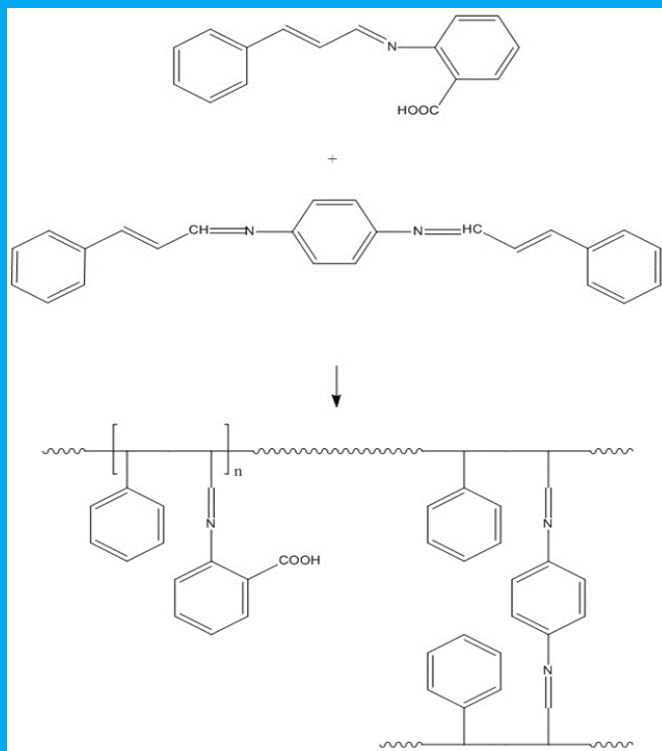


# Eclética Química Journal

Volume 43 • number 2 • year 2018



**A comparative study of Schiff base chelating resins: synthesis, uptake of heavy metal ions, and thermal studies**

## Stratification

Study of the stratification process at the reservoir of the hydroelectric power plant Gov. Pedro Viriato Parigot de Souza (Capivari-Cachoeira), Paraná, Brazil

## Water

Evaluation of the water quality of the Verde River, Ponta Grossa, PR: a study on the conditions of aquatic life maintenance and the eutrophication process

## Glass

Incorporation of  $\text{CdFe}_2\text{O}_4$ - $\text{SiO}_2$  nanoparticles in  $\text{SbPO}_4$ - $\text{ZnO}$ - $\text{PbO}$  glasses by melt-quenching process

## X-Ray

Spatial distribution of atmospheric pollutants through biomonitoring in tree bark using X-Ray fluorescence

## Ecotoxicity

Ecotoxicity of Malathion® 500 CE before and after UVC radiation and  $\text{UV}/\text{H}_2\text{O}_2$  treatment

## Pesticide

Removal of pesticide residues after simulated water treatment: by-products and acetylcholinesterase inhibition

**unesp** 

UNIVERSIDADE ESTADUAL PAULISTA  
"JÚLIO DE MESQUITA FILHO"



Instituto de Química  
UNESP  
Araraquara

ISSN 1678-4618



UNIVERSIDADE ESTADUAL PAULISTA

**Reitor**

Sandro Roberto Valentini

**Vice-reitor**

Sergio Roberto Nobre

**Pró-reitor de Planejamento Estratégico e Gestão**

Leonardo Theodoro Büll

**Pró-reitora de Graduação**

Gladis Massini-Cagliari

**Pró-reitor de Pós-Graduação**

João Lima Sant'Anna Neto

**Pró-reitora de Extensão Universitária**

Cleopatra da Silva Planeta

**Pró-reitor de Pesquisa**

Carlos Frederico de Oliveira Graeff



INSTITUTO DE QUÍMICA

**Diretor**

Eduardo Maffud Cilli

**Vice-Diretora**

Dulce Helena Siqueira Silva

## Editorial Team

### Editors

**Prof. Assis Vicente Benedetti**, Institute of Chemistry Unesp Araraquara, Brazil (Editor-in-Chief)

**Prof. Arnaldo Alves Cardoso**, Institute of Chemistry Unesp Araraquara, Brazil

**Prof. Antonio Eduardo Mauro**, Institute of Chemistry Unesp Araraquara, Brazil

**Prof. Horacio Heinzen**, Faculty of Chemistry, UdelaR, Montevideo, Uruguay

**Prof. Maysa Furlan**, Institute of Chemistry Unesp Araraquara, Brazil

**Prof. Maria Célia Bertolini**, Institute of Chemistry Unesp Araraquara, Brazil

**Prof. Paulo Clairmont Feitosa de Lima Gomes**, Institute of Chemistry, Unesp Araraquara, Brazil

### Editorial Board

**Prof. Jairton Dupont**, Instituto de Química, Universidade Federal do Rio Grande do Sul, UFRGS, RS, Brazil

**Prof. Enric Brillas**, Facultat de Química, Universitat de Barcelona, Spain

**Prof. Verónica Cortés de Zea Bermudez**, Escola de Ciências da Vida e do Ambiente, Universidade de Trás-os-Montes e Alto Douro, Vila Real, Portugal

**Prof. Lauro Kubota**, Instituto de Química, Universidade Estadual de Campinas, Unicamp, SP, Brazil

**Prof. Ivano Gerardt Rolf Gutz**, Instituto de Química, Universidade de São Paulo, USP, SP, Brazil

**Prof. Massuo Jorge Kato**, Instituto de Química, Universidade de São Paulo, USP, SP, Brazil

**Prof. Francisco de Assis Leone**, Faculdade de Filosofia, Ciências e Letras, Universidade de São Paulo, Ribeirão Preto, USP-RP, SP, Brazil

**Prof. Roberto Santana da Silva**, Faculdade de Ciências Farmacêuticas, Universidade de São Paulo, Ribeirão Preto, USP-RP, SP, Brazil

**Prof. José Antônio Maia Rodrigues**, Faculdade de Ciências, Universidade do Porto, Portugal

**Prof. Bayardo Baptista Torres**, Instituto de Química, Universidade de São Paulo, USP, SP, Brazil

### Technical Staff

Gustavo Marcelino de Souza  
Lucas Henrique de Carvalho Machado

## Editorial

The Editor proudly announces the new issue of EQJ in which readers will find several original articles covering areas such as Inorganic Chemistry, Material Chemistry and Environmental Chemistry. According to the editorial profile of EQJ, the following subjects are presented: synthesis and characterization of chelating resins based on Schiff bases and the effect of compositional ratio of chelating moieties and the degree of cross-linking on the uptake behavior of the heavy metal ions; the stratification process at a reservoir of a hydroelectric power plant and changes in quality of the water; developing of glasses containing protected nanoparticles dispersed homogeneously which can be used to prepare new functional glasses useful for magneto-optics devices; evaluation of ecotoxicity and phytotoxicity of the commercial Malathion® 500 CE product using *Aedes aegypti* larvae and *Lactuca sativa* seed; evaluation of the physicochemical parameters that express the water quality of a river and their influence on aquatic life maintenance; spatial distribution of atmospheric pollutants biomonitoring in tree barks to determine the emission sources in a portuary context; water treatment systems and their ability to remove pesticides residues and by-products.

The Editor is convinced of the high quality of the articles and thanks all authors for their valuable contributions.

Assis Vicente Benedetti  
Editor-in-Chief of EQJ

## Instructions for Authors

### Preparation of manuscripts

- **Only manuscripts in English will be accepted.** British or American usage is acceptable, but they should not be mixed.
- **The corresponding author should submit the manuscript online:**  
<http://revista.iq.unesp.br/ojs/index.php/eclética/author>
- **Manuscripts must be sent in editable files as \*.doc, \*.docx or \*.odt.** The text must be typed using font style Times New Roman and size 11. Space between lines should be 1.5 mm and paper size A4.
- **The manuscript should be organized in sections as follows:** Introduction, Experimental, Results and Discussion, Conclusions, and References. Sections titles must be written in bold and numbered sequentially; only the first letter should be in uppercase letter. Subsections should be written in normal and italic lowercase letters. For example: **1. Introduction;** *1.1 History;* **2. Experimental;** *2.1 Surface characterization;* *2.1.1 Morphological analysis*
- **The cover letter should include:** the authors' full names, e-mail addresses, ORCID code and affiliations, and remarks about the novelty and relevance of the work. The cover letter should also contain the suggestion of 3 (three) suitable reviewers (please, provide full name, affiliation, and e-mail).
- **The first page of the manuscript** should contain the title, abstract and keywords. *Please, do not give authors names and affiliation, and acknowledgements since a double-blind reviewer system is used. Acknowledgements should be added to the proof only.*
- **All contributions should include** an Abstract (200 words maximum), three to five Keywords and a Graphical Abstract (8 cm wide and 4 cm high) with an explicative text (2 lines maximum).
- **References should be numbered** sequentially in superscript throughout the text and compiled in brackets at the end of the manuscript as follows:

### Journal:

[1] Adorno, A. T. V., Benedetti, A. V., Silva, R. A. G. da, Blanco, M., Influence of the Al content on the phase transformations in Cu-Al-Ag Alloys, *Eclét. Quim.* 28 (1) (2003) 33-38. <https://doi.org/10.1590/S0100-46702003000100004>.

### Book:

[2] Wendlant, W. W., *Thermal Analysis*, Wiley-Interscience, New York, 3rd ed., 1986, ch1.

### Chapter in a book:

[3] Ferreira, A. A. P., Uliana, C. V., Souza Castilho, M. de, Canaverolo Pesquero, N., Foguel, N. V., Pilon dos Santos, G., Fugivara, C. S., Benedetti, A. V., Yamanaka, H., Amperometric Biosensor for Diagnosis of Disease, In: *State of the Art in Biosensors - Environmental and Medical Applications*, Rincken, T., ed., InTech: Rijeka, Croatia, 2013, Ch. 12.

### Material in process of publication:

[4] Valente Jr., M. A. G., Teixeira, D. A., Lima Azevedo, D., Feliciano, G. T., Benedetti, A. V., Fugivara, C. S., Caprylate Salts Based on Amines as Volatile Corrosion Inhibitors for Metallic Zinc: Theoretical and Experimental Studies, *Frontiers in Chemistry*. <https://doi.org/10.3389/fchem.2017.00032>.

- Figures, Schemes, and Tables should be numbered sequentially and presented at the end of the manuscript.
- Nomenclature, abbreviations, and symbols should follow IUPAC recommendations.
- Figures, schemes, and photos already published by the same or different authors in other publications may be reproduced in manuscripts of **Eclet. Quim. J.** only with permission from the editor house that holds the copyright.
- Graphical Abstract (GA) should be a high-resolution figure (900 dpi) summarizing the manuscript in an interesting way to catch the attention of the readers and accompanied by a short explicative text (2 lines maximum). GA must be submitted as \*.jpg, \*.jpeg or \*.tif.
- **Communications** should cover relevant scientific results and are limited to 1,500 words or three pages of the Journal, not including the title, authors' names, figures, tables and references. However, Communications suggesting fragmentation of complete contributions are strongly discouraged by Editors.
- **Review articles** should present state-of-the-art overviews in a coherent and concise form covering the most relevant aspects of the topic that is being revised and indicate the likely future directions of the field. Therefore, before beginning the preparation of a Review manuscript, send a letter (1page maximum) to the Editor with the subject of interest and the main topics that would be covered in Review manuscript. The Editor will communicate his decision in two weeks. Receiving this type of manuscript does not imply acceptance to be published in **Eclet. Quím. J.** It will be peer-reviewed.
- **Short reviews** should present an overview of the state-of-the-art in a specific topic within the scope of the Journal and limited to 5,000 words. Consider a table or image as corresponding to 100 words. Before beginning the preparation of a Short Review manuscript, send a letter (1page maximum) to the Editor with the subject of interest and the main topics that would be covered in the Short Review manuscript.
- **Technical Notes:** descriptions of methods, techniques, equipment or accessories developed in the authors' laboratory, as long as they present chemical content of interest. They should follow the usual form of presentation, according to the peculiarities of each work. They should have a maximum of 15 pages, including figures, tables, diagrams, etc.
- **Articles in Education in Chemistry and chemistry-correlated areas:** research manuscript related to undergraduate teaching in Chemistry and innovative experiences in undergraduate and graduate education. They should have a maximum of 15 pages, including figures, tables, diagrams, and other elements.
- **Special issues** with complete articles dedicated to Symposia and Congresses can be published by **Eclet. Quim. J.** under the condition that a previous agreement with Editors is established. All the guides of the journal must be followed by the authors.
- **Eclet. Quim. J.** Ethical Guides and Publication Copyright:

Before beginning the submission process, please be sure that all ethical aspects mentioned below were followed. Violation of these ethical aspects may prevent authors from submitting and/or publishing articles in **Eclet. Quim. J.**

- The corresponding author is responsible for listing as authors only researchers who have really taken part in the work, and for informing them about the entire manuscript content and for obtaining their permission for submitting and publishing.
- Authors are responsible for carefully searching for all the scientific work relevant to their reasoning irrespective of whether they agree or not with the presented information.
- Authors are responsible for correctly citing and crediting all data used from works of researchers other than the ones who are authors of the manuscript that is being submitted to **Eclet. Quim. J.**
- Citations of Master's Degree Dissertations and PhD Theses are not accepted; instead, the publications resulting from them must be cited.

- Explicit permission of a non-author who has collaborated with personal communication or discussion to the manuscript being submitted to **Eclét. Quím. J.** must be obtained before being cited.
- Simultaneous submission of the same manuscript to more than one journal is considered an ethical deviation and is conflicted to the declaration has been done below by the authors.
- Plagiarism, self-plagiarism, and the suggestion of novelty when the material was already published are unaccepted by **Eclét. Quím. J.**
- The word-for-word reproduction of data or sentences as long as placed between quotation marks and correctly cited is not considered ethical deviation when indispensable for the discussion of a specific set of data or a hypothesis.
- Before reviewing a manuscript, the *turnitin* anti-plagiarism software will be used to detect any ethical deviation.
- The corresponding author transfers the copyright of the submitted manuscript and all its versions to **Eclét. Quím. J.**, after having the consent of all authors, which ceases if the manuscript is rejected or withdrawn during the review process.
- Before submitting manuscripts involving human beings, materials from human or animals, the authors need to confirm that the procedures established, respectively, by the institutional committee on human experimentation and Helsinki's declaration, and the recommendations of the animal care institutional committee were followed. Editors may request complementary information on ethical aspects.
- When a published manuscript in EQJ is also published in other Journal, it will be immediately withdrawn from EQJ and the authors informed of the Editor decision.
- **Manuscript Submission**

For the first evaluation: the manuscripts should be submitted in three files: the cover letter as mentioned above, the graphical abstract and the entire manuscript.

The entire manuscript should be submitted as \*.doc, \*.docx or \*.odt files.

The Graphical Abstract (GA) 900 dpi resolution is mandatory for this Journal and should be submitted as \*.jpg, \*.jpeg or \*.tif files as supplementary file.

The cover letter should contain the title of the manuscript, the authors' names and affiliations, and the relevant aspects of the manuscript (no more than 5 lines), and the suggestion of 3 (three) names of experts in the subject: complete name, affiliation, and e-mail).

• **Resubmission** (manuscripts “rejected in the present form” or subjected to “revision”): **A LETTER WITH THE RESPONSES TO THE COMMENTS/CRITICISM AND SUGGESTIONS OF REVIEWERS/EDITORS SHOULD ACCOMPANY THE REVISED MANUSCRIPT. ALL MODIFICATIONS MADE TO THE ORIGINAL MANUSCRIPT MUST BE HIGHLIGHTED.**

#### • **Editor's requirements**

Authors who have a manuscript accepted in **Eclética Química Journal** may be invited to act as reviewers.

Only the authors are responsible for the correctness of all information, data and content of the manuscript submitted to **Eclética Química Journal**. Thus, the Editors and the Editorial Board cannot accept responsibility for the correctness of the material published in **Eclética Química Journal**.

#### • **Proofs**

After accepting the manuscript, **Eclét. Quím. J.** technical assistants will contact you regarding your manuscript page proofs to correct printing errors only, i.e., other corrections or content improvement are not permitted. The proofs shall be returned in 3 working days (72 h) via e-mail.

• **Authors Declaration**

The corresponding author declares, on behalf of the other authors, that the article being submitted is original and has been written by the stated authors who are all aware of its content and approve its submission. Declaration should also state that the article has not been published previously and is not under consideration for publication elsewhere, that no conflict of interest exists and if accepted, the article will not be published elsewhere in the same form, in any language, without the written consent of the publisher.

• **Appeal**

Authors may only appeal once about the decision regarding a manuscript. To appeal against the Editorial decision on your manuscript, the corresponding author can send a rebuttal letter to the editor, including a detailed response to any comments made by the reviewers/editor. The editor will consider the rebuttal letter, and if deemed appropriate, the manuscript will be sent to a new reviewer. The Editor decision is final.

• **Contact**

Gustavo Marcelino de Souza ([ecletica@journal.iq.unesp.br](mailto:ecletica@journal.iq.unesp.br))

**Copyright Notice**

The corresponding author transfers the copyright of the submitted manuscript and all its versions to Eclét. Quim. J., after having the consent of all authors, which ceases if the manuscript is rejected or withdrawn during the review process.

The articles published by **Eclética Química Journal** are licensed under the Creative Commons Attribution 4.0 International License.

## SUMMARY

EDITORIAL BOARD.....	3
EDITORIAL.....	4
INSTRUCTIONS FOR AUTHORS.....	5

### ORIGINAL ARTICLES

A comparative study of Schiff base chelating resins: synthesis, uptake of heavy metal ions, and thermal studies.....	10
<i>Fatma A. Al-Yusufy, Mohammed Q. Al-Qadasy, Yasmin M. S. Jamil, Hussein M. Al-Maydama, Moathe M. Akeel</i>	
Study of the stratification process at the reservoir of the hydroelectric power plant Gov. Pedro Viriato Parigot de Souza (Capivari-Cachoeira), Paraná, Brazil.....	23
<i>Sarah Meier Lopes, Nicole Machuca Brassac de Arruda, Thomaz Aurélio Pagioro</i>	
Incorporation of CdFe <sub>2</sub> O <sub>4</sub> -SiO <sub>2</sub> nanoparticles in SbPO <sub>4</sub> -ZnO-PbO glasses by melt-quenching process .....	32
<i>Juliane Resges Orives, Wesley R. Viali, Marina Magnani, Marcelo Nalin</i>	
Ecotoxicity of Malathion® 500 CE before and after UVC radiation and UV/H <sub>2</sub> O <sub>2</sub> treatment.....	44
<i>Eliane Adams, Vinicius de Carvalho Soares de Paula, Rhaissa Dayane Carneiro, Rubia Matos de Lima, Monike Felipe Gomes, Wanessa Algarte Ramsdorf, Adriane Martins de Freitas</i>	
Evaluation of the water quality of the Verde River, Ponta Grossa, PR: a study on the conditions of aquatic life maintenance and the eutrophication process.....	51
<i>Karine Andréa Costa, Elizabeth Weinhardt Oliveira Scheffer, Patrícia Los Weinert, Estevan Luis Silveira</i>	
Spatial distribution of atmospheric pollutants through biomonitoring in tree bark using X-Ray fluorescence.....	59
<i>Bruno Martins Gurgatz, Regiani Carvalho-Oliveira, Gisele Antoniaconi, Paulo Hilário do Nascimento Saldiva, Luciano Fernandes Huergo, Rodrigo Arantes Reis</i>	
Removal of pesticide residues after simulated water treatment: by-products and acetylcholinesterase inhibition.....	65
<i>Rafael Oliveira Costa, Polyana Soares Barcellos, Maria Cristina Canela</i>	

## A comparative study of Schiff base chelating resins: synthesis, uptake of heavy metal ions, and thermal studies

Fatma A. Al-Yusufy<sup>1</sup>, Mohammed Q. Al-Qadasy<sup>1</sup>, Yasmin M. S. Jamil<sup>1</sup>, Hussein M. Al-Maydama<sup>1</sup>, Moathe M. Akeel<sup>1</sup>

<sup>1</sup>Sana'a University, Faculty of Science, Department of Chemistry, Sana'a, Yemen

\* Corresponding author: Fatma A. Al-Yusufy, e-mail address: [f\\_aljusufy@yahoo.com](mailto:f_aljusufy@yahoo.com)

### ARTICLE INFO

#### Article history:

Received: February 5, 2018

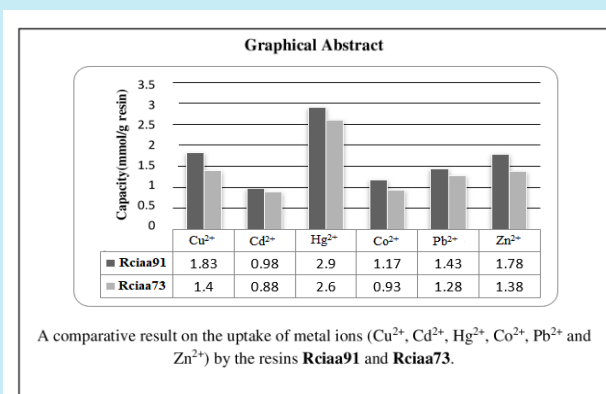
Accepted: May 7, 2018

Published: August 23, 2018

#### Keywords:

1. Schiff bases
2. chelating resins
3. cross-linking
4. metal ion uptake
5. physical parameters

**ABSTRACT:** Two new chelating resins (**Rciaa91** and **Rciaa73**) with different compositional chelating groups and degree of cross-linking were prepared by free radical copolymerization of Schiff bases obtained from condensation reaction of cinnamaldehyde (ci) with anthranilic acid (aa) and 1,4-phenylenediamine (pn) monomers. The synthesized materials were characterized using CHN analyses, FTIR, <sup>1</sup>H-NMR, and thermal analyses (TGA, DTA). Batch technique was applied, and the contact time, pH and initial concentration of the metal ions were investigated as factors affecting the uptake behavior. The results obtained indicated that the chelating resin with larger compositional ratio of chelating moieties and lower degree of cross-linking showed lower optimum reaction time and higher uptake affinity towards the metal ions Cu(II), Cd(II), Co(II), Zn(II), Hg(II), and Pb(II), under the same conditions. Both the chelating resins showed uptake behavior of the metal ions in the following order  $Hg^{2+} > Cu^{2+} > Zn^{2+} > Pb^{2+} > Co^{2+} > Cd^{2+}$  each metal at its optimum pH and at the same reaction time and ion concentration. The thermal degradation behavior and stability of the resins were investigated by using non-isothermal thermogravimetric analysis (TGA/DTG/DTA), at 10 °C min<sup>-1</sup> heating rate and under nitrogen. The Coats-Redfern method was used to evaluate the kinetic and thermodynamic parameters ( $\Delta G^*$ ,  $\Delta H^*$  and  $\Delta S^*$ ) for the prominent degradation steps in the TGA curves at 450-660 °C range.



### 1. Introduction

The removal and separation of metal ions in aqueous solution play an important role for the analysis of wastewaters, industrial and geological samples as well as for environmental remediation<sup>1, 2</sup>. Chelating resins have been widely utilized for the removal of the undesired metal ions from these aqueous solutions<sup>3, 4</sup>. The development of high performance chelating resins for removing heavy metal ions from aqueous solution is considered not only as research priority in the environmental field but also as an area of interest in inorganic catalyst and recovery of valuable trace

metal ions<sup>5-8</sup>. These resins show greater selectivity compared to the conventional types of ion exchangers<sup>9-11</sup>. Besides, they show good physical and chemical properties such as porosity, high surface area, durability and purity<sup>12-14</sup>. Many chelating resins with different functionalities like quaternary amine<sup>11, 12</sup>, sulfonamides<sup>15</sup>, Schiff base<sup>7, 8, 16-20</sup>, sulfonic acid<sup>21</sup>, hydroxamic acid<sup>22</sup> and amidoxime<sup>23, 24</sup> have been emphasized for interaction with metal ions.

Schiff bases having multidentate coordination sites are known to form complexes with transition metal ions readily. Present in a polymer matrix, they are expected to show affinity and selectivity

towards the metal ions at an appropriate pH<sup>7,8,16-20</sup>. This led us to synthesize chelating resins, which will show affinity for the metal ions at appropriate pH.

In the present work Schiff base chelating resins have been prepared. The adsorption behavior of the resin obtained towards heavy metal ions (II); Cu, Cd, Co, Zn, Hg, and Pb have been studied. Both kinetic thermodynamic parameters of the adsorption process were also calculated. It also reported the thermal behavior, degradation kinetic, thermodynamic parameters and the thermal stability of the **Ricaa91** and **Ricaa73** resin at a single heating rate (10 °C min<sup>-1</sup>).

## 2. Experimental

### 2.1 Chemicals

All starting materials were reagent grade: solvents, indicators and metal ions (Cu<sup>2+</sup>, Cd<sup>2+</sup>, Co<sup>2+</sup>, Zn<sup>2+</sup>, Hg<sup>2+</sup>, and Pb<sup>2+</sup>) were purchased from BDH chemical company - England, anthranilic acid, and absolute ethanol from Fluka chemical company-USA, 1,4-phenylenediamine and benzoyl peroxide from Aldrich chemical company-Germany, and cinnamaldehyde and 1,2 azobisisobutyronitrile (AIBN) were from HiMedia laboratories- India.

Anthranilic acid was purified and recrystallized before use from distilled water. 1,4-Phenylenediamine was recrystallized from benzene. Cinnamaldehyde and 1,2 azobisisobutyronitrile were used as received.

### 2.2 Techniques

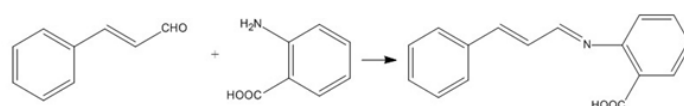
Melting points were determined on Stuart Scientific Electro-thermal melting point apparatus. FTIR spectra were recorded using the KBr disc technique on a JASCO 410 FTIR Spectrophotometer. Elemental analyses (CHN) were performed on an elemental analyses system, GmbH VARIOEL V<sub>2,3</sub>1998 CHNS Mode. <sup>1</sup>H-NMR spectra were recorded in d<sub>6</sub> DMSO on VARIAN 300 MHz FT-NMR Spectrometer (δ in ppm) using TMS as an internal reference. The TGA/DrTGA, DTA/DrDTA thermo-analytical curves were measured in a heating range (25-800 °C) and at a rate of 10 °C min<sup>-1</sup> under nitrogen using Shimadzu TGA-50H and Shimadzu DTA-50H thermal analyzers, respectively.

### 2.3 Synthesis of Schiff bases

#### 2.3.1 Synthesis of cinnamaldehyde anthranilic acid (*ciaa*)

The Schiff base **ciaa** was prepared by adding cinnamaldehyde (0.05 mol, 6.38 mL) to solution of anthranilic acid (0.05 mol, 6.86 gm) in 20 mL absolute ethanol with stirring and gentle heating. The formed precipitate was filtered, washed with ethanol and then dried in air (**Scheme 1**). Color yellow. Mwt. 251. Yield 85%. M.p. 140 °C.

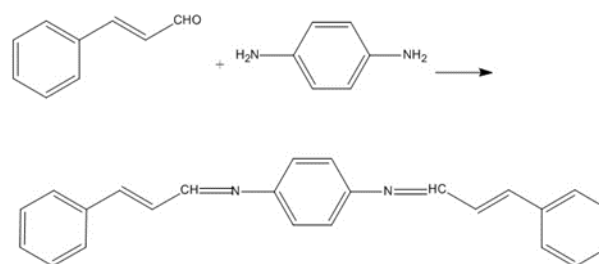
Elemental analysis (% CHN): Calcd. (Found) C: 76.47 (76.23), H: 5.21 (5.07), N: 5.57 (5.32). <sup>1</sup>HNMR data (DMSO-d<sub>6</sub>): (ppm), 47 - 8.00 (m, CH vinyl, CH arm), 9.65(d, CH=N). IR (KBr) v/cm<sup>-1</sup>: 3100 - 2634 (broad band OH<sub>str</sub>), 3063, 3029 (=CH vinyl, arm), 1704 (C=O), 1616 (CH=N), 1603, 1586, 1509 (C=C vinyl, arm), 747, 687 (=CHoop).



**Scheme 1:** Synthesis of the Schiff base **ciaa**

#### 2.3.2 Synthesis of cinnamaldehyde-1,4-phenylenediamine (*cipn*)

To a solution of 1,4-phenylenediamine (0.05 mol, 5.41gm) in 20 mL absolute ethanol, a cinnamaldehyde (0.1 mol, 12.7 mL) was added with stirring and gentle heating. The precipitate obtained was filtered, washed thoroughly with ethanol and then dried in air (**Scheme 2**). Color, pale yellow. Mwt. 336. Yield 80%. M.p. 227 °C.



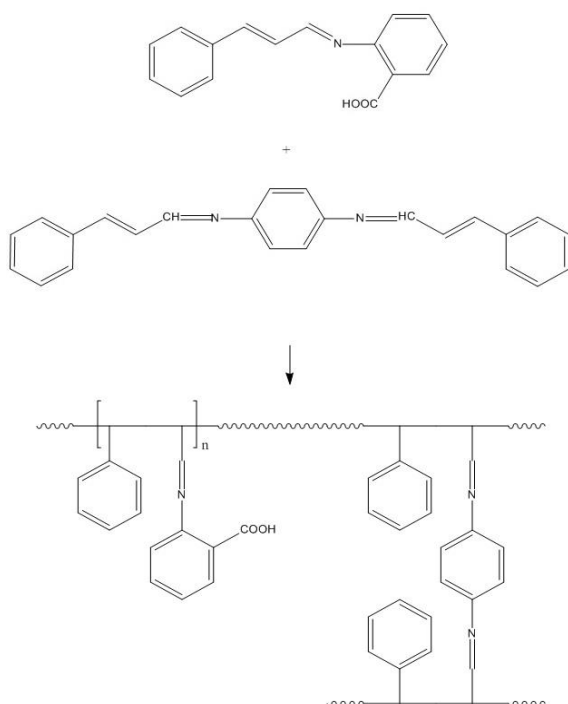
**Scheme 2:** synthesis of the Schiff base **cipn**.

Elemental analysis (% CHN): Calcd. (Found) C: 85.68 (85.06), H: 5.99 (5.86), N: 8.32 (7.90). <sup>1</sup>HNMR data (DMSO-d<sub>6</sub>): δ(ppm), 7.1 - 7.6 (m, CH vinyl, CH arm), 8.4 (d, CH=N). IR (KBr) v/cm<sup>-1</sup>

<sup>1</sup>: 3077, 3039, 3029 (=CHstr), 1626 (CH=N), 1603, 1599, 1586, 1572 (C=C vinyl, arm), 838, 745, 693(=CHoop).

#### 2.4 Synthesis of (*ciaa* – *cipn*) copolymers (chelating resins)

A general heterogeneous copolymerization method was used in the preparation of the chelating resins in this study<sup>25</sup>. Each of the comonomers, **ciaa** and **cipn**, were mixed individually with AIBN (1 mol/100 mol of common mixture) as a polymerization initiator in 5 mL DMF. The radical copolymerization was maintained by mixing together the two comonomer mixture solutions, then heating to 75 °C under reflux for 24 h. After cooling the chelating resin was precipitated in methanol, filtered off, washed several times with methanol and finally, dried in air (Scheme 3). Since the Schiff base **cipn** possess two vinyl (-CH<sub>2</sub>=CH<sub>2</sub>-) moieties on either sides of its chemical structure, it was deliberately used as the cross-linking agent in the preparation of the chelating resins.



**Scheme 3:** Synthesis of Schiff base chelating resins, **Rciaa91** and **Rciaa73**.

The resin of (*ciaa*-*cipn*) copolymer was prepared as crosslinked chelating resins in two different ratios of **ciaa** and **cipn** mixtures<sup>26</sup>; a mixture of **ciaa** (9 gm, 35.9×10<sup>-3</sup> mol) and **cipn** (1

gm, 3×10<sup>-3</sup> mol) to form the resin **Rciaa91**, and that of **ciaa** (7 gm, 27.9×10<sup>-3</sup> mol) and **cipn** (3 gm, 8.9×10<sup>-3</sup> mol) to form the resin **Rciaa73**.

#### 2.5 Metal ion adsorption measurements using a batch method.

Stock solutions of the metal ions were prepared in distilled water. A stock solution of EDTA (5.0 × 10<sup>-3</sup> mol L<sup>-1</sup>) was prepared and standardized against a solution of MgSO<sub>4</sub>·7H<sub>2</sub>O using Eriochrome Black-T (EBT) as an indicator<sup>27</sup>. Buffers of acetic acid/sodium acetate and ammonium hydroxide/ammonium chloride were used for the experiments carried out under a controlled pH.

The metal ion adsorption experiments using the batch method were carried out at a controlled pH by placing 0.05 g chelating resin with 50 mL metal ion at initial concentration 5.0 × 10<sup>-3</sup> mol L<sup>-1</sup>. The contents of the flask were equilibrated on a Gallenkamp flask shaker at room temperature for 60 min at 150 rpm. The pH of the solution was adjusted using a suitable buffer. Then, 5 mL of the solution (free of suspended solid) were taken at the end of the experiment at different intervals. The residual concentration of the metal ion solution was determined via titration against 5.0 × 10<sup>-3</sup> mol L<sup>-1</sup> EDTA using EBT indicator<sup>27,28</sup>.

#### 2.6 Effect of pH on the uptake of metal ions

The effect of pH of the metal ion test solution is an important parameter for adsorption of metal ions because it affects the solubility of the metal ions, concentration of the counter ions, on the functional groups of the adsorbent and the degree of ionization of the adsorbent<sup>29</sup>. Adsorption measurements under pH control were carried out following the above procedures of uptake experiments. The pH was controlled using NH<sub>4</sub>OH/NH<sub>4</sub>Cl buffer solution to study the uptake behavior at the alkaline mediums (pH 6–12) and acetic acid/sodium acetate (AcOH/NaOAc) buffer was used to study the uptake in the acidic medium (pH 4).

### 3. Results and discussion

#### 3.1 Synthesis and Characterization

The Schiff bases, **ciaa** and **cipn** were prepared as described in the experimental part, by the reaction of cinnamaldehyde (ci) with anthranilic acid (aa), and 1,4-phenylenediamine (pn), respectively. The Schemes 1 and 2 display the structures of the synthesized Schiff bases **ciaa**, **cipn**, respectively. Two chelating resins, **Rciaa91** and **Rciaa73** were then synthesized using free radical polymerization reaction of the synthesized Schiff bases with different compositional weight ratios (**ciaa:cipn**), 9:1 and 7:3, respectively, (Scheme 3).

The synthesized Schiff bases were subjected to elemental analysis (CHN) and their found values were in good agreement with those of the calculated values for the suggested formulas of the prepared samples. The melting points were sharp, indicating the purity of prepared Schiff bases.

### 3.2 Spectral analysis FTIR spectra

The chemical structures of the synthesized Schiff bases were confirmed by the IR and  $^1\text{H}$ NMR spectra. The FTIR spectra of the synthesized Schiff bases, **ciaa** and **cipn**, showed sharp and strong characteristic absorption peaks. Figure 1 displays the FTIR spectra of the synthesized Schiff bases, and their corresponding copolymer **Rciaa91**. The disappearance of the aldehydic carbonyl  $\nu(\text{C}=\text{O})$  band and the amino  $\nu(\text{NH}_2)$  bands of the starting materials, and the appearance of the azomethine  $\nu(\text{C}=\text{N})$  band confirmed the formation of the Schiff bases. The  $\nu(\text{C}=\text{N})$  stretching frequencies of the Schiff bases, **ciaa** and **cipn** appeared at 1616, 1626, respectively. Upon copolymerization of the Schiff bases **ciaa** and **cipn**, the IR spectra of the chelating resins showed broader and less intense peaks compared to their corresponding comonomers. The medium broad peak in the range of  $3400 - 3200 \text{ cm}^{-1}$  could be due to the adsorbed water molecules on the Schiff base chelating resin because of its hygroscopic nature<sup>18</sup>.

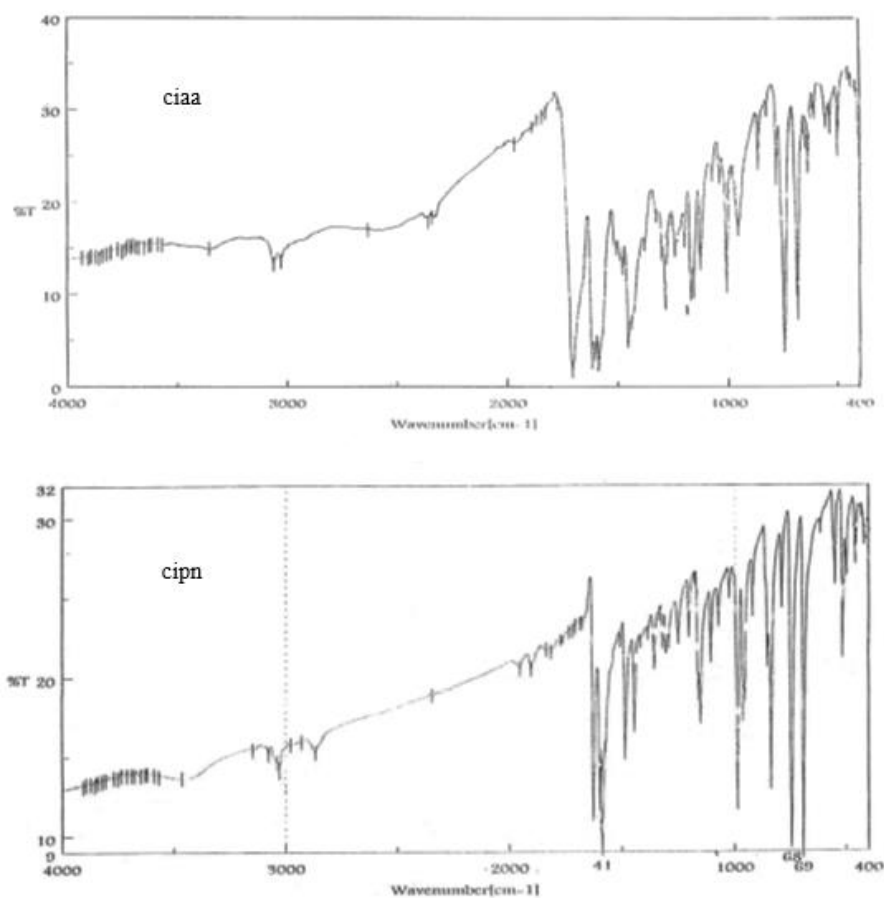


**Figure 1:** FTIR spectra of the Schiff bases, **ciaa** and **cipn**, and the chelating resin **Rciaa91**.

Figure 2 shows the  $^1\text{H}$ NMR spectra of the Schiff base, **ciaa** and **cipn**. The  $^1\text{H}$ NMR spectra of the Schiff bases, **ciaa** and **cipn** showed doublet signals for the  $\delta$  (CH=N) protons at 9.65 and 8.45, respectively. The multiple peaks in the range  $\delta$  6.47 - 8.00 ppm were attributed to the vinyl and aromatic protons of the conjugated structure of the

Schiff bases. The singlet peak at 2.51 ppm in the spectra of is due to the DMSO solvent used in the analysis. The appearance of a broad signal at  $\delta$  3.2 ppm in  $^1\text{H}$ NMR spectrum of the Schiff base **cipn** could be attributed of the presence of traces of unreacted  $\text{NH}_2$  in its chemical structure<sup>30</sup>.

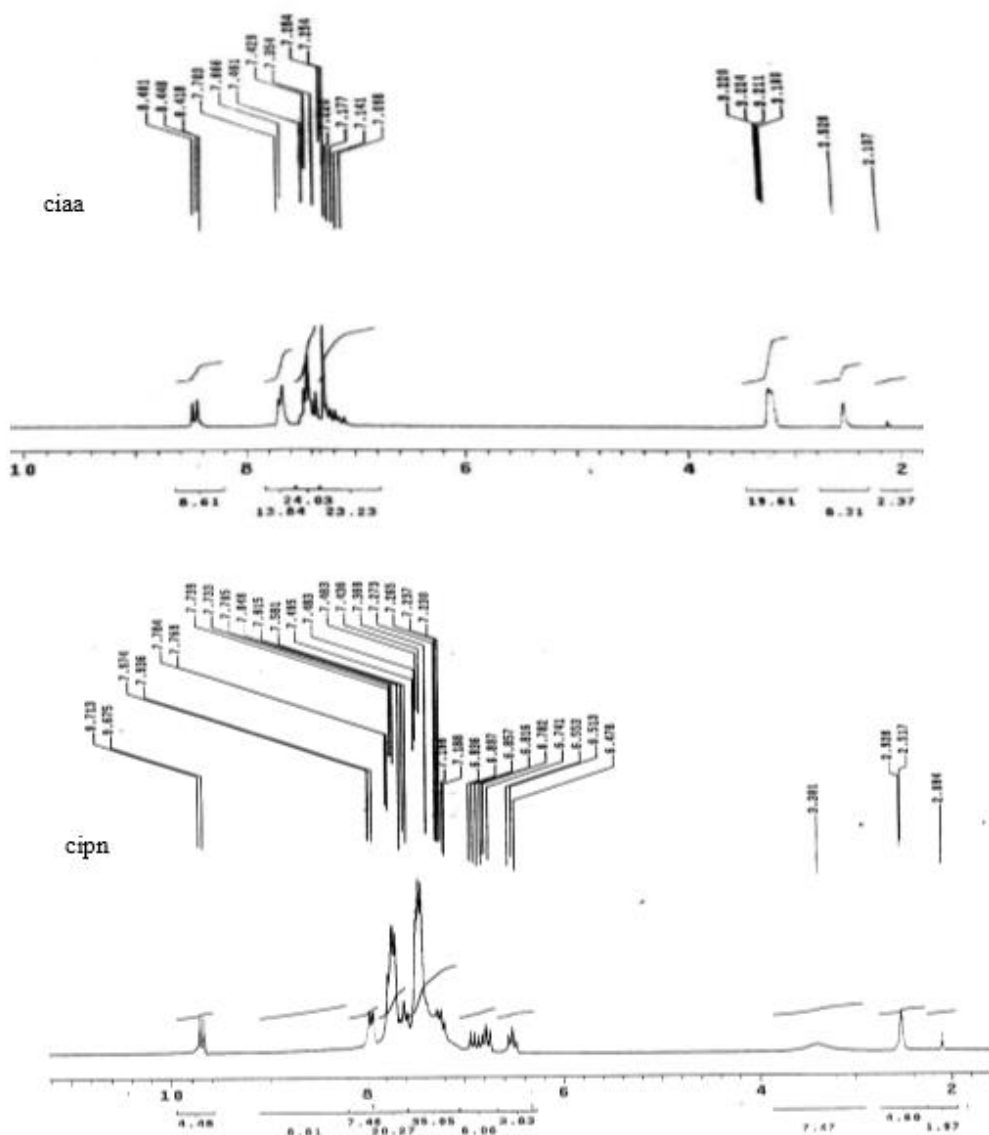


Figure 2:  $^1\text{H}$ NMR spectra of the Schiff bases, **ciaa** and **cipn**.

### 3.3 Uptake of metal ions ( $\text{Cu}^{2+}$ , $\text{Cd}^{2+}$ , $\text{Co}^{2+}$ , $\text{Zn}^{2+}$ , $\text{Hg}^{2+}$ , $\text{Pb}^{2+}$ ) by the chelating resins

#### 3.3.1 Optimum pH of the metal ion uptake

The preliminary uptake experiments of the metal ions;  $\text{Cu}^{2+}$ ,  $\text{Cd}^{2+}$ ,  $\text{Co}^{2+}$ ,  $\text{Zn}^{2+}$ ,  $\text{Hg}^{2+}$  and  $\text{Pb}^{2+}$  by the chelating resin **Rciaa91** and **Rciaa73** at

different pH values between 4 and 10 were examined by batch technique for 60 minutes as a reaction time<sup>26</sup>. The results are shown in Table 1. In general, the uptake of the metal ions increased with increasing pH, until reaching a maximum value and then followed by a decrease in the uptake values at higher pH values, due to the precipitation of the metal hydroxides in the basic solution<sup>31</sup>.

**Table 1.** Effect of pH on the uptake of the metal ions ( $\text{Cu}^{2+}$ ,  $\text{Cd}^{2+}$ ,  $\text{Co}^{2+}$ ,  $\text{Zn}^{2+}$ ,  $\text{Hg}^{2+}$ ,  $\text{Pb}^{2+}$ ) by the chelating resins **Rciaa91** and **Rciaa73** after 60 minutes.

pH	Capacity (mmol/g resin)											
	Rciaa91						Rciaa73					
	$\text{Cu}^{2+}$	$\text{Cd}^{2+}$	$\text{Hg}^{2+}$	$\text{Co}^{2+}$	$\text{Pb}^{2+}$	$\text{Zn}^{2+}$	$\text{Cu}^{2+}$	$\text{Cd}^{2+}$	$\text{Hg}^{2+}$	$\text{Co}^{2+}$	$\text{Pb}^{2+}$	$\text{Zn}^{2+}$
4	1.36	0.13	2.32	0.42	1.10	0.72	1.08	0.13	2.17	0.15	0.70	0.54
5	1.44	0.27	<b>2.92</b>	0.42	1.13	1.02	1.28	0.20	<b>2.60</b>	0.57	0.97	0.87
6	--	--	2.77	--	1.28	--	--	--	2.50	--	1.12	--
7	1.84	0.65	2.4	<b>1.17</b>	<b>1.53</b>	1.48	1.40	0.53	1.75	<b>0.93</b>	<b>1.28</b>	1.22
8	<b>1.84</b>	0.90	--	1.10	--	<b>1.79</b>	<b>1.40</b>	0.76	--	0.79	--	<b>1.38</b>
9	--	<b>1.00</b>	--	--	--	1.66	--	<b>0.88</b>	--	--	--	1.32
10	1.43	0.53	--	--	--	--	1.28	0.50	--	--	--	--

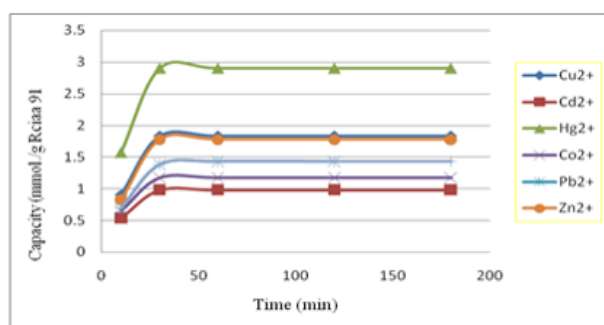
The optimum pH values obtained for the metal ions under study;  $\text{Cu}^{2+}$ ,  $\text{Cd}^{2+}$ ,  $\text{Co}^{2+}$ ,  $\text{Zn}^{2+}$ ,  $\text{Hg}^{2+}$ ,  $\text{Pb}^{2+}$  are 8, 9, 7, 8, 5, 7, respectively.

Table 1 showed that the chelating resins **Rciaa91** and **Rciaa73** absorbed the metal ions in the following order  $\text{Hg}^{2+} > \text{Cu}^{2+} > \text{Zn}^{2+} > \text{Pb}^{2+} > \text{Co}^{2+} > \text{Cd}^{2+}$  each metal at its optimum pH and at the same reaction time and ion concentration. A special feature seen in this study is that  $\text{Hg}^{2+}$  ion showed the highest uptake affinity at low pH compared to the rest of the metal ions under study. This allows separation of  $\text{Hg}^{2+}$  ions, selectively, in the presence of other metal ions.

### 3.3.2 Effect of contact time

The interaction between the resin and metal ion continues until most of effective sites of the resin are occupied by the metal ion. At this point the resin is said to have reached the equilibrium state with the metal ions<sup>32</sup>. The time required to reach the equilibrium state for the uptake processes of each metal ion with the chelating resins **Rciaa91** and **Rciaa73** was evaluated at their optimum pH values. Table 2 and Figures 3 and 4 show the relationship between the uptake processes of each metal ion and the equilibrium reaction time, for the chelating resins **Rciaa91** and **Rciaa73**, respectively. In the case of the chelating resins **Rciaa91**, the equilibrium state was attained within 30 min for all the metal ions and the time required for 50% uptake was about 10 min. On the other

hand, for the chelating resin **Rciaa73**, the equilibrium state was attained within 60 min for the metal ions under investigation and the time required for 50% uptake was about 30 min.



**Figure 3.** Effect of the reaction time on the uptake of the metal ion ( $\text{Cu}^{2+}$ ,  $\text{Cd}^{2+}$ ,  $\text{Hg}^{2+}$ ,  $\text{Co}^{2+}$ ,  $\text{Pb}^{2+}$  and  $\text{Zn}^{2+}$ ) for the resin **Rciaa91**. Resin; 0.05 g, metal ion; 0.005 mol L<sup>-1</sup> and solution volume 50 mL.

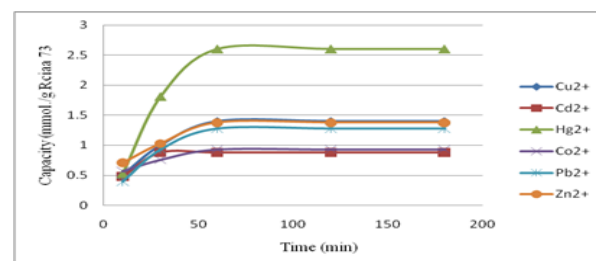


**Figure 4.** Effect of the reaction time on the uptake of the metal ions ( $\text{Cu}^{2+}$ ,  $\text{Cd}^{2+}$ ,  $\text{Hg}^{2+}$ ,  $\text{Co}^{2+}$ ,  $\text{Pb}^{2+}$  and  $\text{Zn}^{2+}$ ) for the resin **Rciaa73**. Resin; 0.05 g, metal ion; 0.005 mol L<sup>-1</sup> and solution volume 50 mL.

**Table 2.** Effect of reaction time on the uptake of the metal ions ( $\text{Cu}^{2+}$ ,  $\text{Cd}^{2+}$ ,  $\text{Co}^{2+}$ ,  $\text{Zn}^{2+}$ ,  $\text{Hg}^{2+}$ ,  $\text{Pb}^{2+}$ ) by the chelating resins **Rciaa91** and **Rciaa73** at optimum pH.

Time (min)	Capacity (mmol/g resin)											
	Rciaa91						Rciaa73					
	$\text{Cu}^{2+}$	$\text{Cd}^{2+}$	$\text{Hg}^{2+}$	$\text{Co}^{2+}$	$\text{Pb}^{2+}$	$\text{Zn}^{2+}$	$\text{Cu}^{2+}$	$\text{Cd}^{2+}$	$\text{Hg}^{2+}$	$\text{Co}^{2+}$	$\text{Pb}^{2+}$	$\text{Zn}^{2+}$
10	0.9	0.54	1.57	0.65	0.69	0.83	0.51	0.48	0.53	0.57	0.39	0.71
30	1.83	0.98	2.90	1.17	1.38	1.78	1.00	0.88	1.81	0.76	0.93	1.03
60	1.83	0.98	2.90	1.17	1.43	1.78	1.40	0.88	2.60	0.93	1.28	1.38
120	1.83	0.98	2.90	1.17	1.43	1.78	1.40	0.88	2.60	0.93	1.28	1.38
180	1.83	0.98	2.90	1.17	1.43	1.78	1.40	0.88	2.60	0.93	1.28	1.38

From the data obtained it could be concluded that the uptake values depend on both the metal ion and the pH values. The uptake capacity of the chelating resins, **Rciaa91** and **Rciaa73** for different metal ions showed a maximum value of  $2.9 \text{ mmol g}^{-1}$  resin and  $2.6 \text{ mmol g}^{-1}$  resin for  $\text{Hg}^{2+}$  ions and a minimum value of  $0.98 \text{ mmol g}^{-1}$  resin and  $0.88 \text{ mmol g}^{-1}$  resin for  $\text{Cd}^{2+}$  ions, respectively. The uptake capacities of the rest of the metal ions were in between for both the chelating resins **Rciaa91** and **Rciaa73** as seen in Figures 3 and 4, respectively.

The differences in the uptake capacities may be attributed to i) the differences in the stability constants of the formed complexes between the different metal ions and the resin<sup>33, 34</sup>. For this reason, the differences in the stability constants may explain the high uptake capacities of  $\text{Hg}^{2+}$  for both the chelating resins, in spite of the large ionic radii of the mercury (II) ion compared to the other ions under investigation, ii) the differences in ionic

radii of the metal ions; the smaller the ion size the easier it can penetrate through the network of the resin<sup>33</sup>. This explains why, the smallest ion  $\text{Cu}^{2+}$ , (ionic radii  $0.72 \text{ \AA}$ ) showed high uptake capacities,  $1.84 \text{ mmol g}^{-1}$  and  $1.40 \text{ mmol g}^{-1}$ , whereas the largest ion  $\text{Cd}^{2+}$ , (ionic radii  $0.97 \text{ \AA}$ ) showed low uptake capacities,  $0.90 \text{ mmol g}^{-1}$  and  $0.88 \text{ mmol g}^{-1}$ , for **Rciaa91** and **Rciaa73**, respectively.

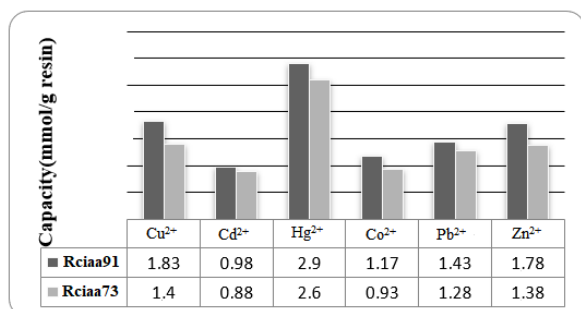
3.4 The effect of compositional ratio of the chelating groups and degree of cross-linking between **Rciaa91** and **Rciaa73** on the uptake processes.

Table 3 and the Figure 5 show the effect of chelating group and degree of cross-linking ratio of **Rciaa91** and **Rciaa73** on the uptake process of the metal ions at the same pH medium, initial metal concentration and reaction time.

**Table 3.** Effect of degree of cross-linking on the uptake of metal ions ( $\text{Cu}^{2+}$ ,  $\text{Cd}^{2+}$ ,  $\text{Hg}^{2+}$ ,  $\text{Co}^{2+}$ ,  $\text{Pb}^{2+}$  and  $\text{Zn}^{2+}$ ) for the resins **Rciaa91** and **Rciaa73** at 60 min.

Chelating resin	Degree of cross-linking (%) by weight	Capacity (mmol/g resin)					
		$\text{Cu}^{2+}$	$\text{Cd}^{2+}$	$\text{Hg}^{2+}$	$\text{Co}^{2+}$	$\text{Pb}^{2+}$	$\text{Zn}^{2+}$

<b>Rciaa91</b>	10	1.84	0.98	2.9	1.17	1.43	1.78
<b>Rciaa73</b>	30	1.4	0.88	2.6	0.93	1.28	1.38
uptake difference (%)		24	10	10	21	10	22



**Figure 5.** A comparative result on the uptake of metal ions (Cu<sup>2+</sup>, Cd<sup>2+</sup>, Hg<sup>2+</sup>, Co<sup>2+</sup>, Pb<sup>2+</sup> and Zn<sup>2+</sup>) by the resins **Rciaa91** and **Rciaa73**.

The results obtained indicated that the resin **Rciaa91** has higher uptake efficiency than **Rciaa73** at the same conditions. This is due to the difference in the compositional ratio of chelating groups and degree of cross-linking of the chelating resins **Rciaa91** and **Rciaa73**. The resin **Rciaa91** with ratio (9:1) by weight, has about 20% of coordinating groups RCH=N-C<sub>6</sub>H<sub>4</sub>-COOH more than the resin **Rciaa73** with compositional ratio (7:3) by weight. Therefore, the low metal ion uptake capacity of the chelating resin **Rciaa73** could be attributed to its higher degree of cross linking. This presumably hinders the approach of the metal ions to the polymeric matrix and, hence, limits the chelating reaction<sup>35</sup>.

The uptake of the resin **Rciaa91** was about 20% more than that of the resin **Rciaa73** for the small metal ions under investigation (Cu<sup>2+</sup>, Co<sup>2+</sup>, Zn<sup>2+</sup>) whose ionic radii was nearly 0.7 Å. This ratio is nearly close to the theoretical ratio of chelating groups between the two resins. On the other hand, the uptake of the large ions (Cd<sup>2+</sup>, Hg<sup>2+</sup> and Pb<sup>2+</sup>) with ionic radii of about 1 Å, by the resin **Rciaa91** was about 11% more than that of the resin **Rciaa73**. This shortage in uptake capacity maybe due to the larger ionic volume of metal ions (Cd<sup>2+</sup>, Hg<sup>2+</sup> and Pb<sup>2+</sup>) and the increasing of degree of cross linking in the resin **Rciaa73**<sup>26, 33</sup>.

### 3.5 The effect of the degree of cross linking on the optimum reaction time for the uptake processes.

The data in the Table 2 and Figures 3 and 4 showed that the resin **Rciaa91** with a lower degree of cross linking reached the optimum reaction time for the uptake process at half time period compared to the resin **Rciaa73**. For example, the equilibrium state for the uptake of Cu<sup>2+</sup> ions by **Rciaa91** at the optimum pH 8 was attained after 30 min, whereas the equilibrium state for the uptake of Cu<sup>2+</sup> ions by **Rciaa73** was reached after 60 min. Also, it was calculated from the data obtained that the time required to achieve 50% of the metal ion uptake was within 5 min for **Rciaa91**, whereas, it was within 20 min for **Rciaa73**.

The comparison between the optimum reaction time for the resins, **Rciaa91** and **Rciaa73**, which have the same chemical structure, but different degree of cross-linking proved that, the higher the degree of cross-linking the higher the optimum reaction time, at the same pH medium.

The resin **Rciaa73** has about 200% more cross linking through RCH=NC<sub>6</sub>H<sub>4</sub>N=CHR than the resin **Rciaa91**. A high degree of cross-linking makes the polymer chains more rigid and more hindering for the metal ions to penetrate the network of the resin in order to act with the active sites. This in turn, will lead to a decrease in the rate of uptake process and increase in the time required to reach the equilibrium state during the uptake<sup>26, 33</sup>.

### 3.6 Thermal Studies

The TGA and DTA curves of the prepared **Rciaa91** and **Rca73** resins are given in Figures 6.1 and 6.2. These curves characterize and compare the thermal degradation of these two resins at 10 °C min<sup>-1</sup> heating rate, under nitrogen and over the range 20-800 °C. For the evaluation of the thermal degradation kinetics parameters at a single heating rate (10 °C min<sup>-1</sup>), the activation energy ( $E_a$ ) and pre-exponential factor ( $Z$ ) are determined by using the Coats-Redfern method<sup>36</sup> for the reaction order  $n \neq 1$ . When the Coats-Redfern method is linearized for a correctly-chosen order of reaction ( $n$ ) yields the activation energy ( $E_a$ ) from the slope of the equation:

$$\log \left[ \frac{1 - (1 - \alpha)^{1-n}}{T^2(1-n)} \right] = \log \left[ \frac{ZR}{qE_a} \left( 1 - \frac{2RT}{E_a} \right) \right] - \frac{E_a}{2.303RT} \text{ for } n \neq 1 \rightarrow 1$$

where:  $\alpha$  = fraction of weight loss,  $T$  = temperature (K),  $Z$  = pre-exponential factor,  $R$  = molar gas constant,  $q$  = heating rate and  $n$  = reaction order; estimated by Horovitz-Metzger method<sup>37</sup>.

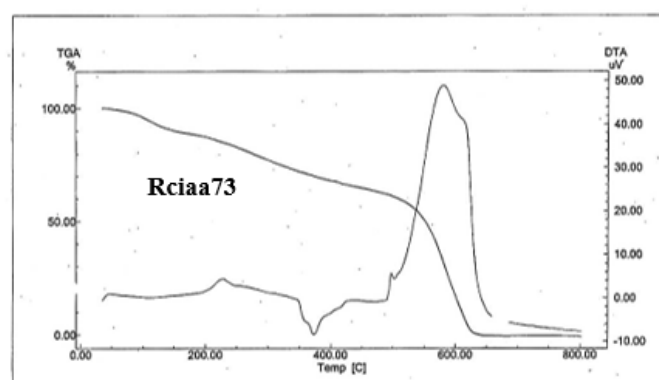
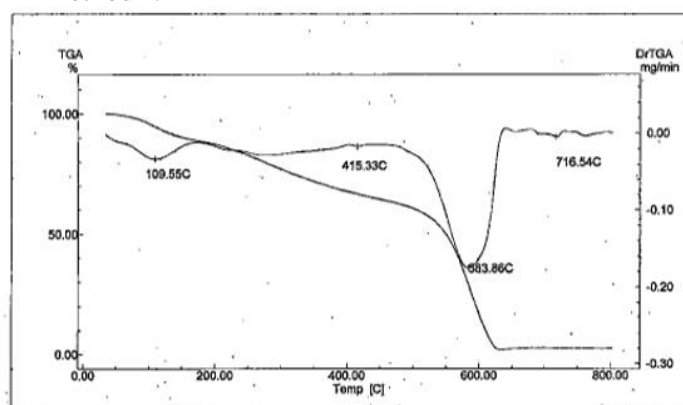
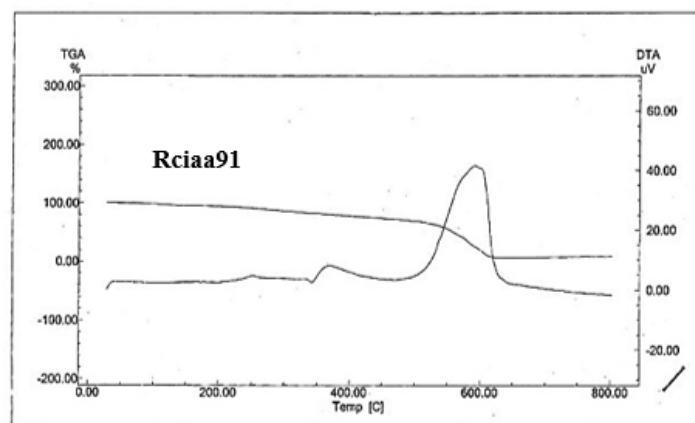


Figure 6.2: DTA thermograms of Rciaa91 and Rciaa73 in nitrogen at 10 °C min<sup>-1</sup> heating rate.

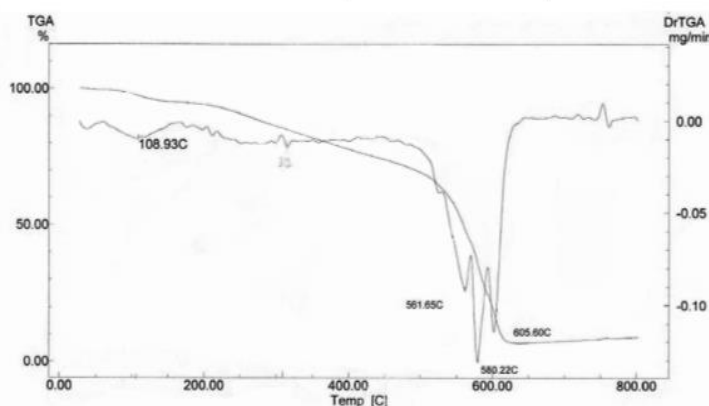


Figure 6.1. TGA thermograms of Rciaa91 and Rciaa73 in nitrogen at 10 °C min<sup>-1</sup> heating rate.

The thermodynamic parameters of the thermal degradation step; enthalpy ( $\Delta H^*$ ), entropy ( $\Delta S^*$ ), and Gibbs energy ( $\Delta G^*$ ) of activation are calculated using the following standard equations:

$$\Delta S^* = R \ln \frac{Zh}{kT_{\max}}$$

$$\Delta H^* = E_a - RT_{\max}$$

$$\Delta G^* = \Delta H^* - T_{\max} \Delta S^*$$

The characteristics of the thermal degradation of these two resins recorded on the TG/DTG/DTA curves, their kinetics and thermodynamics parameters extracted from these curves are given in Tables 4 and 5.

The thermal degradation TG curves of **Rciaa91** and **Rciaa73** resin (Figures 6.1 and 6.2) showed a very slow and continuous mass bleeding (i.e. no plateau from the start up to about 450 °C) of about 37.7% and 27.8%, respectively. Consequently, very small and weak DTG peaks are observed on the DTG curves of these resins and this is indicative to the very slow degradation process in both resins

at the about 35-450 °C range. Therefore, the prominent steps of these two resins that occur at about 470-641 °C range with large and strong DTG peak at 580 °C (**Rciaa91**) and 584 °C (**Rciaa73**) are considered as characteristic steps for which the thermal degradation, kinetics and thermodynamics parameters are determined and hence compared (Tables 4 and 5).

The **Rciaa91** resin showed a mass loss (61.3%) at the prominent step (470-634 °C) with strong  $T_{DTG}$  at 584 °C and exothermic  $T_{DTA}$  peak at 580 °C. The calculated activation energy  $E_a$  of the **Rciaa91** resin for this prominent step is 184 kJ mol<sup>-1</sup>, while -167 J K<sup>-1</sup> mol<sup>-1</sup>, 83 kJ mol<sup>-1</sup> and 226 kJ mol<sup>-1</sup> are the values of entropy ( $\Delta S^*$ ), enthalpy ( $\Delta H^*$ ), and Gibbs energy ( $\Delta G^*$ ) changes. The prominent step (480-641 °C) of the **Rciaa73** resin showed also exothermic mass loss (64.7%) with strong  $T_{DTG}$  (580 °C) and  $T_{DTA}$  (592 °C). The activation energy  $E_a$ , entropy ( $\Delta S^*$ ), enthalpy ( $\Delta H^*$ ), and Gibbs energy ( $\Delta G^*$ ) changes are 180 kJ mol<sup>-1</sup>, -211 J K<sup>-1</sup> mol<sup>-1</sup>, 49 kJ mol<sup>-1</sup> and 226 kJ mol<sup>-1</sup>, respectively.

**Table 4.** Characteristic parameters of the thermal degradation of the resins **Rciaa91** and **Rciaa73**.

Resin	TGA				DTA		$E_a$ kJ mol <sup>-1</sup>
	$\Delta m$ %	$T_i$ °C	$T_f$ °C	$T_{DTG}$ °C	$T_{DTA}$ °C	Peak	
<b>Rciaa91</b>	61.3	470	634	584	580	exo	184
<b>Rciaa73</b>	64.7	480	641	580	592	exo	180

**Table 5.** Kinetic and thermodynamic parameters of the thermal degradation of the resins **Rciaa91** and **Rciaa73**

Resin	$r$	$n$	$T_{\max}$ °C	$Z$ s <sup>-1</sup>	$E_a$ kJ mol <sup>-1</sup>	$\Delta S^*$ kJ mol <sup>-1</sup>	$\Delta H^*$ kJ mol <sup>-1</sup>	$\Delta G^*$ kJ mol <sup>-1</sup>
<b>Rciaa91</b>	0.997	0.9	584	$2.9 \times 10^{17}$	184	80.6	176.9	108.3
<b>Rciaa73</b>	0.998	0.7	580	$8.3 \times 10^{16}$	180	70.3	172.9	112.9

If the initial molecular structure destruction temperature ( $T_i$ ) of the **Ricaa91** and **Ricaa73** resin is taken as a measure of the thermal stability, these two resins are of similar thermal stability for their similar  $T_i$  (35 °C). It can be concluded that although the two resins **Ricaa91** and **Ricaa73** are of similar chemical structure but different degree of cross-linking, their TGA curves and the data extracted from them (Tables 4 and 5) indicate almost similar thermal degradation behavior, kinetics and thermodynamics parameters as well as similar thermal stability regardless the difference in the degree of the cross-linking 1:3 (**Rciaa91**:**Rciaa73**). The resin **Rciaa91** losses 37.7% of its mass slowly and 61.3% rapidly with 1% residue, while **Rciaa73**

losses 28% slowly and 64.7% rapidly with 7.5% residue. This difference in mass loss degradation process may be due to the cross-linking variation.

#### 4. Conclusions

The effect of the compositional ratio of the chelating groups and the degree of the cross-linking of the Schiff base chelating resins, **Rciaa91** and **Rciaa73** on the uptake behavior of the heavy metal ions (Cu<sup>2+</sup>, Cd<sup>2+</sup>, Hg<sup>2+</sup>, Co<sup>2+</sup>, Pb<sup>2+</sup> and Zn<sup>2+</sup>) was the main aim of this research. A special feature observed in this study was that Hg<sup>2+</sup> ions showed the highest uptake affinity at low pH compared to the rest of the metal ions under study for both

resins, **Rciaa91** and **Rciaa73**. The difference in the uptake affinity of the chelating resins may be due to i) the ionic radii of the metal ions; the smaller the ion size the easier it can penetrate through the network of the resin, ii) the stability constants which explains the high uptake capacities of  $\text{Hg}^{2+}$  for both the chelating resins, in spite of the large ionic radii of the mercury (II) ion compared to the other ions under investigation.

When comparing between the uptake affinity and the optimum reaction time for the chelating resins **Rciaa91** and **Rciaa73**, which have the same chemical structure, but different degree of cross linking, one concludes that the higher the degree of cross-linking the higher the optimum reaction time and the lower the uptake affinity towards the heavy metal ions.

The chelating resins showed good thermal stability. The thermal degradation behavior and the kinetic parameters of the resin **Rciaa91** and **Rciaa73** are almost similar, indicating that the differences in the degree of cross-linking are almost of no significant effects.

## 5. References

- [1] Shah, B. A., Shah, A. V., Shah, P. M., Analytical and Morphology Studies of Phthalic acid-Formaldehyde Resorcinol as Chelating Resin, *Malaysian Polymer Journal (MPJ)* 4 (2) (2009) 1-12.
- [2] Cavaco, S. A., Fernandes, S., Augusto, C. M., Quina, M. J., Gando-Ferreira, L. M., Evaluation of chelating ion-exchange resins for separating Cr(III) from industrial effluents, *J. Hazard. Mater.* 169 (2009) 516-523. <https://doi.org/10.1016/j.jhazmat.2009.03.129>.
- [3] Dikshit, D., Polymorphisms in DNA Sequence and Personalized Alternative Herbal Drugs, *Orient Journal of Chemistry (OJC)* 29 (1) (2013) 305-307.
- [4] Hassan, R., Arida, H., Montasser, M., Abdel Latif N., Synthesis of New Schiff Base from Natural Products for Remediation of Water Pollution with Heavy Metals in Industrial Areas, *J. Chem.* 2013 (2013) 1-10. <https://doi.org/10.1155/2013/240568>.
- [5] Cheng-Chien W., Chun-Chih W., Synthesis and characterization of chelating resins with amino moieties and application on removal of copper(II) from EDTA complexes, *J. Appl. Polym. Sci.* 97 (2005) 2457-2468. <https://doi.org/10.1002/app.22019>.
- [6] Shareef, B. A., Waheed, I. F., Jalaot, K. K., Preparation and Analytical Properties of 4-Hydroxybenzaldehyde, Biuret and Formaldehyde Terpolymer Resin, *Orient Journal of Chemistry (OJC)* 29 (4) (2013) 1391-1397. <https://doi.org/10.13005/ojc/290414>.
- [7] Al-Yusufy, F. A., Othman, M. K., Al-Qadri, F. A., Synthesis and Metal Ion Uptake Studies of Formaldehyde and Furfuraldehyde-Condensed Phenol-Schiff Base Chelating Resins, *Sana'a Univ. J. Sci. & Technol.*, 2 (1) (2005) A(9-19).
- [8] Monier, M., Abdel-Latif, D. A., El-Reash, Y. A., Ion-imprinted modified chitosan resin for selective removal of Pd(II) ions, *J. Colloid Interface Sci.* 469 (2016) 344-354. <https://doi.org/10.1016/j.jcis.2016.01.074>.
- [9] Urbano, B. F., Rivas, B. L., Sorption properties of chelating polymer-clay nano-composite resin based on iminodiacetic acid and montmorillonite: water absorbency, metal ion uptake, selectivity, and kinetics, *J. Chem. Technol. Biotechnol.* 89 (2) (2014) 249-258. <https://doi.org/10.1002/jctb.4109>.
- [10] Veliscek-Carolan, J., Separation of actinides from spent nuclear fuel: A review, *J. Hazard. Mater.* 318 (2016) 266-281. <https://doi.org/10.1016/j.jhazmat.2016.07.027>.
- [11] Ling, C., Liu, F. Q., Xu, C., Chen, T. P., Li, A. M., An Integrative Technique Based on Synergistic Coremoval and Sequential Recovery of Copper and Tetracycline with Dual-Functional Chelating resin: Roles of Amine and Carboxyl Groups, *ACS Appl. Mater. Interfaces* 5 (22) (2013) 11808-11817. <https://doi.org/10.1021/am403491b>.
- [12] Laaksonen, T., Heikkinen, S., Wähälä, K., Synthesis of Tertiary and Quaternary Amine Derivatives from Wood Resin as Chiral NMR Solvating Agents, *Molecules* 20 (2015) 20873-20886. <https://doi.org/10.3390/molecules201119732>.
- [13] Monier, M., Adsorption of  $\text{Hg}^{2+}$ ,  $\text{Cu}^{2+}$  and  $\text{Zn}^{2+}$  ions from aqueous solution using formaldehyde cross-linked modified chitosan-

thioglyceraldehyde Schiff's base, *Int. J. Biol. Macromol.* 50 (3) (2012) 773-781. <https://doi.org/10.1016/j.ijbiomac.2011.11.026>.

[14] Donia, A. M., Atia, A. A., Elwakeel, K. Z., Selective separation of mercury(II) using magnetic chitosan resin modified with Schiff's base derived from thiourea and glutaraldehyde, *J. Hazard. Mater.* 151 (2-3) (2008) 372-379. <https://doi.org/10.1016/j.jhazmat.2007.05.083>.

[15] Yang, W., Zheng, F., Xue, X., Lu, Y., Investigation into adsorption mechanisms of sulfonamides onto porous adsorbents, *J. Colloid Interface Sci.* 362 (2) (2011) 503-509. <https://doi.org/10.1016/j.jcis.2011.06.071>.

[16] El-Reash, Y.A., Otto, M., Kenawy, I.M., Ouf, A.M., Adsorption of Cr(VI) and As(V) ions by modified magnetic chitosan chelating resin, *Int. J. Biol. Macromol.* 49 (4) (2011) 513-522. <https://doi.org/10.1016/j.ijbiomac.2011.06.001>.

[17] Othman, M. K., Al-Qadri, F. A., Al-Yusufy, F. A., Synthesis, physical studies and uptake behavior of: Copper(II) and lead(II) by Schiff base chelating resins, *Spectrochim. Acta A Mol. Biomol. Spectrosc.* 78 (5) (2011) 1342-1348. <https://doi.org/10.1016/j.saa.2010.12.073>.

[18] Oo, C. W., Osman, H., Fatinathan, S., Md. Zin, M. A., The Uptake of Copper(II) Ions by Chelating Schiff Base Derived from 4-Aminoantipyrine and 2-Methoxybenzaldehyde, *International Journal of Nonferrous Metallurgy (IJNM)* 2 (2013) 1-9. <https://doi.org/10.4236/ijnm.2013.21001>.

[19] M. Singanan, Biosorption of Hg(II) ions from synthetic wastewater using a novel biocarbon technology, *Eviron. Eng. Res.* 20 (1) (2015) 33-39. <https://doi.org/10.4491/eer.2014.032>.

[20] Hamzaa, M. F., Abdel-Monemb, Y. K., Farag, N. M., El-Tanbouly, A. M., Studies on the Recovery of Cu (II) and U (VI) on Highly Adsorptive Modified Magnetic Amine Resins from Dolostone Leachate Solution, *International Journal of Sciences: Basic and Applied Research (IJSBAR)*, 30 (1) (2016) 149-166.

[21] Daşbaşı, T., Saçmac, Ş., Şahan, S., Kartal, Ş., Ülgen, A., Synthesis, characterization and application of a new chelating resin for on-line

separation, preconcentration and determination of Ag(I) by flame atomic absorption spectrometry, *Talanta* 103 (2013) 1-7. <https://doi.org/10.1016/j.talanta.2012.09.017>.

[22] Haron, M. J., Yunus, W. M. Z., Removal of fluoride ion from aqueous solution by a cerium-poly (hydroxamic acid) resin complex, *J. Environ. Sci. Health. A.* 36 (2001) 727-734. <https://doi.org/10.1081/ESE-100103756>.

[23] El-Hamshary, H., El-Newehy, M. H., Al-Deyab, S. S., Oxidation of phenol by hydrogen peroxide catalyzed by metal-containing poly (amidoxime) grafted starch, *Molecules* 16 (2011) 9900-9911. <https://doi.org/10.3390/molecules16129900>.

[24] Dragan, E.S., Apopei Loghin, D. F., Cocarta, A. I., Efficient Sorption of Cu<sup>2+</sup> by Composite Chelating Sorbents Based on Potato Starch-graft-Polyamidoxime Embedded in Chitosan Beads, *ACS Appl. Mater. Interfaces* 6 (19) (2014) 16577-16592. <https://doi.org/10.1021/am504480q>.

[25] Hazer, O., Kartal, S., Synthesis of a novel chelating resin for the separation and preconcentration of uranium (VI) and its spectrophotometric determination, *Anal. Sci.* 25 (2009) 547-551. <https://doi.org/10.2116/analsci.25.547>.

[26] Othman, M. K., Ph. D. Thesis, Preparation and Thermal Behavior Studies of Some New Polymers and Their Uses in Metal Complexes and Heavy Metal ions Removal from Aqueous Solutions, Zagazig University, Benha Branch, Faculty of Science, Chemistry Department, 2003.

[27] West, T. S., *Complexometry with EDTA and Related Reagents*, BDH Chemicals Ltd, 3rd ed., 1969.

[28] Peters, D. G., Hayes, J. M., Hieftje, G. M., *Chemical Separations and Measurements Theory and Practice of Analytical Chemistry*, Saunders Company, 3rd ed., 1974.

[29] El-Sayed, G. O., Dessouki, H. A., Ibrahiem, S. S., Removal of Zn(II), Cd(II) and Mn(II) from aqueous solutions by adsorption on maize stalks, *Malaysian Journal of Analytical Sciences (MJAS)* 15(1) (2011) 8-21.

[30] Silverstein, R. M., Bassler, G. C., Morrill, T. C., Spectroscopic Identification of Organic Compounds, John Wiley, New York, (1981).

[31] Bhatt, R. R., Shah, B. A., Shah, A. V., Uptake of heavy metal ions by chelating ion-exchange resin derived from p-hydroxybenzoic acid-formaldehydesorcinol: synthesis, characterization and sorption dynamics, The Malaysian Journal of Analytical Sciences (MJAS) 16 (2) (2012) 117-133.

[32] Naiya, T. K., Bhattacharya, A. K., Das, S. K., Adsorptive removal of Cd(II) ions from aqueous solutions by rice husk ash, Environ. Prog. Sustain. Energy 28 (4) (2009) 535–546. <https://doi.org/10.1002/ep.10346>.

[33] Cotton, F. A., Wilkinson, G., Advanced Inorganic Chemistry; A Comprehensive Text, John Wiley & Sons, New York, 3rd ed., 1972.

[34] Malakul, P., Srinivasan, K., Wang, Y. H., Metal Adsorption and Desorption Characteristics of Surfactant-Modified Clay Complexes, Ind. Eng. Chem. Res. 37(11) (1998) 4296-4301. <https://doi.org/10.1021/ie980057i>.

[35] Lezzi, A., Cobianco, S., Roggero, A., Synthesis of thiol chelating resins and their adsorption properties toward heavy metals ions, J. Polym. Sci., Part A 32 (10) (1994) 1877-1883. <https://doi.org/10.1002/pola.1994.080321008>.

[36] Coats, A. W., Redfern, J. P., Kinetic Parameters from Thermogravimetric Data, Nature 201 (1964) 68-69.

[37] Horowitz, H. H., Metzger, G., A New Analysis of Thermogravimetric Traces, Anal. Chem. 35 (10) (1963) 1464-1468. <https://doi.org/10.1021/ac60203a013>.

## Study of the stratification process at the reservoir of the hydroelectric power plant Gov. Pedro Viriato Parigot de Souza (Capivari-Cachoeira), Paraná, Brazil

Sarah Meier Lopes<sup>1+</sup>, Nicole Machuca Brassac de Arruda<sup>2</sup> , Thomaz Aurélio Pagioro<sup>1</sup> 

<sup>1</sup> Technological Federal University of Paraná, 3165 Sete de Setembro Av, Curitiba, Paraná, Brazil

<sup>2</sup> Institute of Technology for Development, Lactec, 8813 BR 116 Hwy, km 98, Curitiba, Paraná, Brazil

+ Corresponding author: Sarah Meier Lopes, e-mail address: [sah.mlopes@gmail.com](mailto:sah.mlopes@gmail.com)

### ARTICLE INFO

#### Article history:

Received: December 7, 2017

Accepted: June 10, 2018

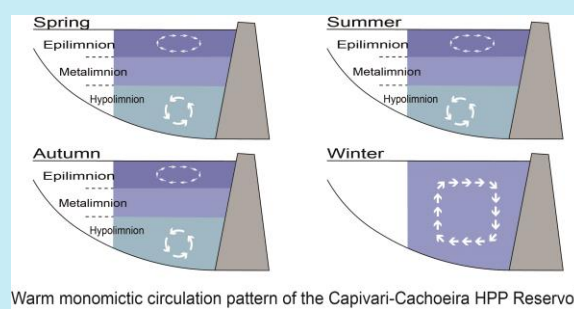
Published: August 23, 2018

#### Keywords:

1. densimetric Froude number
2. residence time
3. hydrology

**ABSTRACT:** The study of the stratification processes in reservoirs is important because they happen along with several physical and chemical changes in the water, as in the distribution of dissolved gases and nutrients. The aim of this work was to study the stratification process of the Capivari-Cachoeira Hydroelectric Power Plant reservoir, based on the data of the vertical profiles of dissolved oxygen and temperature, as well as the comparison of them with the calculation of Densimetric Froude Number, and reservoir residence time. The data used are part of the self-monitoring program carried out by COPEL. These data were collected quarterly between 2005 and 2016. The hydraulic and operational data from the reservoir were used to calculations.

According to the measurements of dissolved oxygen and temperature, the reservoir was considered to be stratified during almost all the year, with a trend of circulation in the colder months, this behavior characterizes lakes with warm monimictic circulation pattern. Therefore, the result of Densimetric Froude Number corresponded correctly with the observed. Regarding the residence time, this was not consistent with the results obtained from the models. The use of different methodologies in evaluating circulation in reservoirs should be used to make the best management decision.



Warm monimictic circulation pattern of the Capivari-Cachoeira HPP Reservoir

### 1. Introduction

The differences in temperature in lakes and reservoirs generate layers with different densities, forming a physical barrier that prevents circulation. This situation happens especially when the wind energy is not sufficient to mix the layers, therefore the heat is not evenly distributed through the water column, generating long lasting thermal stratification<sup>1-3</sup>.

Epilimnion is the upper, hotter and less dense layer of water, being very homogeneous by the action of wind and thermal heating that occurs during the day, and thermal cooling at night. Hypolimnion is the bottommost, dense, lower-

water layer. The layer of water between epilimnion and hypolimnion is the metalimnion. The thermocline is the layer in the metalimnion region that exhibits a temperature drop gradient of at least 1 °C<sup>2-4</sup>. The layers that are formed are often physically, chemically and biologically differentiated from each other<sup>1-6</sup>.

In most water bodies that have thermal stratification, there is also chemical stratification, in which oxygen and other dissolved compounds may, in general, have an inhomogeneous distribution in the water column<sup>1-3</sup>. Thermal stratification is considered the most important limnological characteristic in deep lakes and reservoirs, since it affects from the heterogeneity

and distribution of the chemical elements in the water column until the composition of its biological community<sup>1,2,4-6</sup>.

The study of the stratification processes in reservoirs is important because they occur together with several physical and chemical changes in the water body, such as, distribution of dissolved gases and nutrients in the water, accumulation of substances and chemical elements in the hypolimnion, as reducing substances and the consequent deoxygenation of hypolimnion. These changes may favor eutrophication events, due to the accumulation of internal charge<sup>2-5</sup>.

The study of Governador Pedro Viriato Parigot de Souza hydroelectric power plant (HPP) reservoir, located in Bocaiuva do Sul, in the state of Paraná, Brazil, is very relevant due to the fact that the reservoir is part of the future planning of sources for water supply in the metropolitan region of Curitiba, being important the knowledge of its dynamics of circulation, that directly reflects in its characteristics and quality of its waters<sup>7</sup>.

The Densimetric Froude Number is an indicator, calculated by an equation that tries to predict the possibility of a reservoir being stratified. The Densimetric Froude number equation is based on the comparison between the force of inertia of the flow through the reservoir and the gravitational force that tends to maintain the density stability as established by<sup>8,9</sup>.

This equation was used to evaluate the tendency of stratification in 30 reservoirs of small and medium-sized hydroelectric plants planned for the Taquari-Antas river basin<sup>5</sup>. The stratification processes were also studied in four reservoirs of the Iguaçu Basin by the evaluation of dissolved oxygen and temperature profiles, as well as the calculation of the Densimetric Froude number and the residence time<sup>7</sup>. This model was also used to determine the possibility of stratification and or circulation in the Santo Hipólito reservoir, in Minas Gerais<sup>10</sup>. The behavior of physical, chemical and biological stratification in the Rio das Pedras reservoir, located in São Bernardo do Campo, São Paulo, was studied<sup>4</sup>.

Other studies were also carried out in Brazil. The thermal behavior of the São Pedro reservoir used for water supply, located in the city of Juiz de Fora, Minas Gerais, was studied through mathematical modelling to evaluate the surface water temperature, based on meteorological and hydrological data<sup>11</sup>. The stratification of the water column of the Poxim reservoir was also studied

from the vertical profiles of temperature, conductivity, total dissolved solids, dissolved oxygen and pH<sup>12</sup>. A reservoir located in the Brazilian Pantanal was studied to understand the seasonal variations in the vertical structure of the water column and to quantify the importance of physical forces, radiation, wind and hydraulic retention time in the mixing processes in the water column<sup>6</sup>.

In this concept, the effect of thermal stratification on the water quality of the Tahtali reservoir, Turkey<sup>13</sup>, was also evaluated. Thermal stratification conditions of Heihe Reservoir, Shanxi Province, 2008-2010<sup>14</sup> were studied as well. In addition, studies that evaluate the influence of stratification on physical and chemical parameters in reservoirs, showed its influence on the microbial community. These researches were all performed in Chinese reservoirs<sup>15,16</sup>.

Chinese reservoirs Guanjingkou and Fengdou, that are still under construction, were previously studied using numerical methods with Delft3d software package in order to simulate the water temperature profile in the reservoirs, the water temperature released by the future spillways and the temperature effect of the water released<sup>17</sup>. The stratification of small temperate lakes of the Cárpados basin, in Turkey, and its biological consequences were also studied<sup>18</sup>. Three lakes in the United States of America were studied in order to investigate the response of water temperature and stratification in different morphometry (water depth and surface area) due to changes in temperature and wind speed<sup>3</sup>.

The objective of this study was to evaluate the Governador Pedro Viriato Parigot de Souza hydroelectric power plant reservoir, known as Capivari-Cachoeira, based on the stratification processes, from the data collected in the field from vertical profiles of dissolved oxygen and temperature, and comparing these results with the Densimetric Froude number and the reservoir's calculated water residence time.

## 2. Materials and methods

### 2.1 Study area and analyzed variables

The study area was the Capivari-Cachoeira HPP reservoir, in which the Capivari River was barred for the construction of the reservoir. The reservoir is located in the Ribeira basin, located in the cities of Bocaiuva do Sul, and Campina Grande do Sul,

in the state of Paraná, shown in Figure 1. From the reservoir, waters are transposed to the Litorânea basin, flowing into the Cachoeira River, through an underground adduction tunnel<sup>19</sup>. The analyzed data were collected quarterly between 2005 and 2016, at a sampling station located in the reservoir near the dam and the bottom dump, at the geographic coordinates 25°08'25.7 "S 48°52'19.0" W. In order to carry out a seasonal investigation, the samples were collected in the spring (September, October

and November), summer (December, January, February and March), autumn (April, May) and winter (June, July and August). These data belong to the program of self-monitoring of water quality of hydroelectric reservoirs, carried out by Paranaense Energy Company (COPEL) and developed by the Institute of Technology for Development (LACTEC Institutes).

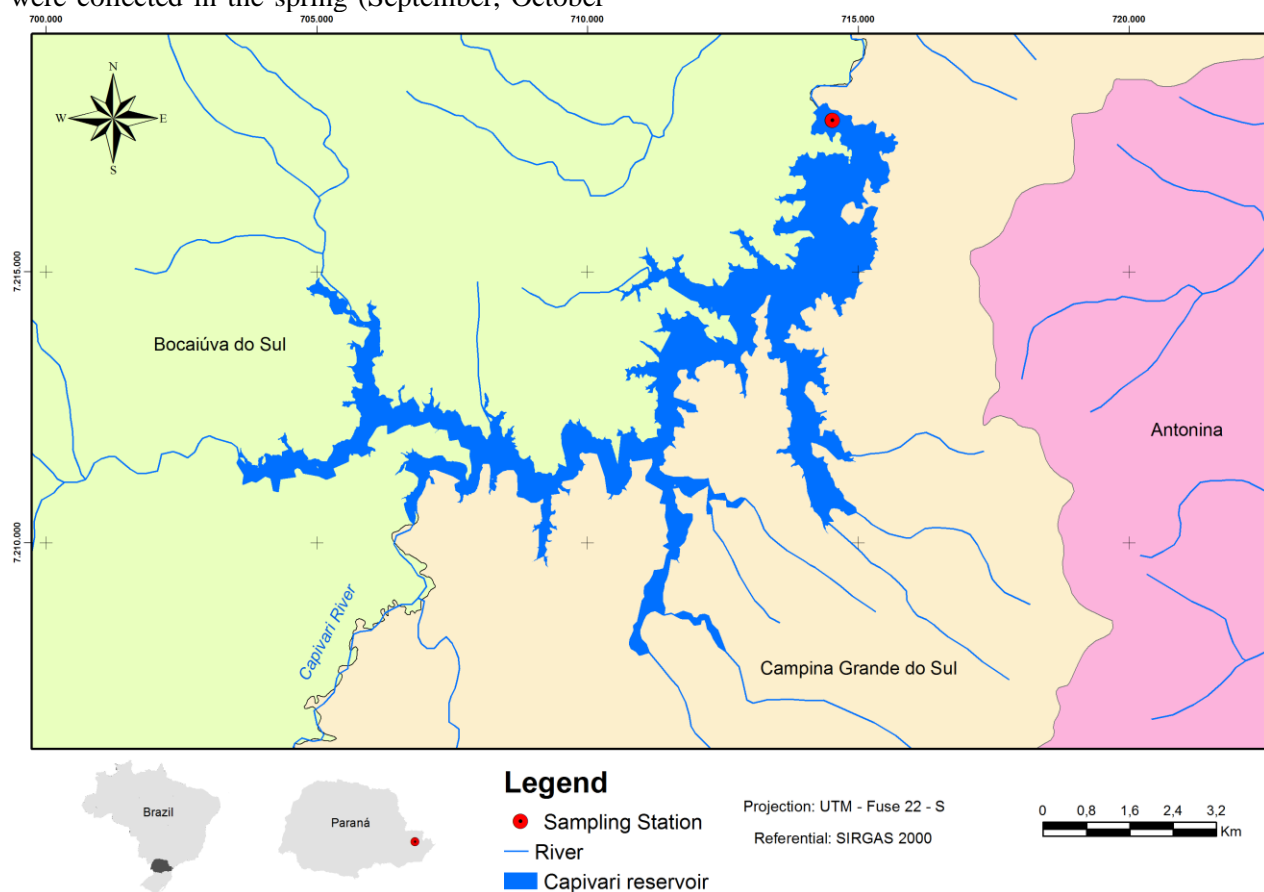


**Figure 1.** Capivari-Cachoeira HPP reservoir's location.  
**Source:** Adapted from ref. 23.

Since 2005, COPEL has been systematically monitoring the water quality of its hydroelectric power plants in Paraná, aiming to meet the environmental licensing conditioners. The LACTEC Institute manages this monitoring activity, conducting and managing laboratorial analysis and maintaining the water quality database of reservoirs and related rivers<sup>19, 20</sup>.

The studied variables were those related to the thermal structure and the distribution of dissolved oxygen in the water column. For this analysis vertical profiles were created, meter by meter, using data of temperature and dissolved oxygen.

Due to the accesses to the sampling station, changes in the coordinates of the collection site may have occurred during the monitoring. The measurements of dissolved oxygen and water temperature were performed in the field by a YSI PRO ODO multiparameter probe, which measures dissolved oxygen from 0-50 mg L<sup>-1</sup> (from 0 to 20 mg L<sup>-1</sup> ± 0.1 mg L<sup>-1</sup>), and temperature from -5 °C to 70 °C (± 0.2 °C)<sup>21</sup>. Through these results, the oxygen and temperature profiles were determined using the Microsoft Excel software<sup>22</sup>, for the analysis of thermal and chemical stratification in the studied reservoir.

Table 1 presents the hydraulic and operational data of the analyzed reservoir, from the power plant's original project<sup>23</sup>. These data were used to perform the calculation of the residence time and the Densimetric Froude number.

**Table 1.** Capivari-Cachoeira reservoir's hydraulic and operational data.

Characteristic	Capivari-Cachoeira HPP Reservoir
Altitud next to the damn (m)	837.50
Medium long term dischard ( $\text{m}^3 \text{s}^{-1}$ )	19.40
Volume ( $\text{hm}^3$ )	186.00
Flooded area ( $\text{km}^2$ )	13.20
Lenght (km)	21.25
Medium Depth (m)	13.60
Maximum Depth (m)	45.00

Source: [23]

## 2.2 Water Residence Time (RT)

The evaluation of the stratification tendency of a reservoir can be calculated using several indices and parameters. The residence time is one of the simplest, which classifies the reservoirs based on the mean water holding time, the average time a reservoir takes to renew its entire volume<sup>5,7,9</sup>. It is expressed by Equation 1:

$$RT = 11.57 \frac{V}{Q} \quad (1)$$

Where RT: residence time in days; V: reservoir volume in cubic hectometers ( $10^6 \text{ m}^3$ ); Q: average long period flow in cubic meters per second.

The classification adopted for the Capivari-Cachoeira reservoir was made considering the volume ratio of the reservoir / average flow affluent to it and the residence time<sup>8,9</sup>. The classification is the following: a) Reservoirs with  $RT > 1$  year: small seasonal variations are observed in the water volume and the outflow is withdrawn from the surface; b) Four months  $< RT < 1$  year: present stratification and great variation in water volume; and c) Reservoirs with  $RT < 4$  months: stratification is difficult to establish, and longitudinal temperature variation may occur. However, this equation should be used only as an

indicator of general conditions of the reservoir, because, for example, there are deep-water reservoirs with a short residence time<sup>9</sup>.

## 2.3 Densimetric Froude Number (Fd) calculation method

The Densimetric Froude number (Fd) is considered the best parameter to evaluate the thermal stratification trend of a reservoir because it brings together the main characteristics of stratification and morphometry. Its expression relates the forces of inertia responsible for mixing the reservoir water mass and the gravitational force, a consequence of the stratification (Equation 2)<sup>5-9</sup>:

$$Fd = 0.322 \frac{L \cdot Q}{H \cdot V} \quad (2)$$

Where Fd: Densimetric Froude Number; L: reservoir length (km); Q: flow ( $\text{m}^3 \text{ s}^{-1}$ ); H: mean depth (m); V: volume ( $10^6 \text{ m}^3$ ).

In this method, the tendency of stratification in a reservoir is classified as following: A) strong: Fd less than or equal to 0.1; b) medium: in which stratification occurs, but horizontal temperature gradients may also occur (Fd greater than 0.1 and less than 0.3); and c) weak: Fd greater than or equal to 0.3 and less than 1.0. Fd values greater than 1.0 indicate mixed regime and, therefore, no stratification<sup>5-9</sup>.

## 3. Results and discussion

The results of the calculation of the residence time and the Densimetric Froude number are presented in Table 2 and were compared with the dissolved oxygen and temperature profiles made by the collected data (between 2005 and 2016). In the Figure 2, as an example of the vertical profiles of the monitoring cycle of 2005-2006, is represented the stratification pattern identified in the reservoir.

**Table 2.** Densimetric Froude number and water residence time results.

Reservoir	RT (days)	Fd
Capivari-Cachoeira	110.90	0.052

Legend: RT: water residence time; Fd: Densimetric Froude number.

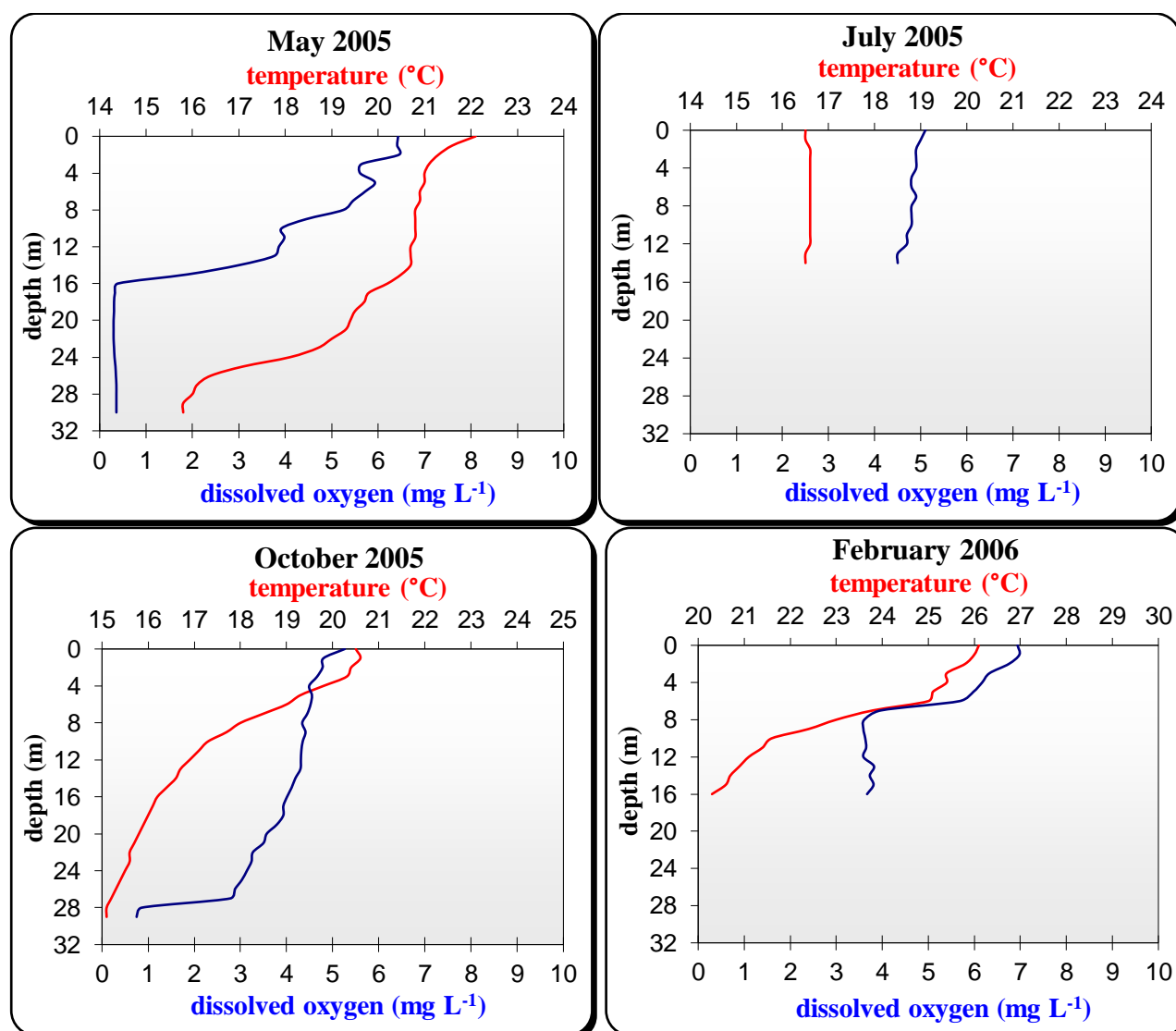


**Figure 2.** Dissolved oxygen and temperature profiles in Capivari-Cachoeira reservoir, examples from 2005 and 2006 data<sup>23</sup>.

The measurements of dissolved oxygen and temperature reflected the behavior of these variables in the vertical profile of the reservoir of the Capivari-Cachoeira HPP. In the evaluation of the temperature profiles it can be observed that the reservoir was stratified predominantly in the warmer months, with a significant drop in surface temperature towards the bottom. While in the months of lower temperatures, the thermal stratification was absent or not very pronounced, with a tendency to water circulation. The change in density of the water molecule varies as a function of temperature, however, this change is not uniform, and with the increase in water temperature, the differences in water density become higher<sup>1</sup>.

A pattern can be observed, in which thermal stratification occurs in most of the annual cycle and the de-stratification and mixing along the water column, once a year, around the month of July and August. This behavior characterizes lakes with warm monomictic circulation pattern. The stratification process in warm monomictic lakes occurs due to the thermal heating of the surface<sup>2</sup>. The warm monomictic circulation pattern was observed in different reservoirs in the state of Paraná, where circulation occurs once a year, predominantly in winter<sup>7, 24-25</sup>.

This stratification pattern was considered a tendency since it occurs in almost every monitored year, as observed in Figure 2. For example, the thermocline was superficial in October'05 and February'06, between 4 meters and 10 meters (m)

reflecting the depth of mixing of the water column on those months, that is, surface circulation, in the first 4 m. In May'05, the thermocline started at 16 m, and presented a second thermocline in 24 m, approximately, showing circulation of the upper layers and in June'05, no stratification occurred. Similar behavior was also observed in a reservoir in the Pantanal, Brazil. The Ponte de Pedra reservoir presented a long stratification period with complete mixing in winter. The vertical structure showed that during the stratification period, the upper layers of the reservoir are homogeneous and that the physical and chemical composition only changes at greater depths<sup>6</sup>.

Evaluating profiles from the years 2005 to 2016, in warmer months (Summer and Spring) it was recorded temperature drops from 3.5 °C to 10 °C, and the thermoclines started near the surface with a depth of around 2 meters to 15 meters, reflecting the depth of mixing of the water column in these months. To illustrate these stratification events, in the months of October'06 and January'07, temperature dropped of up to 5 °C in the first 15 m of the water column. In October'10, the surface temperature loss to the bottom was approximately 10 °C. In January'11, the difference between surface and bottom temperature was almost 6 °C.

In the summers and springs temperatures usually presented a great difference between the surface temperature and the background temperature. A similar situation was observed in three Paraná reservoirs, being the reservoir of the Jordão, Segredo and Foz do Areia, in which thermal stratifications were more pronounced in the months of higher temperatures<sup>7</sup>.

Corroborating these findings, a paper produced in the Rio das Pedras reservoir showed evidences of thermal stratification mainly due to temperature differences, followed by chemical and biological stratification<sup>4</sup>.

Deep reservoirs generally form thermal stratification due to uneven vertical heat distribution. Thermal stratification can hinder vertical water exchange, causing stratification of water quality<sup>7</sup>.

The evaluation of the vertical profile of dissolved oxygen in the Capivari-Cachoeira reservoir showed that it presents stratification during most of the annual period, following the thermal stratification pattern (Figure 2). Similar behavior was found in the reservoir of the HPP Segredo, HPP Salto Caxias, when its stratifications processes were studied<sup>7</sup>. Also, similarities between

the present results and other researches were also verified. In Poxim reservoir, in Sergipe, a decrease of the temperature along the water column was also identified, usually accompanied by a decrease of dissolved oxygen, with more stratification occurring in periods with higher temperatures<sup>12</sup>. The vertical distribution of dissolved oxygen in lakes in the Tisza valley demonstrated a chemical stratification characteristic in summer<sup>18</sup>.

Comparing the results found in other studies, there were also significant differences in the physical and chemical parameters, as well as differences in the microbiological parameters between epilimnion and hypolimnion<sup>15</sup>. Results that indicated that the stratification of the reservoir had great effects on the temperature and oxygen profiles, and both the functional diversity and the composition of the bacterial community strongly reflected the significant vertical stratification were also found in the reservoir studied<sup>16</sup>.

As for the distribution of dissolved oxygen in the Capivari-Cachoeira reservoir: events of hypolimnetic hypoxia, when there are marked deficits of dissolved oxygen in the bottom layer, were recorded in several sampling events. In May'05 and October'05, hypolimnetic hypoxia was observed, with concentrations below 1.0 mg L<sup>-1</sup>, from 15 m in the first case and below 25 m in the second (Figure 2). Also, in October'07 and February'08, oxyline was recorded between 2 m and 3 m depth, with hypoxia from 25 m and also from 12 m, respectively. Hypoxia in the bottom region can stimulate eutrophication processes by internal loading, since it makes phosphorus retention difficult in sediments, making it available for the assimilation of living beings<sup>2-5</sup>.

Events of anoxia were also observed in the Capivari-Cachoeira reservoir, as in April'07, when oxyline was recorded in 6 m, with a decrease of 5.5 mg L<sup>-1</sup> in the concentration of dissolved oxygen towards the bottom and observation of anoxia from 9 m deep. In October'14, anoxia occurred from 10 m depth with dissolved oxygen values below 0.7 mg L<sup>-1</sup> and January'15, from 8 m, dissolved oxygen values were observed below 0.3 mg L<sup>-1</sup>.

During the studied period, in summer the stratification was evident, and the observed concentrations of dissolved oxygen fell well below the standard limit in the thermocline, leading to the development of anoxia<sup>13</sup>.

Lakes of tropical regions have their dissolved oxygen profiles influenced mainly by the morphometry of the lake and by high temperatures,

once the influence of the winds act in the distribution of dissolved oxygen in the water body. Thus, it is common for these lakes to present a strong oxygen deficiency in the water column, especially in the lower bottom<sup>1</sup>.

The results of the calculation of the residence time, 110.9 days (Table 2), considering the classification of WRE (1969)<sup>8,9</sup>, suggests that the Capivari reservoir has little possibility of stratification, due to the great relation flow rate/volume. Thus, because the Capivari-Cachoeira reservoir has a small residence time<sup>9</sup>, less than 4 months, it is suggested that stratification is difficult to be established.

However, according to the result of the Densimetric Froude number, which was equal to 0.052, (Table 2), the Capivari reservoir presents a tendency to strong stratification<sup>5-9</sup>, because for the stratification to be developed, low flow velocities are necessary associated with morphology of the reservoir<sup>3</sup>.

According to the measurements of dissolved oxygen and temperature carried out in the Capivari-Cachoeira HPP reservoir during the studied period, the reservoir was considered to be stratified during most of the year, with a circulation trend in the coldest months, especially in the winter, therefore, the result of the Densimetric Froude number, suggesting tendency to strong stratification, corresponded correctly with the observed. In relation to the residence time, its classification was not consistent with the results obtained in the field and with the calculation of Froude number, because according to the result (110.9 days), and the classification proposed<sup>8,9</sup>, it would be difficult for the reservoir to stratify.

The calculation of residence time does not take into account some important features such as depth, thus allowing a general view of the reservoir. The Densimetric Froude number represents the environment with greater accomplishment, since it considers more factors<sup>9</sup>. Thus, several factors must be taken into account in the studies of the stratification and mixing processes of water columns<sup>9</sup>. For example, it has already been identified that larger surface area lakes have a greater mix do to the wind. And larger lakes tend to have more variability in temperature and stratification than smaller lakes, and this variability increases with higher wind speeds<sup>3</sup>.

In another study, in small temperate lakes of the Carpathian basin, it was concluded that depending on their depth and wind shelter, the lakes could be

characterized by various stratification patterns<sup>18</sup>. In the São Pedro reservoir, Juíz de Fora, because it is a small and shallow reservoir, the temperatures are more limited to the flows of the tributaries, characterizing, therefore, a low capacity of this reservoir to regularize its temperatures<sup>11</sup>.

#### 4. Conclusions

The thermal and dissolved oxygen stratification pattern observed in the Capivari-Cachoeira HPP reservoir is of a warm monomictic lake, in which stratification occurs almost throughout the year, with a higher intensity in summers and tendency to circulate, de-stratification, in the winter. Hypoxia and even anoxia events have been recurrent in the reservoir, in the hipolimnion, and it is also characteristic of warm monomictic environments within periods of reduced circulation.

The calculated Densimetric Froude number corresponded correctly with the stratification trend observed in the monitoring of the oxygen and temperature profiles for the Capivari-Cachoeira reservoir.

On the other hand, the classification adopted for residence time as indicative of the trend of stratification was not consistent with the values obtained in the profiles of temperature and dissolved oxygen and in the calculation of the Densimetric Froude number. In this sense, the use of different methodologies and approaches in evaluating circulation patterns in reservoirs should, whenever possible, be used to make the best management decision.

#### 5. Acknowledgments

The authors would like to thank COPEL (Paranaense Energy Company) for the permission to use the water quality monitoring data used in this study.

The authors also would like to thank CNPq and CAPES for their financial support and LACTEC and UTFPR for logistical support.

#### 6. References

- [1] Esteves, F. A., Fundamentos de Limnologia, Rio de Janeiro: Interciência, 3rd ed., 2011, ch9.
- [2] Tundisi, J. G., Tundisi, T. M., Limnologia. São Paulo: Oficina de Textos, 1rd ed., 2008, ch4.

- [3] Magee, M. R., Wu, C. H., Response of water temperatures and stratification to changing climate in three lakes with different morphometry, *Hydrol. Earth Syst. Sci.* 21 (2017) 6253-6274. <https://doi.org/10.5194/hess-21-6253-2017>.
- [4] Padial, P.R., Pompêo, M., Moschini-Carlos, V., Heterogeneidade espacial e temporal da qualidade da água do reservatório Rio das Pedras (Complexo Billings, São Paulo), *Revista Ambiente & Água*, 4 (3) (2009) 35-53. <https://doi.org/10.4136/ambi-água.101>.
- [5] Benetti, A. D., Tucci, C. E. M., Uso de indicadores para avaliação de usinas hidrelétricas em bacias hidrográficas com múltiplos aproveitamentos, *Revista de gestão de água da América Latina* 3 (1) (2006) 73-83.
- [6] Cruz, I. F., Pedrollo, O., Bonecker, C. C., Zeilhofer, E., Key factor in vertical mixing processes in a reservoir bordering the Pantanal floodplain, Brazil, *Hydrological Sciences Journal* 60 (9) (2015) 1508-1519. <https://doi.org/10.1080/02626667.2014.933224>.
- [7] Miranda, T. L. G., Brassac, N. M., Prestes, E. C., Muller, I. I., Pereira, S., Estudo dos processos de estratificação em grandes reservatórios da Bacia do Rio Iguaçu. In: *Simpósio Brasileiro de Recursos Hídricos 18* (2009), Campo Grande, Anais... Campo Grande – MS: ABRH (2009) 1-12.
- [8] WRE, 1969, *Mathematical Model for Prediction of Thermal Energy Changes in Inpoundments* US EPA 16130.
- [9] Tucci, C. E. M., *Modelos Hidrológicos*. Porto Alegre: ABRH, ed. UFRGS, 1998, ch11.
- [10] Von Sperling, E., Estudo sobre influência na qualidade da água decorrente da implantação da barragem de Santo Hipólito, Rio Das Velhas-MG, Belo Horizonte: Comitê da bacia hidrográfica do Rio das Velhas (2009) 1-28.
- [11] Souza, F. F. C., Ribeiro, C. B. M., Fragoso Junior, C. R., Otenio, M. H., Modelagem do regime térmico de um reservatório tropical de abastecimento público, Juiz de Fora, MG, Brasil, *Rev. Ambient. Água* 11 (1) (2016) 60-74. <https://doi.org/10.4136/ambi-água.1544>.
- [12] Neves, A. M., Fonseca, L. C., Macedo, L. C. B., Alves, J. P. H. A., Estratificação da coluna d'água do reservatório do rio Poxim, São Cristóvão – Sergipe. In: *Simpósio de Recursos Hídricos do Nordeste 8* (2016) Aracajú, Anais... Aracajú-SE:ABRH (2016) 1-9.
- [13] Elçi, Ş., Effects of thermal stratification and mixing on reservoir water quality, *Limnology*, (9) (2008)135–142. <https://doi.org/10.1007/s10201-008-0240-x>.
- [14] Lu, J., Li, Z., Seasonal effects of thermal stratification on the water quality of deep reservoirs: A case study of Heihe Reservoir, Xi'an City, *J. Lake Science* 26 (5) (2014) 698-706. <https://doi.org/10.18307/2014.0507>.
- [15] Yu, Z., Yang, J., Amalfitano, S., Yu, X., Liu, L., Effects of water stratification and mixing on microbial community structure in a subtropical deep reservoir, *Scientific Reports* 25 (4) (2014) 5821. <https://doi.org/10.1038/srep05821>.
- [16] Xiao, Y., Huang, T., Zhang, H., Effects of Seasonal Thermal Stratification on the Functional Diversity and Composition of the Microbial Community in a Drinking Water Reservoir, *Water* 7 (10) (2015) 5525-5546. <https://doi.org/10.3390/w7105525>.
- [17] Jang, J. Y., Zhou, L. Y., Simulation of water temperature in two reservoirs with Delft3d, *International Conference on Water Resource and Environment 2016. Series: Earth and Environmental Science* 39 (2016) 7. <https://iopscience.iop.org/1755-1315/39/1/012073>.
- [18] Borics, G., Abonyi, A., Várbíró, A., Padisák, J., Krasznai, T. E., Lake stratification in the Carpathian basin and its interesting biological consequences, *Inland Waters* 5 (2015) 173-186. <https://doi.org/10.5268/IW-5.2.702>.
- [19] Copel. Usina Parigot de Souza. (2016). Available in: <<http://www.copel.com/hpcopel/root/nivel2.jsp?endereco=%2Fhpcopel%2Froot%2Fpagcopel2.nsf%2F044b34faa7cc1143032570bd0059aa29%2F>>

08013ddc621f4eed03257412005ed73>. Accessed in: 01 ago. 2017.

[20] Arruda, N. M. B., Rizzi, N. E., Miranda, T. L. G., Análise multivariada na avaliação da qualidade de água do reservatório de Foz do Areia, estado do Paraná, *Revista Brasileira de Ciências Ambientais* 37 (2015) 26-37. <https://doi.org/10.5327/Z2176-947820159514>.

[21] YSI. ProODO Optical Dissolved Oxygen Instrument. (2018). Available in: <<https://www.ysi.com/proODO>>. Accessed in: 28 mar. 2018.

[22] Microsoft. Microsoft Office Excel 2013. [S.I.]: Microsoft Inc, (2013).

[23] Lactec – Instituto de Tecnologia para o Desenvolvimento, Relatório Anual do Automonitoramento da Qualidade das Águas Superficiais do Rio Capivari, na região da Usina Governador Pedro Viriato Parigot De Souza (UHE Capivari-Cachoeira), Curitiba: Lactec (2016) 41.

[24] Ferreira, D. M., Cunha, C., Simulação numérica do comportamento térmico do reservatório do Rio Verde, *Eng Sanit Ambient* 18 (1) (2013) 83-93. <https://doi.org/10.1590/S1413-41522013000100010>.

[25] Colombo, G. T., Mannich, M., Estudo da estratificação térmica do reservatório Vossoroca por meio de índices físicos, In: *Simpósio Brasileiro de Recursos Hídricos*, 22 (2017), Florianópolis, Anais... Florianópolis – SC: ABRH (2017) 1-8.

## Incorporation of $\text{CdFe}_2\text{O}_4\text{-SiO}_2$ nanoparticles in $\text{SbPO}_4\text{-ZnO-PbO}$ glasses by melt-quenching process

Juliane Resges Orives<sup>1</sup>, Wesley R. Viali<sup>1</sup>, Marina Magnani<sup>1</sup>, Marcelo Nalin<sup>1</sup>

<sup>1</sup>São Paulo State University (Unesp), Institute of Chemistry, 55 Prof. Francisco Degni St, Araraquara, São Paulo, Brazil

\* Corresponding author: Juliane Resges Orives, e-mail address: [juliane\\_resges@hotmail.com](mailto:juliane_resges@hotmail.com)

### ARTICLE INFO

#### Article history:

Received: March 20, 2018

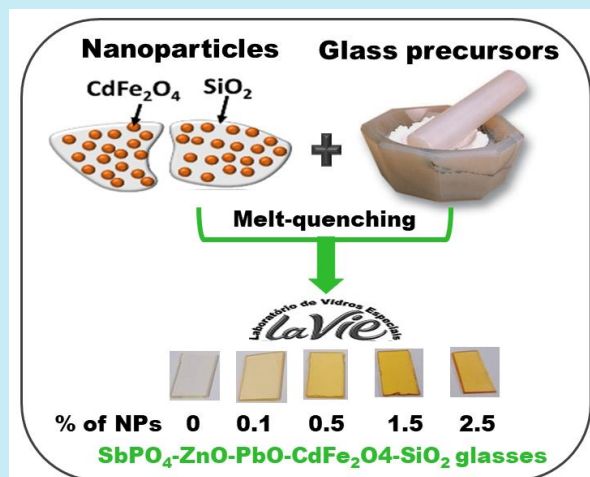
Accepted: August 14, 2018

Published: August 23, 2018

#### Keywords:

1. antimony based glass
2. cadmium ferrite nanoparticles
3. optical properties
4. structural properties

**ABSTRACT:** The development of glasses containing nanoparticles dispersed homogeneously with controlled size and optimum parameters for functionality is a big challenge. In the present work, the ternary system  $60\text{SbPO}_4\text{-}30\text{ZnO-}10\text{PbO}$  containing  $\text{CdFe}_2\text{O}_4\text{-SiO}_2$  nanoparticles was studied.  $\text{CdFe}_2\text{O}_4$  nanoparticles, with average size of 3.9 nm, were synthesized using the coprecipitation method and, in a second step, protected by a silica layer. Different mass percentages of nanoparticles were mixed to the glass precursors and then transformed into glasses by melt-quenching method. Thermal and structural properties were evaluated by differential scanning calorimetry, Raman spectroscopy, scanning electronic microscopy and transmission electron microscopy. While the optical properties were studied by M-Lines spectroscopy and UV-Vis spectroscopy. The glasses obtained were completely transparent, with yellow color and showed no sign of crystallization according to the techniques used. Scanning and transmission electron microscopy confirm that the methodology used for the incorporation of nanoparticles was efficient. The methodology used to protect the nanoparticles prior to incorporate them to glasses, strongly contributes towards the development of new functional glasses useful for magneto-optics devices.



### 1. Introduction

Antimony phosphate glasses containing heavy metal oxides<sup>1, 2</sup> have been studied due to their interesting characteristics like high linear and non-linear refractive indexes<sup>3, 4</sup>, large transmission window<sup>5</sup>, low phonon energy<sup>6, 7</sup>, which make them promising materials for several technological applications in photonics<sup>8-10</sup> and plasmonics<sup>11, 12</sup>.

Another emerging field is related to nanophotonic technologies by incorporating metal, semiconductor or magnetic nanoparticles into such dielectric materials and further to study using

femtosecond lasers, in order to understand the fundamental properties of the interaction of light with this new kind of materials<sup>13-18</sup>.

How it is a very new field it should be noted that several fundamental aspects must be considered, as for example, what size range of nanoparticles can lead to satisfactory results, what is the amount of nanoparticles supported without crystallizes and what is the influence of the glass matrix nature on the properties of the nanoparticles.

In the case of glasses containing magnetic nanoparticles, the functionality of magneto-optical devices and magnetic sensors can be greatly

improved, but the development of magnetic glasses with nanoparticles dispersed satisfactorily remains a major challenge<sup>19, 20</sup>.

For this reason, finding high refractive index matrices that are good hosts for magnetic nanoparticles is important. Despite intensive efforts to study antimony-based glasses, to our knowledge, there is no studies in the literature dedicated to the incorporation of magnetic nanoparticles in these glasses.

The melt-quenching process for the incorporation of nanoparticles has been reported in the literature<sup>20-24</sup>, by mixing the glass precursors and nanoparticles powders before melting the material. As the melting process occurs at high temperatures, it is interesting to protect the nanoparticles to ensure that they do not dissolve after the process.

Cadmium ferrite nanoparticles ( $\text{CdFe}_2\text{O}_4$ ) have been studied due to excellent chemical stability and applicability in magneto-optical devices and semiconductor sensors<sup>25-28</sup>. These nanoparticles can be further functionalized by adding layers of silica, which can act as a protective layer of the nanoparticles during the melting<sup>29-31</sup>.

In this context, the proposal of this work was to incorporate cadmium ferrite nanoparticles, synthesized by co-precipitation and coated with silica ( $\text{CdFe}_2\text{O}_4\text{-SiO}_2$ ) into the glass composition  $60\text{SbPO}_4\text{-}30\text{ZnO}\text{-}10\text{PbO}$  using the melt-quenching technique. A structural, thermal and optical investigations were performed in the glasses containing the nanoparticles by means of, transmission electron microscopy (TEM), scanning electronic microscopy (SEM), atomic force microscopy (AFM), Raman spectroscopy, differential scanning calorimeter (DSC), M-Lines spectroscopy and UV-Vis spectroscopy.

## 2. Experimental

### 2.1 Synthesis of cadmium ferrite nanoparticles protected by a silica layer (CdSiNPs)

The  $\text{CdFe}_2\text{O}_4$  nanoparticles were synthesized by the coprecipitation method, using equal volumes (62.5 mL) of a  $0.005 \text{ mol L}^{-1}$  solution of cadmium nitrate tetrahydrate (Sigma-Aldrich 99%) and  $0.01 \text{ mol L}^{-1}$  solution of iron nitrate nonahydrate (Sigma-Aldrich 99%). Then, under stirring, 125 mL of a  $1 \text{ mol L}^{-1}$  solution of sodium

hydroxide (P.A. Synth) was added slowly. The system was kept under a  $\text{N}_2$  atmosphere at a controlled heating rate of  $10 \text{ }^\circ\text{C min}^{-1}$  up to  $100 \text{ }^\circ\text{C}$  and was maintained at this temperature for 2 h to complete the reaction. The nanoparticles were washed and then dispersed using ultrasound in 250 mL of ethanol 99%. Subsequently, 3.6 mL of tetraethylorthosilicate (TEOS) (Sigma-Aldrich) and 1.3 mL of 25% ammonium hydroxide solution (P.A Synth) were added in the dispersion of the nanoparticles. The system remained under mechanical stirring for 24 h under  $\text{N}_2$  atmosphere. Then, a heat treatment at  $600 \text{ }^\circ\text{C}$ , at room atmosphere, for 5 h was performed to eliminate any organic residue.

### 2.2 $\text{SbPO}_4\text{-PbO-ZnO}$ glasses (SPZ) containing CdSiNPs

Glass samples were prepared by melt-quenching process. The precursors used in the glass preparation for the  $60\text{SbPO}_4\text{-}30\text{PbO}\text{-}10\text{ZnO}$  system were  $\text{SbPO}_4$  (prepared as reported previously by Nalin *et al.*<sup>32</sup>),  $\text{PbO}$  and  $\text{ZnO}$  (grade purity 99%). A sample without nanoparticles (SPZ) and four samples containing 0.1, 0.5, 1.0 and 2.5% in mass of CdSiNPs (SPZ-0.1CdSiNPs, SPZ-0.5CdSiNPs, SPZ-1.0CdSiNPs and SPZ-2.5CdSiNPs) were prepared. The glass composition was weighed (sufficient to prepare 25 g of glass) and subsequently homogenized using an agate mortar. The powder mixture was transferred to a Pt-Au crucible and melted in a furnace at  $1100 \text{ }^\circ\text{C}$  for 30 min. Later, the melt was poured into a brass mold and crushed. The mother glass was separated into 5 portions of 5 g each one and then, the different percentages of nanoparticles (0, 0.1, 0.5, 1.5, 2.5) were mixed. The melting process was repeated for the 5 samples at  $1100 \text{ }^\circ\text{C}$  for 7 min and poured in a brass mold heated at  $340 \text{ }^\circ\text{C}$  and left at such temperature for 2 h for annealing. This procedure is used to eliminate the internal residual stresses of the glass, resulted from the rapid cooling of the liquid and aims to increase the mechanical resistance. The finishing of the samples was obtained by polishing the glasses with SiC sandpaper with different grades. Figure 1a illustrates the silica modification of cadmium ferrite nanoparticles and Figures 1b and c the preparation of glasses by melt-quenching process.

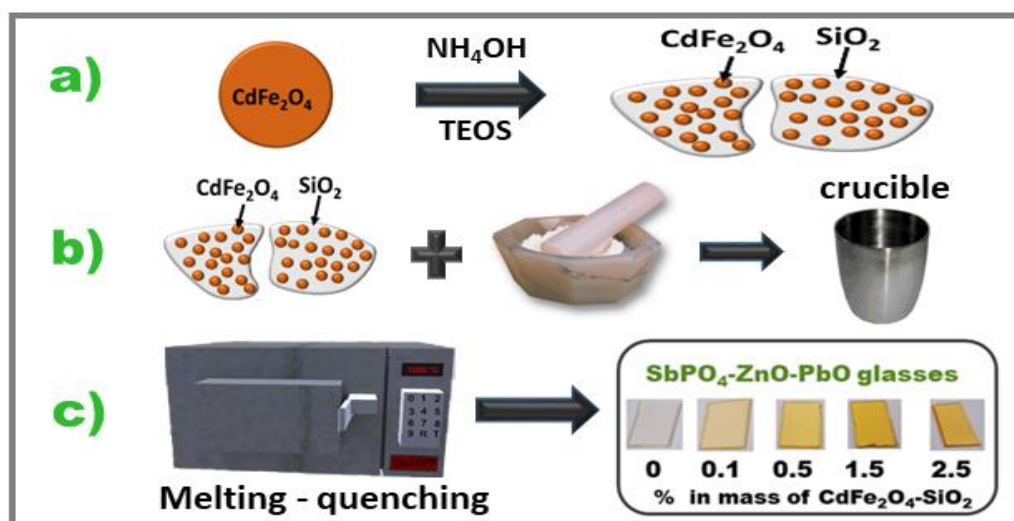


**Figure 1.** Illustration of: a) silica modification of  $\text{CdFe}_2\text{O}_4$ , b) mixture of nanoparticles and glass precursors and c) preparation of glasses containing nanoparticles.

### 2.3 Nanoparticles and glasses characterization

X-ray powder diffraction were carried out for the  $\text{CdSiNPs}$  with a Bruker D8 Advance diffractometer operating with a Ni filtered  $\text{CuK}\alpha$  radiation source at  $2\theta$  angle ranging from 10 to  $80^\circ$  with a step pass of  $0.02^\circ$  and a step time of 2 s. Transmission electron microscopy TEM were carried out using a Philips CM200 equipment operating at 200 kV and equipped with X-ray energy dispersive spectroscopy (EDS) Bruker model XFlash 6TI30. Samples were prepared using 0.1 mg of  $\text{CdSiNPs}$  or SPZ samples containing  $\text{CdSiNPs}$ . After grounding, the powder was dispersed in 1 mL of isopropyl alcohol using ultrasound. Some drops of this suspension were applied on a copper grid coated with carbon film. Reflectance spectrum for the  $\text{CdSiNPs}$  and transmission spectra (in the spectral range from 200 to 800 nm) for the SPZ- $\text{CdSiNPs}$  glasses were recorded using a Varian Cary 5000 UV-Vis-Near infrared (NIR) spectrophotometer from the polished samples with 2 mm in thickness. Scanning electron microscopy images were obtained in a high-resolution Scanning Electron Microscope (SEM-FEG HR) – FEI Inspect F50 equipped with Energy Dispersive X-ray Spectroscopy (EDS) Probe (Inca Energy-Oxford) in the bulk sample covered with carbon film and in the powder dispersed in isopropyl alcohol by dripping the suspension onto a silicon substrate. Topography images of  $\text{SbPO}_4\text{-PbO-ZnO}$  glasses (SPZ) containing  $\text{CdSiNPs}$  were obtained using a Park NX-10 Atomic Force Microscope. PPP-MFM

probes (NanoWorld) with spring constant of 2.8 N/m and resonance frequency within 75 kHz were used for measurements. Topography were acquired in air by single pass scanning at room temperature and humidity between 74.5 and 75.5%. Topography was measured using the intermittent contact mode setup, slightly below the frequency of resonance. Analysis and processing of the AFM images were carried out with Gwyddion<sup>33</sup>. Raman scattering spectra were recorded at room temperature in a frequency range from 200 to  $1150\text{ cm}^{-1}$  in a HORIBA Jobin Yvon model LabRAM HR micro Raman apparatus equipped with a 632.8 nm laser, delivering 17 mW. Differential scanning calorimetry (DSC) measurements were carried out using the DSC Q600 equipment from TA Instruments to study the thermal properties of glasses. Small pieces of glasses, with typically 15 mg, were heated in aluminum crucible from 150 to  $600^\circ\text{C}$  at a heating rate of  $10^\circ\text{C}\cdot\text{min}^{-1}$ , in  $\text{N}_2$  atmosphere ( $70\text{ mL min}^{-1}$ ). The estimated errors are  $\pm 2^\circ\text{C}$  for  $T_g$  and  $T_x$ . The refractive index of the samples was measured at 632.8 nm using a Metricon model 2010 equipment. The estimated error is  $\pm 0.0001$ .

## 3. Results and discussion

### 3.1 $\text{CdFe}_2\text{O}_4$ and $\text{CdSiNPs}$

The X-ray diffraction pattern of the synthesized powder is consistent with a cubic phase of spinel structure (space group:  $\text{Fd-3m}$ ) (Figure 2). The major peak located at  $34.4^\circ$  corresponds to the

(311) plane which can be readily ascribed to the characteristic peaks of the spinel ferrites. Except for the low intensity diffraction peak at  $42.5^\circ$  assigned to the  $\text{Fe}_3\text{O}_4$  plane (400) according to the standard (JCPDS 19-0629) the remaining diffraction peaks match well with standard (JCPDF 22-1063). The broadening of diffraction peaks indicates the nanocrystalline nature of the synthesized powder<sup>34</sup>.

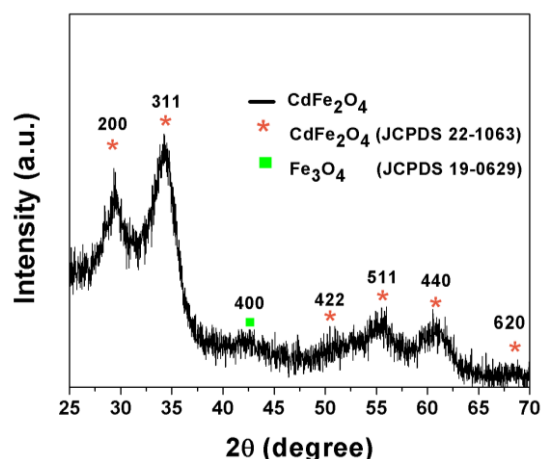


Figure 2. XRD pattern of  $\text{CdFe}_2\text{O}_4$ .

A TEM image, obtained for the  $\text{CdSiNPs}$ , is shown in Figure 3. The upper inset displays the histogram obtained from several TEM images, with size distribution of  $3.9 \pm 0.1$  nm. Moreover, is observed that the nanoparticles present a spherical-like morphology. Plocek *et al.*, prepared nanoparticles of  $\text{CdFe}_2\text{O}_4@SiO_2$ , via sol gel methodology, with average size of 3.4 nm, and the TEM profile obtained is very similar to those obtained in this work<sup>29</sup>.

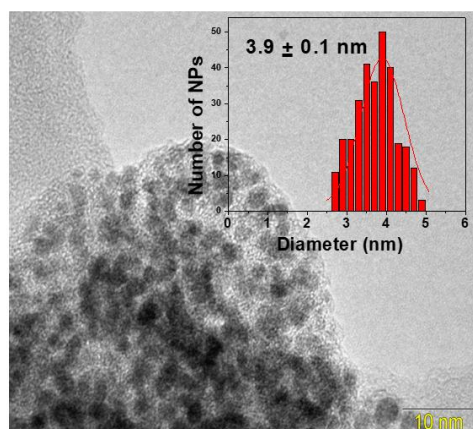


Figure 3. TEM and histogram with the size distribution of  $\text{CdSiNPs}$ .

The nanoparticles were synthesized by coprecipitation method and was used a surfactant-free synthesis in order to avoid remaining organic compounds, that can induce bubbles during the synthesis of the glass and react with the Pt-Au crucible during the melting process. After coating the  $\text{CdSiNPs}$  with silica, the nanoparticles were heated at  $600^\circ\text{C}$  for 5 h. For this reason, the nanoparticles are not isolate and monodisperses, but rather in the form of silica agglomerates.

Figure 4a shows the diffuse reflectance spectrum for the  $\text{CdSiNPs}$ . This technique allows to obtain the band gap energy of the material. The Kubelka-Munk remission function is the most used for interpreting diffuse reflectance data. The absorption coefficient close to the edge of the absorption band is a function of the frequency according to Equation 1:

$$(ah\nu)^{\frac{1}{n}} = K' \cdot h\nu - K' \cdot E_{bg} \quad (1)$$

In which  $K'$  is the absorption constant that depends on the properties of the material and  $h\nu$  is the photon energy of the incident radiation; the exponent  $n$  can have values of 1/2, 2, 3/2 and 3 corresponding to direct transition, indirect transition, prohibited direct transition and prohibited indirect transition, respectively<sup>35</sup>.

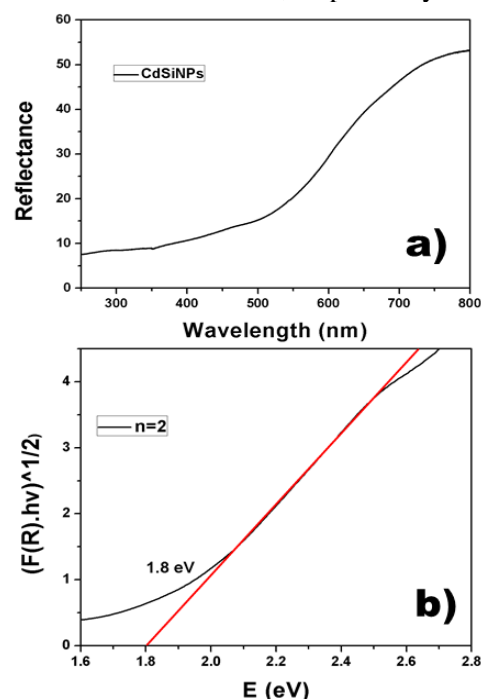


Figure 4. a) Diffuse Reflectance Spectra of  $\text{CdSiNPs}$ , b)  $(F(R).h\nu)^{1/2}$  as a function of the photon energy.

The absorption coefficient ( $a$ ) is related to the reflectance ( $R$ ) measured by means of Equation 2:

$$a = F(R) \quad (2)$$

where  $F(R)$  is the Kubelka-Munk function which has the form expressed in Equation 3:

$$F(R) = (1 - R)^2 / 2R \quad (3)$$

If  $F(R) \cdot h\nu^{\frac{1}{n}}$  is plotted as a function of the energy of the incident photon and the straight-line portion is extrapolated to  $F(R) \cdot h\nu^{\frac{1}{n}} = 0$ , with  $n = \frac{1}{2}$  or 2, the band gap energy can be estimated.

In Figure 4b is shown the graph of  $F(R) \cdot h\nu^{\frac{1}{n}}$  as a function of photon energy ( $E$ ) for  $n=2$ , which provided lower deviation in the linear regression, the indirect band gap obtained was 1.8 eV. Miao *et al.*<sup>36</sup> calculated an indirect gap for a thin film of  $\text{CdFe}_2\text{O}_4$  of 1.97 eV and Shi *et al.*<sup>37</sup> also obtained a band gap of 1.97 eV for nanoparticles of  $\text{CdFe}_2\text{O}_4$  with 24 nm of diameter. Naseri<sup>28</sup> obtained in his work a band gap of 2.06 eV for nanoparticles with a size of 47 nm treated at 673 °C. Based on these results, and due to the reduced size of the nanoparticles the band gap value obtained is in agreement with the literature.

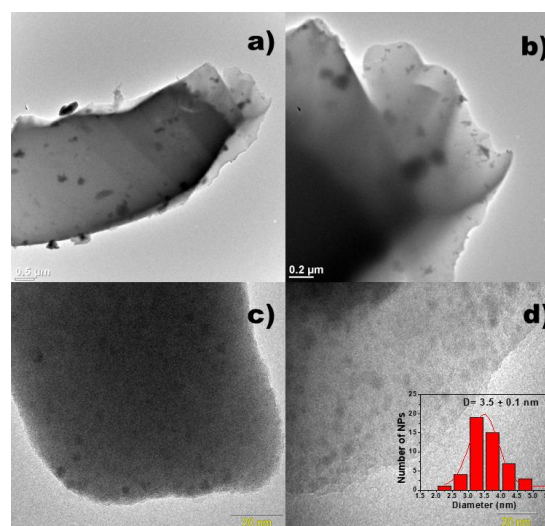
### 3.2 SPZ glasses containing CdSiNPs

Figure 1c showed the profile of the matrix and vitreous samples containing nanoparticles obtained. The matrix color is light yellow and when the nanoparticles were incorporated to the samples, they became darker with intensification of the tonality with increasing the percentage of CdSiNPs. The color is characteristic of the presence of iron ions in the glasses<sup>38</sup>. The obtained samples are totally transparent and visually homogeneous. For compositions containing concentrations higher than 3.0% of nanoparticles the total crystallization of the samples occurred, indicating that the limit of nanoparticles supported by the SPZ matrix is between 2.5 and 3.0% in mass of CdSiNPs.

By means of the TEM image of the sample SPZ-2.5CdSiNPs it is seen in Figures 5a and 5b that the sample presents regions with different contrast from the glass without nanoparticles. When these regions were analyzed closely, the presence of the CdSiNPs were confirmed, showing that the

incorporation occurred satisfactorily, although it did not occur homogeneously in the nanoscale.

The Figures 5c and 5d were obtained in two different regions in which the nanoparticles present average diameter of 3.5 nm (histogram inserted in Figure 5d, obtained from images 5c and 5d), showing that silica coating was efficient to protect nanoparticles during melting at high temperatures. The smaller size with respect to the nanoparticles prior to incorporation can be explained by the low count number of nanoparticles in the glass, and also due to a possible dissolution of the silica layer at the edges of the agglomerates, consequently causing the dissolution of part of the nanoparticles. In this way, iron ions were dispersed into the matrix and explains the dark yellow color.



**Figure 5.** TEM images of SPZ-2.5CdSiNPs sample in different regions: a) b) c) and d). The insert in d) shows the histogram made from TEM images for the sample including images c) and d).

The morphology of the  $\text{SbPO}_4\text{-PbO-ZnO}$  glasses (SPZ) containing 2.5% CdSiNPs were studied by SEM and AFM microscopy, Figure 6 and Figure 7, respectively. Figure 6a and 6b displayed silica agglomerates containing  $\text{CdFe}_2\text{O}_4$  nanoparticles with different formats in the glass surface. Figure 6c shows the energy dispersive spectra (EDS) of the general area of Figure 6b. The Cd, Fe, Si peaks were clearly visible in EDS showing the presence of NPs within the glass. The Figure 6d shows the image of a suspension obtained from the sample deposited on a silicon substrate. Agglomerates are observed with different sizes and forms concentrated in certain regions of the sample, and these results are in agreement with the images obtained by TEM.

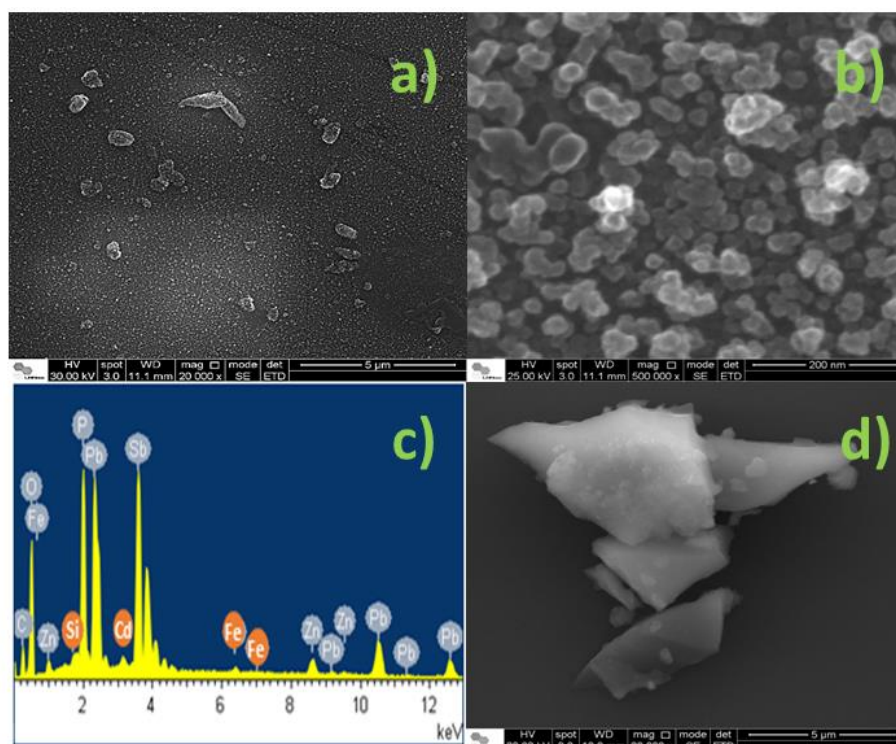


**Figure 6.** SEM-HR images of SPZ-2.5CdSiNPs sample covered with carbon film a) 20.000x; b) 500.000x, c) EDX spectra of the general area of image (b) and d) SEM-HR image for SPZ-2.5CdSiNPs suspension deposited on silicon substrate (20.000x).

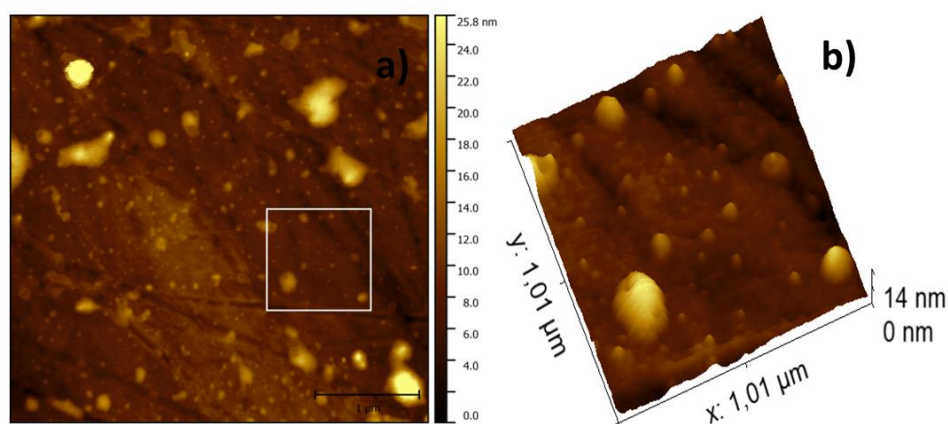


**Figure 7.** AFM topography images of  $4 \times 4 \mu\text{m}^2$  (a) 3D surface topography associated with the region ( $1 \times 1 \mu\text{m}^2$ ) square draw on (a).

Figure 7 shows AFM images corresponding to the  $\text{SbPO}_4\text{-PbO-ZnO}$  glasses (SPZ) containing 2.5% CdSiNPs. The topography of the SPZ-2.5.0CdSiNPs sample and 3D AFM image clearly reveals the presence of different sizes of agglomerates containing the nanoparticles (30 nm until  $0.3 \mu\text{m}$ ) uniformly disperses on glass, corroborating with TEM and SEM images. We assign the presence of the silica agglomerates to the low melting time (7 min), which was not enough to

dissolve all the silica in the sample, protecting the nanoparticles.

### 3.3 Thermal analysis

Figure 8 shows the DSC curves for the matrix and for the samples containing nanoparticles in different percentage in mass. It is observed that the profile of the curves is the same for all samples. The values found for characteristic temperatures of

glass transition ( $T_g$ ), onset of crystallization ( $T_x$ ) and maximum crystallization ( $T_p$ ) of each sample are resumed in Table 1. The addition of nanoparticles leads to a small increase in the value of  $T_g$  and  $T_x$ , attributed to the increase in the degree of structural rigidity due to the incorporation of the silica in the matrix. The parameter  $T_x - T_g$ , referring to the thermal stability of the glass, remains constant, showing that the addition of the nanoparticles to the glass did not destabilizes the composition. This behavior is important for applications when glass pieces with different sizes (for example, 10 x 10 cm) are required.

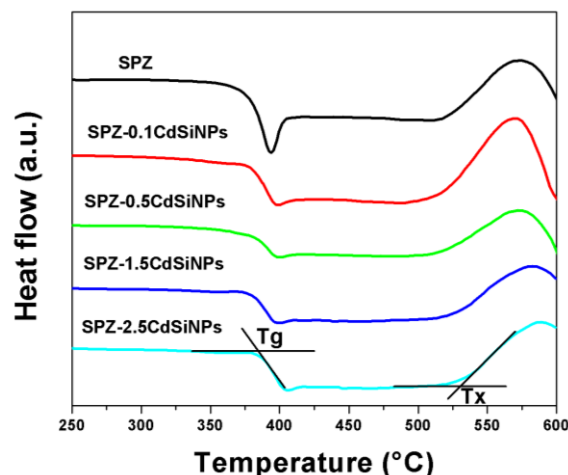


Figure 8. DSC curves of the SPZ and SPZ-CdSiNPs glasses.

Table 1. Characteristic temperatures of the SPZ-CdSiNPs glasses.

Samples	$T_g$ (°C)	$T_x$ (°C)	$T_p$ (°C)	$T_x - T_g$ (°C)
SPZ	375	515	573	140
SPZ-0.1CdSiNPs	379	519	571	140
SPZ-0.5CdSiNPs	380	518	574	138
SPZ-1.5CdSiNPs	381	523	582	142
SPZ-2.5CdSiNPs	385	530	588	145

### 3.4 Raman Spectroscopy

The prepared samples were analyzed by Raman spectroscopy (Figure 9). Due to the higher proportion of  $SbPO_4$  in the glasses studied, the curves predominantly present bands characteristic of the phosphate groups, and can be attributed as published by Nalin *et al.*<sup>4</sup>

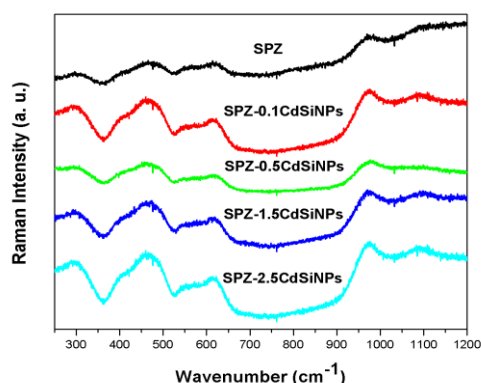


Figure 9. Raman spectra of the SPZ and SPZ-CdSiNPs glasses.

The band at  $300\text{ cm}^{-1}$  is assigned to group modes.<sup>1</sup> The bands at  $461$  and  $404\text{ cm}^{-1}$  are assigned to symmetrical deformation of the  $PO_4$  and the asymmetric deformation of  $Sb-O$ , respectively. While the bands at  $617$  and  $551\text{ cm}^{-1}$  are assigned to the asymmetrical stretches of vibrational modes  $P-O-Sb$  and asymmetrical stretching  $Sb-O$ . Finally, the bands at  $1100$  and  $972\text{ cm}^{-1}$  can be assigned to asymmetrical stretches of the  $PO_4$  and symmetrical stretching of  $PO_4$ , respectively.

Assignments for samples containing CdSiNPs are shown in Table 2. The positions of the bands remain constant and no evidence that the addition of the nanoparticles is modifying the structure of the glass was found.

**Table 2.** Assignments of the bands observed in the Raman spectrum for the glasses studied.

Samples	Raman/cm <sup>-1</sup>						
	G.M.*	$\delta_{as}$ Sb-O	$\delta_s$ PO <sub>4</sub>	$\nu_{as}$ Sb-O	$\nu_{as}$ P-O-Sb	$\nu_s$ PO <sub>4</sub>	$\nu_{as}$ PO <sub>4</sub>
SPZ	300	404	461	546	617	972	1100
SPZ-0.1CdSiNPs	298	404	465	547	617	973	1097
SPZ-0.5CdSiNPs	299	405	467	547	619	972	1098
SPZ-1.5CdSiNPs	300	405	465	547	617	973	1198
SPZ-2.5CdSiNPs	298	405	467	549	619	972	1198

G.M.: Group Modes

### 3.5 Optical measurements

The refractive index values for glasses were obtained using the prism coupling technique, M-lines spectroscopy and the values can be observed in the Table 3.

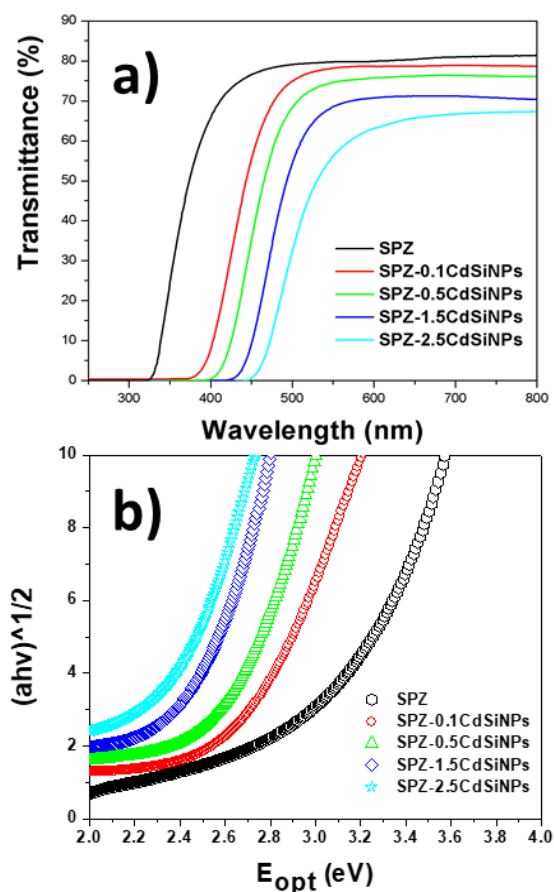
The increase in nanoparticle concentration slightly reduced the refractive index, which can be attributed to the contribution of silica and the substitution of PbO and SbPO<sub>4</sub> in the matrix, which have much higher polarizabilities, leading to a decrease in refractive index values. While Siqueira<sup>39</sup> found to the same vitreous matrix a behavior of increase of refractive index with increase of the concentration of Fe<sub>2</sub>O<sub>3</sub>, which was attributed to the ability of iron ions to polarize neighboring atoms.

**Table 3.** Refractive Indexes obtained for the SPZ and SPZ-CdSiNPs glasses.

Samples	Refractive Index
SPZ	1.887
SPZ-0.1CdSiNPs	1.886
SPZ-0.5CdSiNPs	1.885
SPZ-1.5CdSiNPs	1.883
SPZ-2.5CdSiNPs	1.880

Spectroscopy in the UV-Vis region was used to obtain transmission spectra of the matrix and samples containing CdSiNPs. Figure 10 shows that it occurs a red shift of the absorption edge with the increase in the percentage in mass of CdSiNPs. The decrease of the transmittance is due to light scattering from scratches on the surface of the glasses and also due to the scattering coming from the presence of agglomerates. Higher is the

percentage of nanoparticles, higher is the agglomerates and, as consequence, lower is the transmission of the glasses.

**Figure 10.** a) Transmittance spectra obtained for the SbPO<sub>4</sub>-PbO-ZnO containing CdSiNPs and b)  $(ah\nu)^{1/2}$  as function of the energy of the photon ( $E$ ).

The absorption limit in the visible region is called band gap energy and involves optical transitions between the valence and conduction

bands. Its value can be obtained from the transmission spectra using the PARAV software in which the transmission spectra of the glasses is inserted and also the values of the refractive indexes and thicknesses of the glasses are supplied to the software, which then generates the graph of  $(ah\nu)^{1/2}$  versus  $E^{40}$ .

As already mentioned above, the absorption coefficient is a function of the frequency, so plotting a graph of  $(ah\nu)^{1/2}$  as a function of the energy of the photon ( $E$ ), is possible to obtain the band gap energy values of the glasses (Figure 10b).

The Figure 11 shows the values of the optical band gap ( $E_{opt}$ ) of the glasses (which were determined from a tangent drawn in the intercession of the curve  $(ah\nu)^{1/2}$  versus  $E$ ). Band gap energies decrease with increasing percentage in mass of CdSiNPs and it can be attributed to the fact that the nanoparticles and iron ions introduce new energy levels between the valence band and the conduction band of the matrix, showing that  $E_{opt}$  of the SPZ glass is strongly sensitive to the presence of CdSiNPs.

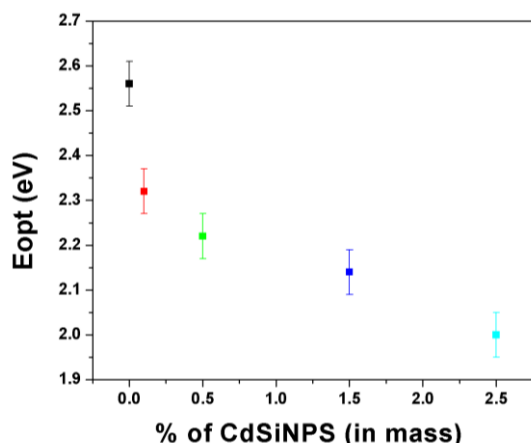


**Figure 11.** Optical band gap energy values obtained for the SPZ and SPZs containing CdSiNPs.

The results obtained in this work are important from the fundamental point of view because demonstrate the possibility to use glass as a medium to disperse nanoparticles without dissolves them. Glasses containing nanoparticles are interesting system for several applications in photonics, however the nanoparticles usually are growth from the vitreous phase by means of a controlled heat treatment. The main drawback of such method is linked to the fact that most of glasses crystallize heterogeneously leading to non-homogeneous optical properties.

The innovation in this paper is related to the fact that we proved that nanoparticles with controlled sizes can be dispersed into glass matrix. Such results open the possibility to explore new functionalities for such materials in the field of photonics and magneto-photonics. It is important to remember the reader that conventional glasses, like those used for optical fibers, are not suitable to changes in the electromagnetic fields close to them, however, using this new hybrid glasses the magnetic properties of the nanoparticles may play a very interesting role on the manipulation of the light by means of changes in the magnetic field. Applications such as, sensors may be idealized using such new materials. These possibilities are currently under investigation in our laboratory.

#### 4. Conclusion

In this work, the  $60\text{SbPO}_4\text{-}30\text{ZnO-}10\text{PbO}$  glass system was used as host for incorporation of CdSiNPs using melt-quenching process. We have shown that the method of protection of the nanoparticles with a silica layer is efficient and the incorporation in the vitreous matrix occurred satisfactorily, as presented in TEM and SEM images, although it is still necessary to improve the quality of the silica coating in order to obtain monodisperse nanoparticles and more homogeneous glasses. The DSC analysis showed that the matrix acquired greater thermal stability while Raman spectroscopy did not present evidence that the presence of the CdSiNPs modified the glass structure. This is interesting because nanocrystals were added in an amorphous matrix without causing crystallization of the sample. The presence of the nanoparticles induced a decrease in the refractive index and  $E_{opt}$  of the glass, showing that the CdSiNPs have influence on the optical properties of the material. The results obtained in this work may contribute towards the development of glasses containing nanoparticles useful for magneto-optics devices. In addition, it is important to emphasize that this methodology can be used for other types of nanoparticles such as bimetallic nanoparticles or nanoparticles with plasmonic properties, for example, thus expanding the range of possibilities of studies in the area of nanoparticles containing glasses.

## 5. Acknowledgements

The authors are grateful to the Brazilian funding agencies CNPq (grant number 141258/2014-4) and São Paulo Research Foundation FAPESP (grant number #2013/07793-6). We would like to thank LME and LCS -LNNano/CNPEM, which provides the equipments for SEM and AFM measurements.

## 6. References

- [1] Manzan, R. S., Donoso, J. P., Magon, C. J., Silva, I. d'A. A., Rüsseld, C., Nalin, M. Optical and Structural Studies of Mn<sup>2+</sup> Doped SbPO<sub>4</sub>-ZnO-PbO Glasses, *J. Braz. Chem. Soc.* 26 (12) (2015), 2607-2614. <https://doi.org/10.5935/0103-5053.20150289>.
- [2] Franco, D. F., Hssen Fares, H., Souza, A. E., Santagneli, S. H., Nalin, M., Glass formation and the structural study of the Sb<sub>2</sub>O<sub>3</sub>-SbPO<sub>4</sub>-WO<sub>3</sub> system, *Eclét. Quim. J.* 42 (1) (2017) 51-59. <https://doi.org/10.26850/1678-4618eqj.v42.1.2017.p51-59>.
- [3] Falcão Filho, E. L., Bosco, C.A.C., Maciel, G. S., Araujo, C. B., Nalin, M., Messaddeq, Y., Ultrafast nonlinearity of antimony polyphosphate glasses, *Appl. Phys. Lett.* 83 (2003) 1292-1294. <https://doi.org/10.1063/1.1601679>.
- [4] Volpi, V., Montesso, M., Ribeiro, S. J. L., Viali, W. R., Magon, C. J., Silva, I. D. A., Donoso, J. P., Nalin, M., Optical and structural properties of Mn<sup>2+</sup> doped PbGeO<sub>3</sub>-SbPO<sub>4</sub> glasses and glass-ceramics, *J. Non-Cryst. Sol.* 431(2016) 135-139. <https://doi.org/10.1039/C8DT00560E>.
- [5] Moustafa, S.Y., Sahar, M.R., Ghoshal, S.K., Comprehensive thermal and structural characterization of antimony-phosphate glass, *Results phys.* 7 (2017) 1396-1411. <https://doi.org/10.1016/j.rinp.2017.04.006>.
- [6] Miller, P. J., Cody, C. A., Infrared and Raman investigation of vitreous antimony trioxide, *Spectrochim. Acta A-M.* 38 (5) (1982) 555-559. [https://doi.org/10.1016/0584-8539\(82\)80146-3](https://doi.org/10.1016/0584-8539(82)80146-3).
- [7] Nalin, M., Poirier, G., Messaddeq, Y., Ribeiro, S. J. L., Carvalho, E. J., Cescato, L., Characterization of the reversible photoinduced optical changes in Sb-based glasses, *J. Non-Cryst. Sol.* 352 (2006) 3535-3539. <https://doi.org/10.1016/j.jnoncrsol.2006.03.087>.
- [8] Manzani, D., Montesso, M., Mathias, C. F., Krishanaiah, K. V., Ribeiro, S. J. L., Nalin, M., Visible up-conversion and near-infrared luminescence of Er<sup>3+</sup>/Yb<sup>3+</sup> co-doped SbPO<sub>4</sub> GeO<sub>2</sub> glasses, *Opt. Mater.* 57 (2016) 71-78. <https://doi.org/10.1016/j.optmat.2016.04.019>.
- [9] Ouannes, K., Lebbou, K., Walsh, B. M., Poulain, M., Alombert-Gotet, G., Guyot, Y., Antimony oxide based glasses, novel laser materials, *Opt. Mater.* 65 (2017) 8-14. <https://doi.org/10.1016/j.optmat.2016.11.017>.
- [10] Rao, V. H., Prasad, P. S., Rao, P. V., Santos, L. F., Veeraiah, N., Influence of Sb<sub>2</sub>O<sub>3</sub> on tellurite based glasses for photonic applications, *J. Alloys Compd.* 687 (2016) 898-905. <https://doi.org/10.1016/j.jallcom.2016.06.256>.
- [11] Shasmal, N., Karmakar, B., Tuneable and Au-enhanced yellow emission in Dy<sup>3+</sup>/Au co-doped antimony oxide glass nanocomposites, *J. Non-Cryst. Solids.* 463 (2017) 40-49. <https://doi.org/10.1016/j.jnoncrsol.2017.02.019>.
- [12] Franco, D. F., Sant'Ana, A. C., Oliveira L. F. C., Silva, M. A. P., The Sb<sub>2</sub>O<sub>3</sub> redox route to obtain copper nanoparticles in glasses with plasmonic properties, *J. Mater. Chem. C.* 3 (2015) 3803-3808. <https://doi.org/10.1039/C5TC00102A>.
- [13] Prasad, P.N. *Nanophotonics*, Wiley, New Jersey, 2004.
- [14] Gonella, F., Mazzoldi, P. *Handbook of nanostructured materials and nanotechnology*, Academic Press, San Diego v. 4, 2000, ch2.
- [15] Sharma, S., Singh, S., Prajapat, C.L., Bhattacharya, S., Preparation and study of magnetic properties of silico phosphate glass and glass-ceramics having iron and zinc oxide, *J. Mag. Mat.* 321(22) (2009) 3821-3828. <https://doi.org/10.1016/j.jmmm.2009.07.047>.
- [16] Bigot, J.-Y., Mircea, V., Beaurepaire, E., Coherent ultrafast magnetism induced by femtosecond laser pulses, *Nature Phys.* 5 (2009) 515-520. <https://doi.org/10.1038/nphys1285>.
- [17] Boeglin, C., Beaurepaire, E., Halté, V., López-Flores, V., Stamm, C., Pontius, N., Dürr, H. A., Bigot, J.-Y. Distinguishing the ultrafast dynamics of spin and orbital moments in solids, *Nature.* 465 (2010) 458-461. <https://doi.org/10.1038/nature09070>.

- [18] Nakashima, S., Sugioka, K., Tanaka, k., Midorikawa, k., Mukai, k., Optical and magneto-optical properties in Fe-doped glasses irradiated with femtosecond laser, *Appl. Phys. B.* 113 (3) (2013) 451- 456. <https://doi.org/10.1007/s00340-013-5489-z>.
- [19] Kim, K.D., Kim, S.S., Choa, Y.H., Kim, H.T., Formation and surface modification of Fe<sub>3</sub>O<sub>4</sub> nanoparticles by co-precipitation and sol-gel method, *J. Ind. Eng. Chem.* 7 (2007) 1137-1141.
- [20] Widanarto, W., Sahar, M.R., Ghoshal, S.K., Arifin, R., Rohani, M.S., Effendi, M., Thermal, structural and magnetic properties of zinc-tellurite glasses containing natural ferrite oxide, *Mat. Lett.* 108 (2013) 289–292. <https://doi.org/10.1016/j.matlet.2013.06.109>.
- [21] Anigrahawati, P., Sahar, M. R., Ghoshal, S. K., Influence of Fe<sub>3</sub>O<sub>4</sub> nanoparticles on structural, optical and magnetic properties of erbium doped zinc phosphate glass, *Mater. Chem. Phys.* 155 (2015) 155-161. <https://doi.org/10.1016/j.matchemphys.2015.02.014>.
- [22] Widanarto, W., Sahar, M. R., Ghoshal, S. K., Arifin, R., Rohani, M.S., Hamzah, K., Effect of natural Fe<sub>3</sub>O<sub>4</sub> nanoparticles on structural and optical properties of Er<sup>3+</sup> doped tellurite glass, *J. Mag. Mat.* 326 (2013) 123-128. <https://doi.org/10.1016/j.jmmm.2012.08.042>.
- [23] Farag, H. K., Marzouk, M. A., Preparation and characterization of nanostructured nickel oxide and its influence on the optical properties of sodium zinc borate glasses *J. Mater. Sci: Mater. Electron.* 28 (2017) 15480–15487. <https://doi.org/10.1007/s10854-017-7435-z>.
- [24] Chen, Q. Wan, L. Chen, Zhang, Q. M., Effect of Magnetite Nanoparticles Doped Glass with Enhanced Verdet Constant for Magnetic Optical Current Transducer Applications, *Adv. Mater. Res.* 270 (2011) 13-18. <https://doi.org/10.4028/www.scientific.net/AMR.271-273.13>.
- [25] Lou, X., Liu, S., Shi, D., Chu, M., Ethanol-sensing characteristics of CdFe<sub>2</sub>O<sub>4</sub> sensor prepared by sol–gel method, *Mater. Chem. Phys.* 105 (2007) 67-70. <https://doi.org/10.1016/j.matchemphys.2007.04.038>.
- [26] Bakuzis, A. F., Skeff, N. K., Gravina, P. P., Figueiredo, L. C., Morais, P. C., Magneto-optical properties of a highly transparent cadmium ferrite-based magnetic fluid, *Appl. Phys. Lett.* 84 (2004) 2355- 2357. <https://doi.org/10.1063/1.1690497>.
- [27] Kaur, H., Singh, J., Randhawa, B. S., Essence of superparamagnetism in cadmium ferrite induced by various organic fuels via novel solution combustion method, *Ceram. Int.* 40 (2014) 12235-12243. <https://doi.org/10.1016/j.ceramint.2014.04.067>.
- [28] Naseri, M. Optical and magnetic properties of monophasic cadmium ferrite (CdFe<sub>2</sub>O<sub>4</sub>) nanostructure prepared by thermal treatment method, *J. Magn. Magn. Mater.* 392 (2015) 107-113. <https://doi.org/10.1016/j.jmmm.2015.05.026>.
- [29] Plocek, J., Hutlová, A., Niznanský, A., D., Bursík, J., Rehspringer, J.-L. Micka, Z. Preparation of ZnFe<sub>2</sub>O<sub>4</sub>/SiO<sub>2</sub> and CdFe<sub>2</sub>O<sub>4</sub>/SiO<sub>2</sub> nanocomposites by sol–gel method, *J. Non-Cryst. Sol.* 315 (2003) 70-76. [https://doi.org/10.1016/S0022-3093\(02\)01595-8](https://doi.org/10.1016/S0022-3093(02)01595-8).
- [30] Dippong, T., Cadar, O., Levei, E. A., Bibicu, I., Diamandescu, L., Leostean, C., Lazar, M., Borodi, G., Tudoran, L. B., Structure and magnetic properties of CoFe<sub>2</sub>O<sub>4</sub>/SiO<sub>2</sub> nanocomposites obtained by sol-gel and post annealing pathways, *Ceram. Int.* (2017) 2113-2122. <https://doi.org/10.1016/j.ceramint.2016.10.192>.
- [31] Silva, J. B., Characterization of Porous Nanocomposites Formed by Cobalt Ferrites Dispersed in Sol-Gel Silica Matrix, *J. Sol-Gel Sci. Technol.* 35 (2015) 115–122. <https://doi.org/10.1007/s10971-005-1378-1>.
- [32] Nalin, M., Poulain, M., Poulain, Mi., Ribeiro, S. J. L., Messaddeq, Y., Antimony oxide based glasses, *J. Non-Cryst. Sol.* 284 (2011) 110-116. [https://doi.org/10.1016/S00223093\(01\)00388-X](https://doi.org/10.1016/S00223093(01)00388-X).
- [33] Nečas, D., Klapetek, P., Gwyddion: an open-source software for SPM data analysis, *Open Physics*, 10 (1) (2011) 2391-5471. <https://doi.org/10.2478/s11534-011-0096-2>.
- [34] Cullity, B. D., Stock, S. R., *Elements of X Ray Diffraction*, Prentice Hall, Upper Saddle River, New Jersey, 3<sup>rd</sup> ed., 2001.

[35] Tauc, J. Amorphous and Liquid Semiconductor. Plenum Publishing Company Ltd; New York, 1974.

[36] Miao, F., Deng, Z., LV, X., Gu, G., Wan, S., Fang, X., Zhang, Q., Yin, S., Fundamental properties of CdFe<sub>2</sub>O<sub>4</sub> semiconductor thin film, Solid State Commun. 150 (2010) 2036–2039. <https://doi.org/10.1016/j.ssc.2010.08.010>.

[37] Shi, W., Liu, X., Zhang, Wang, Q., Zhang, L. Magnetic nano-sized cadmium ferrite as na efficient catalyst for the degradation of Congo red in the presence of microwave irradiation. RSC adv. 5 (2015) 51027-51034. <https://doi.org/10.1039/C5RA07591B>.

[38] Navarro, J. M. F., El Vidrio, CSIC Press, Madrid, Spain, 3<sup>rd</sup> ed., 2003.

[39] Siqueira, F. R. Preparação de vidros e vitrocerâmicas contendo metais de transição. Dissertação (Mestrado em Química) – Instituto de Química, Universidade Federal de São Carlos, São Carlos. 2014.

[40] Ganjoo, A., Gollovchak, R., Computer program PARAV for calculating optical constants of thin films and bulk materials: Case study of amorphous semiconductors, J. of Optoe. and adv. Mat. 10 (2008) 1328-1332.

## Ecotoxicity of Malathion® 500 CE before and after UVC radiation and UV/H<sub>2</sub>O<sub>2</sub> treatment

Eliane Adams<sup>1</sup>, Vinicius de Carvalho Soares de Paula<sup>1</sup>, Rhaissa Dayane Carneiro<sup>1</sup>, Rubia Matos de Lima<sup>1</sup>, Monike Felipe Gomes<sup>1</sup>, Wanessa Algarte Ramsdorf<sup>1</sup>, Adriane Martins de Freitas<sup>1+</sup>

<sup>1</sup> Technological Federal University of Paraná (UTFPR), 5000 Deputado Heitor de Alencar Furtado St., Curitiba, Brazil

+ Corresponding author: Adriane Martins de Freitas, e-mail address: [adrianefreitas@utfpr.edu.br](mailto:adrianefreitas@utfpr.edu.br)

### ARTICLE INFO

#### Article history:

**Received:** May 4, 2018

**Accepted:** July 31, 2018

**Published:** August 23, 2018

#### Keywords:

1. advanced oxidative processes
2. photolysis
3. *Lactuca sativa*
4. *Aedes aegypti*

**ABSTRACT:** Since 2008, Brazil has been the largest consumer of agrochemicals in the world, using pesticides to combat pests and vectors, impacting both microbiota and human health. Aiming at the degradation of the contaminants present in the environment, treatments by advanced oxidative processes are based on the synthesis of free radicals that allow the degradation of the pollutant. Among these processes are included UV/H<sub>2</sub>O<sub>2</sub>. By evaluating the ecotoxicity and phytotoxicity of the commercial Malathion® 500 CE product, using *Aedes aegypti* larvae and *Lactuca sativa* seed, the high toxicity of this formulation was observed. EC<sub>50</sub> values for *A. aegypti* being equal to 0.4 µg L<sup>-1</sup> and for *L. sativa* equal to 550 µg L<sup>-1</sup>. The commercial agrochemical degradation was carried out by UVC radiation and UV/H<sub>2</sub>O<sub>2</sub>, and the toxicity was evaluated after 30 and 120 min. After both treatments, the percentage of immobility was zero for *A. aegypti*, inferring the efficiency of the processes. However, for *L. sativa*, no treatment was able to remove or reduce initial toxicity.



EC<sub>50</sub> values of the pesticide Malathion® 500 CE for *Aedes aegypti* and *Lactuca sativa* were calculated by means of ecotoxicological tests, being 0.40 µg L<sup>-1</sup> and 550 µg L<sup>-1</sup>, respectively. Photolysis and UV/H<sub>2</sub>O<sub>2</sub> degradation evidence the treatment efficiency and removal of toxicity.

### 1. Introduction

Recently, epidemics of dengue, chikungunya, yellow fever and zika caused by the vector *Aedes aegypti* affected a large part of the Brazilian population. From this, government campaigns and control measures were adopted, providing large quantities of malathion insecticide to the environment<sup>1-3</sup>. Malathion is an organophosphate type C widely used in rural and urban areas to control of aphids, flies. It is formulated as household sprays and being sprayed in areas with high proliferation rate of *Aedes aegypti*<sup>2, 4</sup>. It presents the advantage of not being persistent in the environment and does not bioaccumulate.

However, it presents high toxicity in animals due to its action mechanism, which inhibits the enzyme acetylcholinesterase, forming a complex with the esterase center of the enzyme. This results in accumulation of the neurotransmitter acetylcholine, interrupting the breakage of this substance in choline and acetic acid, causing several symptoms, such as nervous hyperactivity<sup>5-9</sup>.

Aiming at the degradation of this pesticide as an alternative to make it less available in the environment, it is possible resort to simple and effective treatments, which includes advanced oxidative processes (AOPs). These processes are based on the generation of highly reactive and

oxidizing species such as hydroxyl radicals, it can be obtained in various forms, including heterogeneous and homogeneous systems, with or without radiation. The main objective is to generate at the end of the process species less toxic such as water and carbon dioxide<sup>10-12</sup>. Recent works have shown the efficiency of AOPs, as photo-Fenton process<sup>13</sup>, UVC/H<sub>2</sub>O<sub>2</sub><sup>14</sup> and others<sup>15</sup>, in the degradation of malathion in aqueous solutions. However, for the degradation of malathion, it is possible to obtain several by-products of the oxidation reaction, including substances like phorate sulfoxide, diethyl phosphate, pharatoxon sulfone and malaaxon, the latter being very toxic, which inhibition power under the enzyme acetylcholinesterase is 40 times higher than the parent compound<sup>16,17</sup>.

Like pesticides, their treatment products can also cause effects on the environment, which highlights the need for ecotoxicological assessments that can demonstrate and quantify possible adverse effects to organisms exposed to these substances<sup>18, 19</sup>. In this sense, the present work evaluated the acute ecotoxicity of malathion before and after degradation by UVC radiation and UV/H<sub>2</sub>O<sub>2</sub> using *Lactuca sativa* seeds and *Aedes aegypti* larvae as bioindicators. Lettuce seed (*Lactuca sativa*) was chosen as the indicator organism, using the observation of interferences in seed germination and root growth<sup>20-22</sup>. The species *Aedes aegypti* was also chosen for toxicity and larvicide evaluation because it is the target organism of malathion<sup>23</sup>.

## 2. Experimental

For ecotoxicity evaluation, samples were collected at initial (0 min), intermediate (30 min), and final treatment times (120 min) in previously washed glass flasks. The pH was adjusted to 6~7, and when necessary, bovine catalase (Sigma-Aldrich) was added for residual H<sub>2</sub>O<sub>2</sub> removal. Samples were analyzed immediately or, when this was not possible, they were kept frozen at -20 °C for a maximum of 20 days until the tests were performed. Two tests were selected: *Aedes aegypti* (acute toxicity) and *Lactuca sativa* seeds (phytotoxicity).

### 2.1 Ecotoxicological tests with *Aedes aegypti*

*Aedes aegypti* tests were performed according to methodology described by the World Health

Organization<sup>24</sup>. Healthy eggs (Rockefeller variety) were used, provided by the Laboratory of Physiology and Control of Arthropod Vectors of the Oswaldo Cruz Foundation – RJ. Egg hatching was performed in a 1 L Becker containing 500 mL of mineral water with the addition of a small amount of fish feed. Packing was carried out in a B.O.D. incubator, with photoperiod of 16 h clear and 8 h dark, maintained at a temperature of 28 °C.

Commercial product Malathion<sup>®</sup> 500 CE were used for the test solutions preparation, which were diluted with ultrapure water. In all of them, there were three preliminary tests (data not show). The concentration in focus refers to that recommended by the manufacturer, which indicates the dilution of 30 mL of the pesticide in 10 L of water<sup>25</sup>.

Preliminary tests were performed in order to determine the concentration range necessary to determine the effective concentration at 50% of the organisms (EC<sub>50</sub>), being the range of 0.05; 0.1; 0.2; 0.4; 0.8 and 1 µg L<sup>-1</sup><sup>16</sup>. Tests were performed in triplicate, the definitive ones and the treated samples were done in quadruplicate, in each replicate, containing 25 mL of solution and 20 organisms, whose life stage is between the 3<sup>rd</sup> and 4<sup>th</sup> larval stage, approximately 96 h of life. The assays were maintained in B.O.D. at 23 °C, without photoperiod, for 24 h. After that, the number of immobile organisms was counted, thus obtaining the percentage of immobility.

### 2.2 Phytotoxicity with *Lactuca sativa*

In order to obtain the EC<sub>50</sub>, solutions of the commercial product Malathion<sup>®</sup> 500 CE were prepared for the realization of the bioassay with *L. sativa*. Preliminary tests were performed with concentrations ranging from 1 µg L<sup>-1</sup> to 400 µg L<sup>-1</sup>, and the concentration range selected for the final test was 250, 350, 450, 550, 600 and 700 µg L<sup>-1</sup>, where adverse effects were observed.

The seed germination/root elongation phytotoxicity assays were performed according to the methodology described by Sobrero and Ronco<sup>22</sup> and Young *et al.*<sup>26</sup>. Tests were carried out in Petri dishes lined with filter paper (Unifil, weight 80 g m<sup>-2</sup>) and with 15 seeds each (cv. Boston), containing 4 mL of sample dilution or negative/positive control, with osmosis water and commercial glyphosate 3% (Dipil), respectively. The assay was done in triplicate. Seeds were incubated at 22 ± 2 °C, in the dark, for 120 h. At the end of the test, the number of germinated seeds

and the root elongation data were used to calculate the germination index (GI)<sup>20</sup> and the relative growth index (RGI)<sup>26</sup>. The RGI values were divided into three categories according to the observed toxicity effects: (a) inhibition of the root elongation:  $0 < \text{RGI} < 0.8$ ; (b) no significant effects:  $0.8 \leq \text{RGI} \leq 1.2$ ; and (c) stimulation of the root elongation:  $\text{RGI} > 1.2$ <sup>26</sup>.

### 2.3 Statistical analysis

Statistical data evaluation was performed with the BioEstat 5.3 software (BioEstat Software, Belém, Brazil). The effective concentrations 50% (EC<sub>50</sub>) were calculated using the Probit method. When the EC<sub>50</sub> was not reached by the tested effluent samples, toxicity was expressed as percentage of toxic effect. For *L. sativa* tests, data were subject to Kolmogorov-Smirnov normality test. As data were normally distributed, they were submitted to one-way analysis of variance (ANOVA) and Tukey test ( $p < 0.05$ ). Significance values are indicated as follows:

\* $p < 0.05$  and \*\* $p < 0.01$ .

### 2.4 Treatment of Malathion® 500 CE by UVC radiation and UV/H<sub>2</sub>O<sub>2</sub>

Photolysis (UVC radiation) and UV/H<sub>2</sub>O<sub>2</sub> treatments of the commercial product Malathion® 500 CE were performed using the concentrations that gave rise to 50% of test organisms (EC<sub>50</sub>), which were 550 µg L<sup>-1</sup> for *L. sativa* and 0.4 µg L<sup>-1</sup> for *A. aegypti*. The experiments were conducted in a borosilicate bench photoreactor with 300 mL capacity, equipped with a water-cooled system and a magnetic stirrer. Artificial radiation was provided by a high-pressure mercury vapor lamp (125 W, Philips) placed in the solution through a quartz jacket. The initial concentration of H<sub>2</sub>O<sub>2</sub> was 1000 mg L<sup>-1</sup> and the residual hydrogen peroxide was determined by UV-Vis spectroscopy, using method based on ammonium metavanadate<sup>27</sup>.

## 3. Results and discussion

### 3.1 Determination of EC<sub>50</sub> of Malathion® 500 CE to *A. aegypti* and *L. sativa*

When it is intended to determine EC<sub>50</sub> of one (or more than one) substance to organisms that have not been reported yet, preliminary tests are of great

value to explore and determine it correctly. Preliminary concentrations to *A. aegypti* were based on EC<sub>50</sub> of Malathion 500 CE to *Daphnia magna*, which ranges between 0.36-3.8 ng L<sup>-1</sup><sup>28-30</sup>.

After preliminary results, new limits of concentration were settled down and this new range of values (0.05; 0.1; 0.2; 0.4; 0.8 and 1 µg L<sup>-1</sup>) allowed determine a reliable EC<sub>50</sub> to *A. aegypti* larvae. In the definitive assays, EC<sub>50</sub> value obtained was 0.4 µg L<sup>-1</sup>.

From data obtained at definitive assay (250, 350, 450, 550, 600 and 700 µg L<sup>-1</sup>) with *Lactuca sativa*, it was possible to calculate the EC<sub>50</sub> (550 µg L<sup>-1</sup>).

Comparing both organisms, it is possible to recognize their sensibility difference. *L. sativa* is about one hundred times more resistant than *A. aegypti*. This result was already expected once *A. aegypti* is a target organism, but comparing with literature, species like *D. magna* are two times more sensible than the target larvae showing the importance to treat this compound before achieve aquatic ecosystems<sup>19</sup>.

Brazilian and American legislation indicates maximum permissible values of pesticides in drinking water, but malathion is not contemplated<sup>31, 32</sup>. In Brazil, resolution n°. 357/2005 stipulates the maximum concentration range of organophosphates in water, which ranging from 0.1 µg L<sup>-1</sup> (freshwater, saline and brackish class 1) to 100 µg L<sup>-1</sup> (freshwater class 3). This means that the higher values would bring acute toxicity effects, according to the value of EC<sub>50</sub> determined in this work<sup>33</sup>.

Preliminary tests are of great value when it is intended to determine the EC<sub>50</sub> of organisms when exposed to one or more substances, therefore, preliminary tests with *A. aegypti* have been carried out using the EC<sub>50</sub> value of known organisms, such as *Daphnia magna*, which effective concentration varies between 0.36-3.8 ng L<sup>-1</sup> for Malathion 500 CE<sup>28-30</sup>.

### 3.2 Ecotoxicity of Malathion® 500 CE to *A. aegypti* and *L. sativa* after treatment by photolysis and UV/H<sub>2</sub>O<sub>2</sub>

It was observed in both treatments that there was no immobility for *A. aegypti* (Table 1), inferring that the degradation of Malathion 500 CE was efficient, losing its larvicidal property, besides that; the byproducts generated were not toxic to the organisms<sup>17</sup>.

**Table 1.** Evaluation of the ecotoxicity of Malathion®500 CE ( $0.4 \mu\text{g L}^{-1}$ ) using *Aedes aegypti* before and after treatment with UVC radiation and UV/H<sub>2</sub>O<sub>2</sub>

	Negative control	T0	UVC 30 min	UVC 120 min	UV/H <sub>2</sub> O <sub>2</sub> 30 min	UV/H <sub>2</sub> O <sub>2</sub> 120 min
Average*	0	10	0	0	0	0
Immobility (%)*	0	50	0	0	0	0

\*Three replicates with 20 organisms.

Comparing the results obtained before and after treatment, the toxicity of the commercial product reduced 100% when tested on *A. aegypti*, demonstrating that it is a viable alternative on the treatment of this organophosphate. This process has the advantage of no needing high pressures, temperatures, elevated times of exposure and the oxidizing agent (hydrogen peroxide) can be removed through catalase abatement<sup>34-36</sup>.

The values of p (probability of significance) for ANOVA followed by Tukey's test, obtained from *L. sativa* bioassays (Table 2), indicate that in all samples there was statistical significance and RGI (Relative Growth Index) less than 0.80, it means that all treatments inhibited root growth. The Germination Index (GI) was greater than 90% in all samples, indicating that there was no inhibition of germination.

**Table 2.** Evaluation of the phytotoxicity of Malathion®500 CE ( $550 \mu\text{g L}^{-1}$ ) using *Lactuca sativa* seeds before and after treatment with UVC radiation and UV/H<sub>2</sub>O<sub>2</sub>

Sample	Mean root length (cm)	RGI	GI%	Effect
Control	2.50±0.7 <sup>a</sup>	---	100	-----
T0	1.25±0.1 <sup>b**</sup>	0.5	97.8	I
UVC 30 min	1.98±0.3 <sup>c*</sup>	0.7	100	I
UVC 120 min	1.62±0.1 <sup>c**</sup>	0.6	100	I
UV/H <sub>2</sub> O <sub>2</sub> 30 min	1.39±0.3 <sup>d**</sup>	0.5	100	I
UV/H <sub>2</sub> O <sub>2</sub> 120 min	1.92±0.5 <sup>c*</sup>	0.7	100	I

Three replicates with 15 seeds. Abbreviations: GI%, germination index; I, inhibition; RGI, relative growth index. Mean values with different letters (a, b, c, d) are significantly different (Tukey's test,  $p < 0.05$ ). \* $p < 0.05$ ; \*\* $p < 0.01$ .

It can be verified that the treatments showed an efficiency in reduction of effects on root growth of lettuce seedlings in comparison to pre-treatment sample (T0 =  $550 \mu\text{g L}^{-1}$ , with RGI = 0.50), since after UVC and UV/H<sub>2</sub>O<sub>2</sub> processes all samples had RGI higher than 0.50.

However, UVC 120 min photolysis likely generated toxic degradation byproducts for lettuce, once in 30 min of radiation exposure there was 21% of inhibition in root growth (RGI = 0.79), while at 120 min the percentage of inhibition growth increased to 36% (RGI = 0.64). Even though there

were no significant differences between them, this increase of the toxicity can be associated to the formation of inorganic anions such as sulfates and phosphates due to cleavage of the P-S bonds<sup>17, 18</sup>.

For UV/H<sub>2</sub>O<sub>2</sub>, rootlets growth had high inhibition at 30 min of treatment (RGI = 0.55) and in 120 min was observed decrease of toxic effects (RGI = 0.76). It is possible that at the initial 30 min were formed intermediates by sulfur oxidation and generation of molecules from the combination of phosphorus, sulfur, carbon, hydrogen and oxygen,

for example, phorate sulfoxide and phoratoxon sulfone<sup>17,18</sup>.

The influence of concentration of treated compound on processes efficiency is evident when comparing treatments carried out based on ecotoxicity of Malathion to *A. aegypti*, since concentration used was ten times lower in relation to *L. sativa* and after both treatments no toxic effects were obtained, it shows that, despite the objective of the treatment was to degrade the pesticide and eliminate sources of toxicity, the concentration of treated compound may interfere in the efficiency of the process and even increase toxic effects<sup>17,36</sup>.

#### 4. Conclusions

As an insecticide, Malathion<sup>®</sup> 500 CE was shown to be more toxic to *Aedes aegypti* larva, evidenced by EC<sub>50</sub>, which is much lower than that obtained for *L. sativa*. As regards phytotoxicity, it was found that the *L. sativa* seed presented moderate resistance to the pesticide studied, with an EC<sub>50</sub> value of 536.11 µg L<sup>-1</sup>, however; it was a low concentration, inferring that lower concentrations of Malathion<sup>®</sup> 500 CE can cause damage to terrestrial plants.

Degradation of the commercial product in both treatments was efficient and the byproducts generated were not harmful to *A. aegypti* larvae. However, in the phytotoxicity assays, it was evidenced that there was inhibition of root growth.

This compound is present in agriculture for biological control and in urban areas being used in the fight against vectors of several diseases like dengue requiring several ecotoxicological and toxicological studies of this insecticide. In the present work, it is possible to see that low concentrations can cause harmful effects to target and non-target organisms.

#### 5. References

[1] Diretoria de Vigilância Epidemiológica, Orientações para o uso de Malathion Emulsão Aquosa - EA 44% para o controle de *Aedes aegypti* em aplicações espaciais a Ultra Baixo Volume (UBV). Estado de Santa Catarina, Secretaria de Estado da Saúde, Superintendência de Vigilância em Saúde. Florianópolis, 2016.

[2] Instituto Oswaldo Cruz, Considerações técnicas sobre a aplicação aérea de inseticidas em área

urbana, Nota Técnica nº 4/2016/IOC-FIOCRUZ/DIRETORIA, Rio de Janeiro, 2016.

[3] Brasil. Ministério da Saúde. Dispõe sobre a adoção de medidas de vigilância em saúde quando verificada situação de iminente perigo à saúde pública pela presença do mosquito transmissor do vírus da dengue, do vírus Chikungunya e do vírus da Zika, Lei nº 13.301, de 27 de junho de 2016.

[4] World Health Organization (WHO), Report of the fifteenth whopes working group meeting. Review of: Olyset<sup>®</sup>Plus, Interceptor<sup>®</sup>LN, Malathion 440 EW, Vectobac<sup>®</sup> GR. World Health Organization, Geneva, Switzerland, 2012.

[5] Barata, C., Solayan, A., Porte, C., Role of B-esterases in assessing toxicity of organophosphorus (chlorpyrifos, malathion) and carbamate (carbofuran) pesticides to *Daphnia magna*, *Aquatic Toxicology* 66 (2) (2004) 125-139. <https://doi.org/10.1016/j.aquatox.2003.07.004>.

[6] Saler, S., Saglan, N., Acute toxicity of Malathion on *Daphnia magna* Straus, 1820, *Journal of Biological Sciences* 5 (3) (2005) 297-299. <https://doi.org/10.3923/jbs.2005.297.299>.

[7] Damásio, J., Guilhermino, L., Soares, A. M., Riva, M. C., Barata, C., Biochemical mechanisms of resistance in *Daphnia magna* exposed to the insecticide fenitrothion. *Chemosphere*. 70 (1) (2007) 74-82. <https://doi.org/10.1016/j.chemosphere.2007.07.026>.

[8] Oga, S., Camargo, M. A., Batistuzzo, J. A. O., Fundamentos de toxicologia, Atheneu, São Paulo, 3<sup>rd</sup> ed., 2008.

[9] Rebechi, D., Efeitos ecotoxicológicos em *Chironomus sanctiparoli* Strixino & Strixino, 1981 (*Diptera: Chironomidae*) expostos ao Malathion. 2012. 85f Dissertação (Mestrado em Entomologia) – Universidade Federal do Paraná, Curitiba, 2012.

[10] Teixeira, C. P. A. B., Jardim, W. F., Advanced Oxidative Processes: theoretical concepts. Thematic Notebook, v. 3, State University of Campinas (UNICAMP), Institute of Chemistry - IQ, Laboratory of Environmental Chemistry - LQA. Campinas, 2004 (Português).

- [11] Badawy, M. I., Ghaly, M. Y., Gad-Allah, T. A., Advanced oxidation processes for the removal of organophosphorus pesticides from waste water, *Desalination* 194 (1-3) (2005) 166-175. <https://doi.org/10.1016/j.desal.2005.09.027>.
- [12] Loures, C. C. A., Alcântara, M. A. K., Izário Filho, H. J., Teixeira, A. C. S. C., Silva, F. T., Paiva, T. C. B., Samanamud, G. R. L., Advanced oxidative degradation processes: Fundamentals and Applications, *International Review of Chemical Engineering* 5 (2) (2013) 102-120.
- [13] Zhang, Y, Pagilla, K., Treatment of malathion pesticide wastewater with nanofiltration and photo-Fenton oxidation, *Desalination* 263 (1-30) (2010) 36-44. <https://doi.org/10.1016/j.desal.2010.06.031>.
- [14] Chenna M., Messaoudi, K., Drouche, N., Lounici, H., Study and modeling of the organophosphorus compound degradation by photolysis of hydrogen peroxide in aqueous media by using experimental response surface design, *Journal of Industrial and Engineering Chemistry* 33 (2016) 307-315. <https://doi.org/10.1016/j.jiec.2015.10.016>.
- [15] Clark, K. K., Mezyk, S. P., Abbott, A., Kiddle, J. J., Kinetic Studies of the AOP Radical-Based Oxidative and Reductive Destruction of Pesticides and Model Compounds in Water, *Chemosphere* 197 (2018) 193-199. <https://doi.org/10.1016/j.chemosphere.2017.12.190>.
- [16] Brenner, L., Malathion Fact Sheet, *Journal of Pesticide Reform* 12 (4) (1992) 29-37.
- [17] Konstantinou, I. K., Antonopoulou, M., Lambropoulou, D. A., Transformation products of emerging contaminants formed during advanced oxidation processes. In *Transformation products of emerging contaminants in the environment: Analysis, processes, occurrence, effects and risks*, Lambropoulou, D. A., Nollet, L. M. L., ed., John Wiley & Sons: Chinchester, United Kingdom, 2014, Ch. 6.
- [18] Kralj, M. B., Černigoj, U., Franko, M., Trebše, P., Comparison of photocatalysis and photolysis of malathion, isomalathion, malaaxon, and commercial malathion - Products and toxicity studies, *Water Research* 41 (19) (2007) 4504-4514. <https://doi.org/10.1016/j.watres.2007.06.016>.
- [19] Zagatto, P. A., Bertoletti, E., *Ecotoxicologia aquática: princípios e aplicações*, RiMa, São Carlos, Brasil, 2<sup>nd</sup> ed., 2008.
- [20] Garcia, J. C., Simionato, J. I., Cinque Almeida, V. de, Palácio, Z., Rossi, F. L., Schneider, M. V., Souza, N. E. de, Evolutive follow-up of the photocatalytic degradation of real textile effluents in TiO<sub>2</sub> and TiO<sub>2</sub>/H<sub>2</sub>O<sub>2</sub> systems and their toxic effects on *Lactuca sativa* seedlings, *Journal of the Brazilian Chemical Society* 20 (9) (2009) 1678-4790. <https://doi.org/10.1590/S0103-50532009000900005>.
- [21] United States Environmental Protection Agency (USEPA), *Protocols for short term toxicity screening of hazardous waste sites – 600/3-88/029*, Washington, United States, 1989.
- [22] Sobrero, M. C., Ronco, A., Ensayo de toxicidad aguda con semillas de lechuga *Lactuca sativa L.*, In *Ensayos toxicológicos para la evaluación de sustancias químicas em água y suelo - La experiencia en México*, Romero, P. R., Cantú, A. M., ed., Secretaria de Medio Ambiente y Recursos Naturales, Ciudad de México, México, 2004, 56-67.
- [23] Muturi, E. J., Larval rearing temperature influences the effect of malathion on *Aedes aegypti* life history traits and immune responses, *Chemosphere* 92 (9) (2013) 1111-1116. <https://doi.org/10.1016/j.chemosphere.2013.01.055>.
- [24] World Health Organization (WHO), *Instructions for Determining the Susceptibility or Resistance on Mosquito Larvae to Insecticides*, World Health Organization, Geneva, Switzerland, 1981.
- [25] Dipil., *Ficha técnica do produto: Malathion 500 CE Inseticida Líquido*, Dipil Indústria Química.
- [26] Young, B. J., Riera, N. I., Beily, M. E., Bres, P. A., Crespo, D. C., Ronco, A. E., Toxicity of the effluent from an anaerobic bioreactor treating cereal residues on *Lactuca sativa*, *Ecotoxicology*

and Environmental Safety 76 (2) (2012) 182-186. <https://doi.org/10.1016/j.ecoenv.2011.09.019>.

[27] Nogueira, R. F. P., Oliveira, M. C., Paterlini, W. C., Simple and fast spectrophotometric determination of H<sub>2</sub>O<sub>2</sub> in photo-Fenton reactions using metavanadate, *Talanta* 66 (2005) 86. <https://doi.org/10.1016/j.talanta.2004.10.001>.

[28] U. S. Environmental Protection Agency (USEPA), Reregistration Eligibility Decision (RED) for Malathion Revised, U. S. Office of Prevention, Pesticides and Toxic Substances, Washington, United States, 2009.

[29] Toumi, H., Boumaiza, M., Millet, M., Radetski, C. M., Camara, B. I., Felten, V., Ferard, J. F., Investigation of differences in sensitivity between 3 strains of *Daphnia magna* (Crustacean: Cladocera) exposed to malathion (organophosphorus pesticide), *Journal of Environmental Science and Health* 50 (1) (2014) 34-44. <https://doi.org/10.1080/03601234.2015.965617>.

[30] Nagato, E. G., Simpson, A. J., Simpson, M. J., *Metabolomics reveals energetic impairments in *Daphnia magna* exposed to diazinon, malathion and bisphenol-A*, *Aquatic Toxicology* 170 (1) (2016) 175-186. <https://doi.org/10.1016/j.aquatox.2015.11.023>.

[31] Brasil, Ministério da Saúde, Portaria nº 2914, de 12 de dezembro de 2011, “Dispõe sobre os procedimentos de controle e de vigilância da qualidade da água para consumo humano e seu padrão de potabilidade”, 2011.

[32] U. S. Environmental Protection Agency (USEPA), 2018 Edition of the Drinking Water Standards and Health Advisories, U. S. Office of Water, Washington, United States, 2018.

[33] Brasil, Ministério do Meio Ambiente, Conselho Nacional do Meio Ambiente, Resolução CONAMA no 357, de 17 de março de 2005, “Dispõe sobre a classificação dos corpos de água e diretrizes ambientais para o seu enquadramento, bem como estabelece as condições e padrões de lançamento de efluentes, e dá outras providências”, 2005.

[34] Lofrano, G., Pedrazzani, R., Libralato, G., Carotenuto, M., *Advanced Oxidation Processes for Antibiotics Removal: A Review*, *Current Organic Chemistry* 21 (12) (2017) 1054-1067. <https://doi.org/10.2174/1385272821666170103162813>.

[35] Santos, K. A., Antonelli, R., Gaydeczka, B., Granato, A. C., Pointer Malpass, G. R., *Processos oxidativos avançados: uma revisão de fundamentos e aplicações no tratamento de águas residuais urbanas e efluentes industriais*, *Ambiente & Água- An Interdisciplinary Journal of Applied Science* 11 (2) (2016) 387-401. <https://doi.org/10.4136/ambiente.1862>.

[36] Pignatello, J. J., Oliveros, S. E., Mackay, A., *Advanced oxidation processes of organic contaminant destruction based of the Fenton reaction and related chemistry*, *Critical Reviews in Environmental Science and Technology* 36 (1) (2006) 1-84. <https://doi.org/10.1080/10643380500326564>.

## Evaluation of the water quality of the Verde River, Ponta Grossa, PR: a study on the conditions of aquatic life maintenance and the eutrophication process

Karine Andréa Costa<sup>1</sup>, Elizabeth Weinhardt Oliveira Scheffer<sup>1</sup>, Patrícia Los Weinert<sup>1</sup>, Estevan Luis Silveira<sup>2</sup>

<sup>1</sup> State University Ponta Grossa, Praça Santos Andrade, Ponta Grossa, Paraná, Brazil

<sup>2</sup> Federal University of Paraná, 1299 XV de Novembro St., Curitiba Paraná, Brazil

\* Corresponding author: Karine Andréa Costa, e-mail address: [karine.ambiental@gmail.com](mailto:karine.ambiental@gmail.com)

### ARTICLE INFO

#### Article history:

Received: February 10, 2018

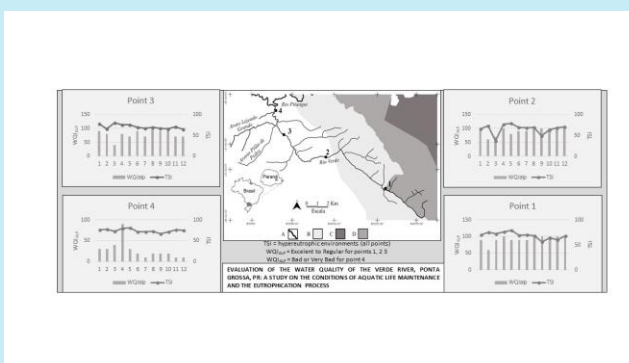
Accepted: June 4, 2018

Published: August 23, 2018

#### Keywords:

1. aquatic biota
2. index of quality
3. river

**ABSTRACT:** This study was to evaluate the physicochemical parameters that express the water quality of the Verde River, in the city of Ponta Grossa, Paraná. Multivariate Analysis was used, and quality indexes were obtained, such as the Trophic State Index (TSI) and the Water Quality Index for Aquatic Life Protection (WQIALP). River samples were collected at 4 points along the Verde River for 12 months. The results indicated that, at point 4, downstream from the Sewage Treatment Plant (STS), the aquatic environment is very poor for the biota. The calculation of the WQIALP showed BAD to VERY BAD quality, and the disposal of the effluent was indicated as the cause. It was also concluded that points 1 and 2 correspond to more preserved sites but are not totally favourable to aquatic life either because they receive surface drainage from agricultural areas in the basin. Point 3, of urban character, suffers an impact caused by irregular connections of sewers, and contribution of streams that flow into the river. For all sampling points,  $TSI > 67$  for more than 90% of the samples, indicating hypereutrophic environments throughout the river. The quality indexes applied in this work were faithful to the reality found for the water of the Verde River.



### 1. Introduction

Even if water is considered a renewable natural resource, the growing impact on natural sources, due to the disordered increasing population density and the many interferences resulting from it, have made the degradation of water resources a public health problem. Improper disposal of domestic and industrial effluent, large-scale use of agricultural input and destruction of riparian forests are examples of anthropogenic pressure which contribute to their degradation<sup>1</sup>. However, when a water body is monitored, there is a great number of

parameters to be analyzed, and the interpretation of this data set requires technical knowledge as well as awareness of the current law. Therefore, aiming to help disseminate water quality data, indices can be employed, which represent the consolidation of information from different analyses<sup>2</sup>. Among the quality indices, this work employed WQIALP (Water Quality Index for Aquatic Life Protection), based on ammoniacal nitrogen and dissolved oxygen (DO), and the TSI (trophic state index) based on phosphorous and chlorophyll concentrations. The integrated evaluation of Verde River also included the determination of 14

physicochemical parameters, studied individually, and their set submitted to multivariate analysis.

Verde River is one of the main tributaries of Pitangui River, a source of water supply to Ponta Grossa, and is in an area classified as “high to extremely high” importance for conservation<sup>3</sup>, with its course including the Environmental Preservation Area (EPA) of the Devonian Escarpment and the National Park of Campos Gerais. Therefore, it plays a relevant role in the city of Ponta Grossa. However, it still suffers with the disposal of raw sewage, STS effluents, domestic waste irregular disposal, degradation of the riparian forest and intensive farming activities on its margins. All these activities potentially affect water quality and biodiversity, they decrease the diversity of ecological niches available in the environment and provoke serious damage to the ichthyofauna.

The objective of this work was to express the water quality of the Verde River through quality indexes, calculated from the physicochemical parameters obtained experimentally. We also promote simplified data dissemination and encourage environmental protection actions.

### 1.1 WQI<sub>ALP</sub> and TSI

The commonly adopted surface water quality indicators are not directed to the aquatic life maintenance, they usually refer to drinkability criteria and the different uses of water by the population. Taking into consideration the importance of parameters such as DO and ammoniacal nitrogen, Silva and Jardim<sup>4</sup> proposed the WQI<sub>ALP</sub> in which the numerical value of the index is the lowest normalized value of such parameters. Ammoniacal nitrogen, for example, presents concentrations accepted by the regulations which can be lethal to many aquatic organisms, since legal limits do not consider toxicity to the biota. On the other hand, the biota requires minimum DO levels. According to the United States Environmental Protection Agency (USEPA), a 0 to 2 mg L<sup>-1</sup> concentration is not enough to keep aquatic life and between 2 and 4 mg L<sup>-1</sup> DO few fish species can survive<sup>5</sup>. In Brazil, according to the Resolution CONAMA n° 357/05<sup>6</sup> the minimum DO concentration set forth for water Class 2 is 5 mg L<sup>-1</sup>, which is not enough for many species of the ichthyofauna.

TSI is an indicator of eutrophication, a phenomenon that is characterized by the increase

in the nutrient concentration, mainly phosphorous and nitrogen, in aquatic ecosystems, resulting in problems such as algae growth, increase in the organic matter decomposition rate with reduction of dissolved oxygen, and, consequently, water quality deterioration<sup>7,8</sup>. This index is obtained from the total phosphorous and chlorophyll analyses and was developed to evaluate water quality regarding its enrichment by nutrients and the consequent effect, revealed by the growth of algae or macrophytes, obtaining a classification in different degrees of trophic status. The TSI determination might aid the management of hydric resources, favouring the control of eutrophication, a phenomenon that is of global concern<sup>7,8,9</sup>.

### 1.2 Physicochemical parameters and Multivariate analysis

The physicochemical parameters that are used to characterise water quality present great variability over time and space, and it is necessary to keep a continuous monitoring program when the actual quality of superficial water is to be evaluated. From monitoring programs, data sets containing several parameters are obtained, which are measured in different scales and units, which makes their interpretation complex. The Multivariate Analysis is made up by a set of statistical methods able to analyse simultaneously the measures of  $n$  variables, providing useful results for the understanding of large and complex data sets. Among the multivariate analysis techniques, the Principal Component Analysis, PCA, is widely used in environmental data base analyses<sup>10,11</sup>. The PCA objective is to reduce the complexity of data making its interpretation easier.

## 2. Experimental

Searching for differentiated characteristics along the Verde River, this study established four sampling points. Monthly collection of surface water was carried out from May 2016 to April 2017. Polyethylene bottles (1 L) were used and three bottles were collected in each point. The bottles were packet in plastic bags, in portable cool box with ice and transported to the laboratory where they were stored at 4 °C. Aliquots of water samples were immediately filtered in a reduced pressure device, using 0.45 µm cellulose acetate membranes. Analyses regarding DO, temperature, conductivity and turbidity were carried out *in situ*,

with a portable analyser Lutron, and in the laboratory, following the techniques described in the Standard Methods for the Examination of Water and Wastewater<sup>12</sup>, the analyses performed were: total alkalinity, dissolved chloride, total suspended solids (TSS), chlorophyll-a, oxygen biochemical demand (OBD), total phosphorous, total nitrogen and ammoniacal nitrogen. Analytical grade reagents and ultrapure water were used in all analyses.

### 3. Results and Discussion

The data analysed covered 14 physicochemical parameters, obtained monthly for one year from 4 monitoring points, resulting in 48 samples. Initially, the principal component analysis of the monitored data was carried out aiming at identifying which water quality parameters were more significant in the characterization of the water quality in Verde River.

**Table 1.** Eigenvalues and total variance explained by the principal components.

Principal component	Eigenvalue	Explained variance (%)	Accumulated explained variance (%)
1	5.956	42.540	42.540
2	1.946	13.900	56.439
3	1.462	10.440	66.879
4	0.995	7.108	73.987
5	0.819	5.851	79.837
6	0.681	4.868	84.705
7	0.576	4.115	88.820
8	0.446	3.186	92.006
9	0.423	3.019	95.025
10	0.247	1.764	96.789
11	0.228	1.626	98.415
12	0.120	0.854	99.269
13	0.064	0.454	99.723
14	0.039	0.277	100.000

To calculate the principal components, the Kaiser criterion was employed, in which the components with eigenvalues higher than 1 were retained<sup>13</sup>. Eigenvalues obtained from the correlation matrix are presented in Table 1 in descending order and define the importance of the principal components, since they correspond to the variance explained by each of them. When the variables present different units and/or when they present magnitude difference, self-scaling is recommended to minimize the dominant effect that one variable might have<sup>14</sup>. Data pre-treatment is fundamental for the success of the multivariate analysis and, it seems relevant to emphasise that for PCA when the correlation matrix is employed, self-scaling can be dismissed. The Program *Statistica*, version 13 was used to analyse the data.

The number of principal components to be retained according to the Kaiser criterion (eigenvalues higher than 1 are retained) were four and, together they explain approximately 74% variance. It seems important to highlight that for the fourth component the eigenvalue 0.995 was

considered as 1. This study considered that a correlation equal or over 0.5 would be reasonable to state that the parameters correlated, since this type of data presents natural variability.

The variables influencing each of the 4 principal components are shown in Table 2. The table also shows the total variance explained by the components, so that the evaluation of the importance of each one is presented when explaining the data set collected. When considering one important variable for the composition of the component, the numerical value of the correlation is recommended to be over 0.7.

In the first component, the outstanding variables were total nitrogen, ammoniacal nitrogen, OBD, TSS, alkalinity, total chloride and conductivity, all with a negative signal. This component reflects the water quality for these parameters, lower values indicate better quality. In this component, DO did not reach a correspondence value over 0.7 presenting 0.525 with a positive signal. However, this opposition of signals is justified by the fact that an increase in the OBD and ammoniacal nitrogen

variables is associated to the presence of organic matter, that is, higher DO consumption. The DO concentration is important for the self-clearing capacity, which is the recovery of balance in the aquatic environment through natural mechanisms.

In this sense, the self-clearing capacity of Verde River is related to the characteristic relief, which includes several rapids. Component 1 can be considered an indication of aspects related to organic matter degradation.

**Table 2.** Weight of the variables in the composition of principal components.

Variable	Factor 1	Factor 2	Factor 3	Factor 4
Water temperature	-0.207	-0.548	0.575	0.093
DO	0.525	-0.478	-0.092	0.251
Cond	-0.825	-0.091	0.163	0.032
Environment temperature	0.175	0.100	0.833	-0.054
Chl	-0.879	0.163	-0.142	0.123
Alkalinity	-0.951	-0.062	0.005	0.030
Turbidity	-0.440	-0.385	-0.430	-0.106
TSS	-0.705	-0.156	0.356	0.001
OBD	-0.855	0.071	-0.097	-0.118
Chlorophyll	-0.185	0.614	-0.004	-0.558
P	-0.073	0.719	0.231	0.115
Total N	-0.946	-0.046	-0.010	0.129
Ammoniacal N	-0.941	-0.079	-0.016	0.005
pH	0.075	-0.538	0.079	-0.733
eigenvalue	5.956	1.946	1.462	0.995
Explained variance (%)	42.5	13.9	10.4	7.1

Component 2 was only formed by the total P content following the correlation criterion over 0.7 and positive. If a value over 0.6 is to be accepted, the variable chlorophyll-a can be aggregated to this component. Component 2 can be considered to express the influence of the farming activity in the neighbourhood of the river and the higher the P content is, the higher the resulting impact is. In component 3, there is also a single variable with correlation over 0.7, which was the environmental temperature. In this component, the hypothesis of accepting a value over 0.6 can also be considered, which would mean that the variable water temperature would also be aggregated. The fourth component presented moderate influence of the variable pH. However, since the data set under analysis involved parameters of natural variability it does not seem reasonable to affirm that the relations between the parameters are strong or weak.

Figure 1 presents the scores for the components 1 and 2 and the samples collected from 4 distinct monitoring points and the formation of some

groups as a function of these components can be observed. In component 1, the growing impact in the quality of the Verde River water was verified in all points in the spring-mouth direction. Point 1 is located closer to the spring, in a place called “Capão da Onça”, and point 2 in a place called “curva do cemitério”, both present preserved margins and clear water. Samples 1-24 (Figure 1) collected from these points, generally presented the highest DO concentrations ( $> 6 \text{ mg L}^{-1}$ ) and the lowest dissolved chloride concentrations ( $< 8 \text{ mg L}^{-1}$ ), total nitrogen and ammoniacal nitrogen, as well as the lowest OBD, conductivity and total alkalinity ( $< 24 \text{ mg L}^{-1}$ ) values, exactly as indicated in the data obtained from the PCA. These are in fact less impacted when compared to points 3 and 4, but still present total phosphorous concentration above the limit set forth in the law, which is  $0.1 \text{ mg L}^{-1}$ . Despite the river presenting margins apparently preserved in these points, the basin is characterized by farming activities, suggesting that the input of this nutrient in the water body occurs via surface drainage.

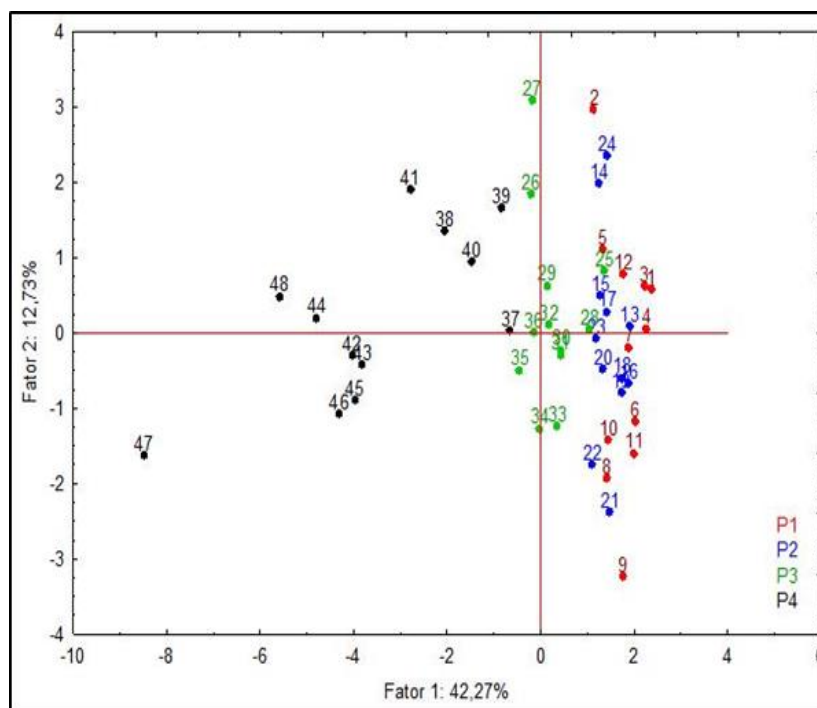


**Figure 1.** CP1 x CP2 scores of the samples collected in Verde River.  
 ● Collection point 1; ● Collection point 2; ● Collection point 3 and ● Collection point 4.

Point 3 (samples 25-36, [Figure 1](#)) is located in the place called “Passadouro”, in the urban area, after Verde River receives the input of the stream Pilão de Pedra, which crosses the city centre, through an underground gallery, but where irregular links provoke leaking resulting in high pollution indices. This point, according to the parameters, is only less impacted than point 4. It presented, for example, OBD over  $3\text{mg L}^{-1}$  in more than 50% of the collections, that is, over the legal limit CONAMA 357/05 for rivers Class 2, in addition to higher turbidity and conductivity than points 1 and 2. The analysis shows that component 1 can differentiate from them by the parameters that indicate the worse quality of the river, considering the way the samples from Point 3 were distributed in the score graph presented in [Figure 1](#). Sample 27 in point 3 was collected in July 2016 and presented high chlorophyll-a content ( $52.45\ \mu\text{g L}^{-1}$ ), for this reason it was separated from the remaining samples of this point in relation to component 2.

Point 4 is located downstream to the Verde River effluent treatment station, around 50 m from the local where the effluent flow into the river, and close to the river mouth which is tributary to the Pitangui River. It is, undoubtedly, the most impacted place in the whole course, with DO below

$5\ \text{mg L}^{-1}$  in most of the samples and organic matter, represented by the ODB, over  $4\ \text{mg L}^{-1}$ , even reaching  $11.5\ \text{mg L}^{-1}$  in December 2016 (sample 44, [Figure 1](#)). For the same point 4, the samples collected from June 2016 and September 2016 (samples 38 to 41, [Figure 1](#)) presented total P content three times higher on average than samples (42-48, [Figure 1](#)) collected in the period from October 2016 to April 2017, being grouped in higher scores in relation to component 2, which represented exactly the P content in the samples.

One characteristic of Verde River, throughout its course, is the presence of rock paved bottom and small rapids, factors that dissimulate the impact when analysed regarding parameters such as DO, turbidity and TSS, and which can also interfere when used to calculate quality indices. Numerous studies have shown that multivariate statistical analysis is useful for the assessment of the spatial water quality variations in a river<sup>15, 16, 17</sup>.

### 3.1 TSI – Trophic state index calculation

Considering the trophic status of its aquatic ecosystem, Verde River is classified, practically in all its points, as eutrophic or superior, with predominance of hypereutrophic features ([Table 3](#)). Undoubtedly, the presence of phosphorous was

determining for this condition. The total phosphorous concentration was mainly above the regulations ( $0.1 \text{ mg L}^{-1}$ ) for lotic environments, such as the Verde River. This fact is due to the characteristics of the neighborhood of this river. In points 1 and 2, the presence of farming activities in the basin, and the surface drainage carrying

phosphorous into the water. While for the urban area, corresponding to points 3 and 4, the raw sewage and the treatment station effluent in a volume that supersedes its flow and dissolution capacity.

**Table 3.** Trophic state index for Verde River within 12 months (May-2016 to April-2017).

Points	2016								2017			
	May	Jun	Jul	Aug	Sep	Oct	Nov	Dec	Jan	Feb	Mar	Apr
P1	70	75	72	76	79	69	70	68	56	64	60	68
P2	66	73	37	77	79	69	68	69	49	63	68	71
P3	78	66	80	75	75	69	67	69	67	66	70	64
P4	76	77	73	80	81	71	72	73	67	71	76	75

Legend: Ultra oligotrophic  $\text{TSI} \leq 47$ ; Oligotrophic  $47 < \text{TSI} \leq 52$ ; Mesotrophic  $52 < \text{TSI} \leq 59$ ; Eutrophic  $59 < \text{TSI} \leq 63$ ; Super eutrophic  $63 < \text{TSI} \leq 67$ ; Hypereutrophic  $\text{TSI} > 67$ .

As well as the phosphorous, the chlorophyll-a concentration is high in Verde River, close to the limit value  $30 \mu\text{g L}^{-1}$ , or even higher than this limit set forth by the Resolution CONAMA n° 357/05. The results corresponding to chlorophyll-a are considered as a measure of response from the water body to the causing agent, therefore, indicating the level of algae growth in the place. According to Cunha *et al.*<sup>18</sup>, eutrophication in would be unusual, due to the characteristics of this system, such as the turbulence, low residence time and continuous community transportation phytoplankton downstream.

### 3.2 $\text{WQI}_{\text{ALP}}$ – Water Quality Index for aquatic life protection

When evaluating the parameters used to calculate the  $\text{WQI}_{\text{ALP}}$ , the ammoniacal concentrations of all points were seen to be within the legal limits set forth for rivers Class 2 ( $3.7 \text{ mg L}^{-1}$  para  $\text{pH} \leq 7.5$ ), since they were below  $1.3 \text{ mg L}^{-1}$ . However, even in low concentrations, this compound might cause impacts to the biota, regarding chronic toxicity with effects on the reproduction capacity, growth as well as biochemical and physiological changes. In this study, the ammoniacal nitrogen was seen to increase along the river, in the spring-mouth direction, mainly after the STS, where it was up to 100 times higher than the concentrations in Point 3. It is possible to promote the biological removal of nitrogen in treatment systems; however, the

efficacy of the removal depends on the efficiency of the STS treatment. Regarding DO, it is a variable whose reduction might affect significantly the aquatic biota, and that in surface waters suffers influence of factors such as temperature and natural oxygenation, as well as the impact of organic matter<sup>19</sup>. The reduction in DO concentrations in point 4 is related to the input of the STS, which impacts the river both for its organic charge and for the disparity between the effluent flow and the river capacity. Despite Verde River having small rapids throughout its course, which increase OD concentration, some samples presented concentrations below  $5 \text{ mg L}^{-1}$ , that is, this fact can be associated to oxidation processes that consume oxygen, indicating the presence of organic matter associated to the impact in the water body.

The calculation of the  $\text{WQI}_{\text{ALP}}$  (Table 4), where 100 represents the best environmental quality, showed between EXCELLENT and REGULAR quality for points 1 and 2, which were less impacted, but also for point 3, since despite several parameters having pointed its low quality, it presented increased DO qualities due to the river oxygenation. On the other hand, downstream the STS, point 4, presented variation from BAD to VERY BAD, clearly indicating the effluent impact even after treatment. The case study of Wu *et al.*<sup>20</sup> confirmed the hypothesis that water remediation pollutants based on replanting vegetation can alleviate increased pollution and enable rehabilitation of the degraded aquatic ecosystem.

**Table 4.** Water quality index for aquatic life preservation in Verde River (May-2016 to Apr-2017).

POINTS	2016								2017			
	May	Jun	Jul	Aug	Sep	Oct	Nov	Dec	Jan	Feb	Mar	Apr
P1	90	60	90	100	90	90	90	100	100	100	100	100
P2	100	60	70	100	80	90	90	100	100	100	100	100
P3	90	80	40	80	70	90	70	100	90	100	70	70
P4	30	30	40	90	30	20	10	20	20	20	10	10

The critical situation of Verde River, at this point, in terms of aquatic life maintenance capacity should be highlighted. Its ranking as a Class 2 river requires that the water presents physicochemical characteristics that favor the presence of the river natural biota. The input of the STS is the main cause of the impact, since even if the data gathered indicated that there is monitoring of the effluent in the STS, so that it is following the legal disposal regulations, the impact faced by the river is evident, suggesting that the STS flow is above the river capacity to receive input without changing its class.

#### 4. Conclusions

The trophic state index (TSI) at the points evaluated in Verde River indicated that its eutrophication status tends to hypereutrophication. The highest phosphorous concentrations in the water are associated to the domestic effluent load and the farming activity. The phosphorous and chlorophyll concentrations were over the legal limit set forth by the Resolution CONAMA n° 357 de 2005, for fresh water courses class 2. The results also revealed that the STS represent an impact factor to the Verde River, in conditions that might change the ecological balance, both for the species that occupy the river as their habitat and for other predator species that feed from other living organisms in this river. The WQI<sub>ALP</sub> results showed the critical situation of the river regarding its capacity of aquatic life maintenance, mainly downstream the effluent treatment station, which disagrees with the law that include the protection of aquatic life among the features of Class 2 waters.

#### 5. Acknowledgements

The authors would like to thanks to CAPES (Coordenação de Aperfeiçoamento de Pessoal do Ensino Superior, Brazil), PPGQA-UEPG (Programa de Pós-Graduação em Química Analítica, Universidade Estadual de Ponta Grossa, Brazil), and C-LABMU (Complexo de

Laboratórios Multiusuários) for grants and scholarships.

#### 6. References

- [1] Beghelli, F. G. de S., Carvalho, M. E. K., Peche Filho, A., Machado, F. H., Moschini-Oschini-Carlos, V., Pompêo, M. L. M., Ribeiro, A. I., Medeiros, G. A., Uso do índice de estado trófico e análise da comunidade de macroinvertebrados como indicadores da qualidade ambiental, *Brazilian Journal of Aquatic Science and Technology* 19 (1) (2015) 13-22. <https://doi.org/10.14210/bjast.v19n1.p13-22>.
- [2] Almeida, A. A., Avaliação da aplicação do IQA-CCME na divulgação da qualidade de água de Bacias Hidrográficas. Dissertação Mestrado. Universidade Federal da Bahia – UFBA, Salvador, 2014. Available from: <<http://www.ppec.ufba.br/site/publicacoes/avaliacao-da-aplicacao-do-iqa-ccme-na-divulgacao-da-qualidade-de-agua-de-bacias-hidrogr>>.
- [3] MMA. MINISTÉRIO DO MEIO AMBIENTE. SECRETARIA DE BIODIVERSIDADE E FLORESTAS. Áreas Prioritárias para a Conservação – Portaria MMA n° 9/2007, Brasília: MMA, 2007
- [4] Silva, G. S. da, Jardim, W. de F., Um novo índice de qualidade das águas para proteção da vida aquática aplicado ao rio Atibaia, região de Campinas/Paulínia - SP, *Quím. Nova* 29 (4) (2006) 689-694. <https://doi.org/10.1590/S0100-40422006000400012>.
- [5] USEPA (Environmental Protection Agency of United State), Ambient Water Quality Criteria for Dissolved Oxygen – EPA 440586003, Washington, DC, 1986.
- [6] CONAMA - CONSELHO NACIONAL DO MEIO AMBIENTE. 2005. Resolução CONAMA

357/2005. Brasil. Available from: <[www.mma.gov.br/port/conama](http://www.mma.gov.br/port/conama)>.

[7] Esteves, F. A., Fundamentos de Limnologia. 2ª ed. Rio de Janeiro: Interciência, 1988.

[8] Cavenaghi, A. L., Caracterização da qualidade de água e sedimento relacionados com a ocorrência de plantas aquáticas em reservatórios. Tese de Doutorado, Botucatu: UNESP, 2003. Available from: <<http://200.145.6.238/handle/11449/105456>>.

[9] Lamparelli, M. C., Grau de trofia em corpos d'água do estado de São Paulo: avaliação dos métodos de monitoramento, 238f, 2004. Tese de Doutorado, Universidade de São Paulo, São Paulo, 2004.

[10] Nonato, E. A., Viola, Z. G. G., Almeida, K. C. B., Schor, H. H. R., Tratamento estatístico dos parâmetros da qualidade das águas da bacia do alto curso do Rio das Velhas, Quim. Nova 30 (4) (2007) 797-804. <https://doi.org/10.1590/S0100-40422007000400008>.

[11] Ouyang, Y., Evaluation of river water quality monitoring stations by principal component analysis, Water Research, Amsterdam 39 (12) (2005) 2621-2635. <https://doi.org/10.1016/j.watres.2005.04.024>.

[12] AMERICAN PUBLIC HEALTH ASSOCIATION – APHA, 2012. Standard methods for the examination of water and wastewater, 22<sup>nd</sup> ed. Washington: APHA.

[13] Smilde, A. K., Bro, R., Principal component analysis, Anal. Methods 6 (2014) 2812-2831. <https://doi.org/10.1039/c3ay41907j>.

[14] Ferreira, M. M. C., Quimiometria - conceitos, métodos e aplicações. Campinas, SP: Editora da Unicamp, 2015.

[15] Ruzdjak, A. M., Ruzdjak, D., Evaluation of river water quality variations using multivariate statistical techniques: Sava River (Croatia): A Case Study, Environmental Monitoring and Assessment 187 (4) (2015) 1–14. <https://doi.org/10.1007/s10661-015-4393-x>.

[16] Muangthong, S., Shrestha S., Assessment of surface water quality using multivariate statistical techniques: case study of the Nampong River and Songkhram River, Thailand, Environmental Monitoring and Assessment 187 (9) (2015) article 548. <https://doi.org/10.1007/s10661-015-4774-1>.

[17] Olsen, R. L., Chappell, R. W., Loftis, J. C., Water quality sample collection, data treatment and results presentation for principal components analysis—literature review and Illinois River watershed case study, Water Research 46 (9) (2012) 3110–3122. <https://doi.org/10.1016/j.watres.2012.03.028>.

[18] Cunha, D. G. F., Falco, P. B., Calijuri, M. C., Densidade fitoplanctônica e estado trófico dos rios Canha e Pariquera-Açu, bacia hidrográfica do rio Ribeira de Iguape, SP, Brasil, Revista Ambiente & Água 3 (2) (2008). <https://doi.org/10.4136/ambiente.55>.

[19] Silva, J. A., Silva, G. H. R., Sarti, A., Tratamento de esgoto sanitário de baixa carga utilizando reator compartimentado anaeróbio/aeróbio em escala piloto, Eng. Sanit. Ambient., Rio de Janeiro 22 (3) (2017) 539-549. <https://doi.org/10.1590/s1413-41522016144668>.

[20] Wu, J., Cheng, S., Li, Z., Guo, W., Zhong, F., Yin, D., Case study on rehabilitation of a polluted urban water body in Yangtze River Basin, Environmental Science and Pollution Research 20 (2013) 7038-7045. <https://doi.org/10.1007/s11356-012-1351-9>.

## Spatial distribution of atmospheric pollutants through biomonitoring in tree bark using X-Ray fluorescence

Bruno Martins Gurgatz<sup>1</sup>, Regiani Carvalho-Oliveira<sup>2</sup>, Gisele Antoniaconi, Paulo Hilário do Nascimento Saldiva<sup>2</sup>, Luciano Fernandes Huergo<sup>1</sup>, Rodrigo Arantes Reis<sup>1\*</sup>

<sup>1</sup> Federal University of Paraná – Litoral, 512 Jaguariaíva St, Matinhos, Paraná, Brazil

<sup>2</sup> Medical School of São Paulo University (FMUSP), 455 Dr. Arnaldo Av, Cerqueira César, São Paulo

\* Corresponding author: Rodrigo Arantes Reis, phone: +55 51 3717-7545, e-mail address: [reisra@gmail.com](mailto:reisra@gmail.com)

### ARTICLE INFO

#### Article history:

Received: January 28, 2018

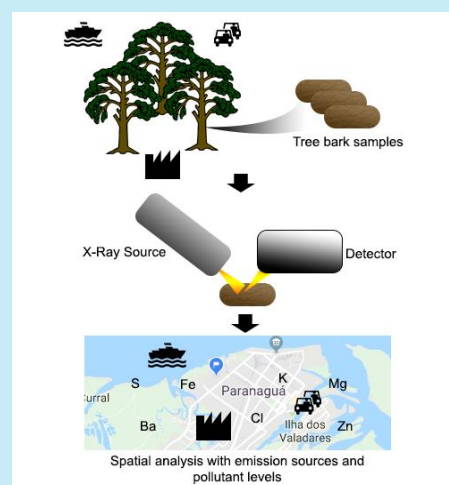
Accepted: July 4, 2018

Published: August 23, 2018

#### Keywords:

1. air pollution
2. biomonitoring
3. harbor
4. fertilizer

**ABSTRACT:** Several studies have shown that tree barks can absorb air contaminants, therefore, trees can be used as biomonitors to identify the distribution of atmospheric pollutants. The city of Paranaguá, located at the coast of the Paraná State in Brazil, hosts the largest bulk cargo port in Latin America and an elevated number of fertilizer processing industries. In this study we used tree barks coupled to X-ray fluorescence spectrometer analysis to biomonitor the distribution of air pollutants in the city of Paranaguá. We identified correlation between the levels of the elements K and Cl, with high levels detected near fertilizer warehouses. High levels of Fe were detected near railways and train stations. The low levels of Zn, Al, Ba and Mg detected in a traffic restricted zone confirmed that these elements are good indicators of vehicles traffic and validate our experimental approach of using tree barks for air pollution biomonitoring.



### 1. Introduction

It is estimated that air pollution-related diseases killed seven million people in 2012 worldwide, and air pollution it is known to be the single largest environmental risk today<sup>1</sup>. In Latin America, approximately 35,000 people die annually because of air pollution. The air pollution is the result of urbanization and industrialization processes along with a heavy dependence on fossil fuels and<sup>2,3</sup>.

Traditional methods for monitoring air quality are generally time consuming and expensive, an alternative method for air quality surveys is the use

of living organisms, a process known as biomonitoring. A biomonitor is an organism that accumulates pollutants in its tissues, acting as a sampler of pollutants<sup>4</sup>. Several studies have shown that tree barks can absorb air contaminants. Hence, trees can be used as biomonitors to identify the distribution of atmospheric pollutants<sup>5-7</sup>. In Brazil, studies have validated the use of tree barks as air biomonitor for urban traffic<sup>5</sup>, industrial activities<sup>8</sup> and environmental injustice assessment<sup>9</sup>.

The operation of ports rely on the use of several equipments contribute to air pollution including ships, trucks, and train engines<sup>10</sup>. Diesel

is widely used in port activities and is directly related to asthma, rhinitis, and the development of cancer<sup>11–13</sup>. A recent study has estimated the annual environmental costs of the Port of Kaohsiung in Taiwan at approximately 123 million dollars<sup>14</sup>.

The city of Paranaguá, located at the coast of the Paraná State in Brazil, hosts the largest bulk cargo port in Latin America. Most of the soybean produced in Brazil is exported at the Paranaguá port, this port is also a stream for the import of fertilizers that supply Brazilian crops. The Paranaguá port also attends demands of other general cargo and chemical products<sup>15</sup>. The transport of goods in and out the port is achieved mostly by the use of heavy trucks and by a railway service. The city of Paranaguá also hosts a number of fertilizer processing industries. The portuary and industry activities are the main sources of atmospheric pollution that can negatively impact in human health in the region. In this study we used tree barks coupled to X-ray fluorescence spectrometer analysis to biomonitor the distribution of air pollutants in the city of Paranaguá.

## 2. Experimental

A map of the Paranaguá city is depicted in Figure 1. The map shows the location of the port, major roads, railway, fertilizer industries, terminals and the location where samples were collected.

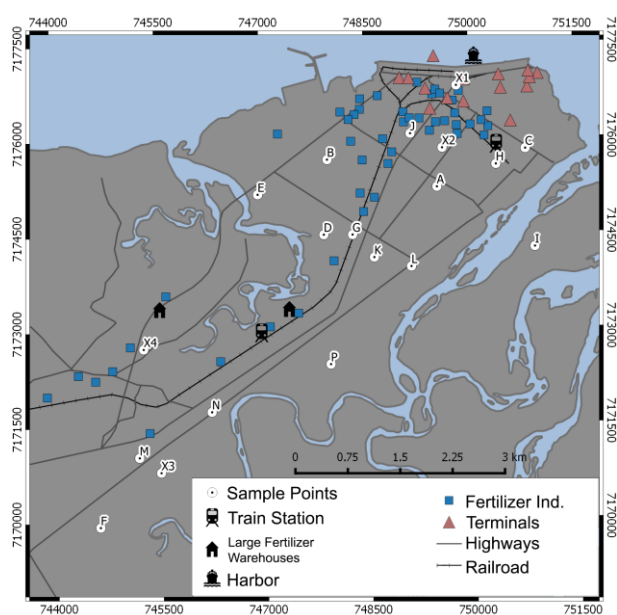


**Figure 1.** Sample points and location of the potential air pollution emission sources in Paranaguá.

Due to their wide distribution and importance, elementary schools were used as references to determine the sampling areas, 20 sampling points were selected (A-N and P). The (O) sample was lost due to sampling problems (Figure 1). Additional samples were collected in the front of the port (X1); in the center of the port area (X2); in a residential area next to the city access (X3); in the fertilizer industrial area (X4).

Due to its wide use in tropical urban environments, the barks of the tree *Terminalia catappa*, also known in Brazil as “Sombreiro” (shadow maker), were used as a bioindicator of air pollutants. The samples of the tree barks were collected using an ultrapure titanium knife at a height of 1.5–2.5 m from the soil. At each sampling site, two bark samples were collected located on different regions of the tree. To minimize the possible effects of variation due to different patterns of accumulation, these barks were mixed into a single sample for analysis. Each sample was stored in a paper bag. Information concerning the sampling site, such as the geographical coordinates and the land use around the sampling site were registered.

The tree barks were cleaned using disposable white dental brushes with nylon soft bristles to remove loosely attached particles, and then, barks were manually ground using a titanium grater until samples of 3-mm thickness were obtained. Each sample was then ground to powder using a vibratory micro mill with an agate mortar (Frisch Pulverisette 0). To ensure the homogeneity of the particle sizes, all bark samples were sieved using a 400-mesh sieve. Approximately 0.5 g of each powdered sample was transformed into 20-mm diameter tablets by applying 15 tons of pressure for 60 s. A duplicate tablet was made for each sampling site.

The content of the prepared sample was measured using an energy dispersive X-ray fluorescence spectrometer (EDX 700-HS, Shimadzu Corporation Analytical Instruments Division, Kyoto, Japan). The instrument employed a low-power Rh-target tube, at a voltage of 5–50 kV and a current of 1–1000  $\mu$ A. The characteristic X-ray radiation emitted was detected using a Si(Li) detector. X-ray fluorescence emission spectra were collected for 240 s for the elements Na–Sc and 400 s for the elements in the range of T–U on a 10 mm surface area of the samples in a vacuum. Each tree bark sample tablet was analyzed twice. The sample intensities were converted into element

concentrations ( $\mu\text{g g}^{-1}$ ) according to fundamental parameter calibrations using the NIST Standard, SRM 1547 Peach Leaves (National Institute of Standards, Gaithersburg, MD, USA). Finally, carbon, in the form of cellulose, was used as the mass balance. The sampling and analysis method was validated by Carneiro *et al.*<sup>5</sup>.

A geographic information system was used to spatialize the results obtained using X-ray fluorescence. The method of “Pretty Breaks”, traditional in geospatial software and geospatial analysis was used to create a pollutant scale. Using this method, a sequence of equally spaced and rounded values in the range of the values obtained in the samplings is calculated. The values are chosen to be 1, 2 or 5 the power of 10.

### 3. Results and discussion

The levels of the chemical elements in tree bark are shown in Table 1. In order to differentiate the pollutant emission sources in the city the following indicators were used: Cl, K and P, as indicators of the manufacture of fertilizers; Zn, Al, Ba and Mg indicators of traffic<sup>5, 16</sup>, S as heavy oils burn indicator<sup>10</sup> and Fe as indicator of railway activity<sup>17</sup>.

Potassium is one of the most used elements for crops fertilization. It is commonly applied in the salt form KCl, the association with Cl<sup>-</sup> makes the K<sup>+</sup> less leachable when applied to the soil<sup>18</sup>. The results depicted in Figure 2A shows that K and Cl have the same distribution profile, both more abundant in sites next the major fertilizer warehouses (Figure 2A). Crop chemical fertilizers are usually manufactured as a mixture of K, N and P to give the so called NPK fertilizer mixture. The results obtained showed that P has a less clear distribution than K, however, in one sample, high values of P were detected near a fertilizer warehouse (Figure 2A).

It was not possible to identify patterns for traffic-related elements (Zn, Al, Ba and Mg), the exception occurred in the sampling point I, which presented low values for all traffic-related elements. This particular sampling site is located on an Island (Ilha dos Valadares) which is a traffic restricted area with access only to emergency vehicles<sup>19</sup>. This data corroborates the use of Zn, Al, Ba and Mg as traffic indicators (Figure 2B).

**Table 1.** Sample points with coordinates and the results of the elemental tree bark analysis in ppm.

Id	Lat.	Long.	Ba	Fe	Zn	Mg	Al	P	S	K	Cl									
A	749525	7175230	94.4	-	151.7	-	32.3	-	1840.0	-	115.6	-	910.0	-	1930.0	-	1820.0	-	855.5	-
B	747958	7175679	55.5	-	104.7	-	28.9	-	2050.0	-	78.1	-	880.0	-	1890.0	-	2480.0	-	1945.6	-
C	750800	7175816	280.7	-	353.5	-	20.5	-	3150.0	-	305.5	-	810.0	-	1880.0	-	420.0	-	178.0	-
D	747891	7174497	144.8	+22.1	573.6	+87.0	26.9	+0.8	1715.0	+106.1	141.4	+3.5	1325.0	+35.4	1985.0	+7.1	1430.0	+14.1	417.8	+28.5
E	746954	7175143	330.4	-	202.4	-	21.0	-	2300.0	-	168.0	-	930.0	-	1660.0	-	4540.0	-	2983.4	-
F	744613	7169931	145.2	+55.9	184.2	+6.4	98.8	+12.5	1440.0	+14.1	151.0	+7.3	780.0	+0.0	1970.0	+14.1	2165.0	+7.1	955.2	+2.6
G	748303	7174492	106.5	+39.9	291.8	+7.1	33.9	+1.7	2090.0	+0.0	189.1	+18.2	980.0	+28.3	2570.0	+14.1	7365.0	+49.5	5504.7	+72.1
H	750376	7175575	72.3	+5.1	117.7	+15.6	20.5	+1.0	2815.0	+21.2	97.6	+18.8	1005.0	+35.4	1915.0	+21.2	780.0	+28.3	188.2	+30.5
I	750913	7174270	38.5	+10.9	49.9	+5.6	13.4	+0.9	1400.0	+14.1	43.6	+2.4	790.0	+14.1	1655.0	+7.1	980.0	+14.1	165.1	+42.8
J	749156	7176074	57.4	+24.7	139.2	+3.9	41.8	+2.9	1645.0	+21.2	143.1	+11.9	865.0	+21.2	1765.0	+35.4	1770.0	+84.9	1473.1	+68.2
K	748609	7174131	103.2	-	122.7	-	27.5	-	1290.0	-	89.9	-	990.0	-	1790.0	-	1610.0	-	897.0	-
L	749138	7173980	121.3	-	228.0	-	43.6	-	2430.0	-	137.2	-	950.0	-	1860.0	-	420.0	-	125.8	-
M	745190	7171020	22.6	-	37.7	-	11.5	-	1770.0	-	41.7	-	840.0	-	1670.0	-	1760.0	-	1415.0	-
N	746240	7171727	106.4	-	226.2	-	36.8	-	1910.0	-	150.9	-	860.0	-	1520.0	-	1750.0	-	1119.1	-
P	747957	7172455	160.3	+30.3	234.6	+0.5	25.6	+2.6	2490.0	+56.6	179.9	+15.9	985.0	+35.4	1825.0	+21.2	1010.0	+42.4	168.7	+19.0
X1	749827	7176824	186.0	+63.3	302.0	+37.6	28.0	+0.8	1090.0	+14.1	180.5	+5.4	930.0	+0.0	2495.0	+7.1	2490.0	+14.1	1183.1	+33.4
X2	749610	7175844	79.1	+9.1	101.6	+28.5	12.0	+0.0	1250.0	+14.1	67.9	+5.8	985.0	+7.1	1355.0	+7.1	1430.0	+28.3	360.5	+29.0
X3	745498	7170781	224.3	+222.2	71.3	+8.0	15.9	+0.9	2330.0	+14.1	109.9	+7.4	800.0	+14.1	1890.0	+14.1	660.0	+14.1	206.2	+35.4
X4	745278	7172728	165.7	-	240.6	-	32.7	-	2070.0	-	203.0	-	1140.0	-	2220.0	-	7780.0	-	5155.6	-

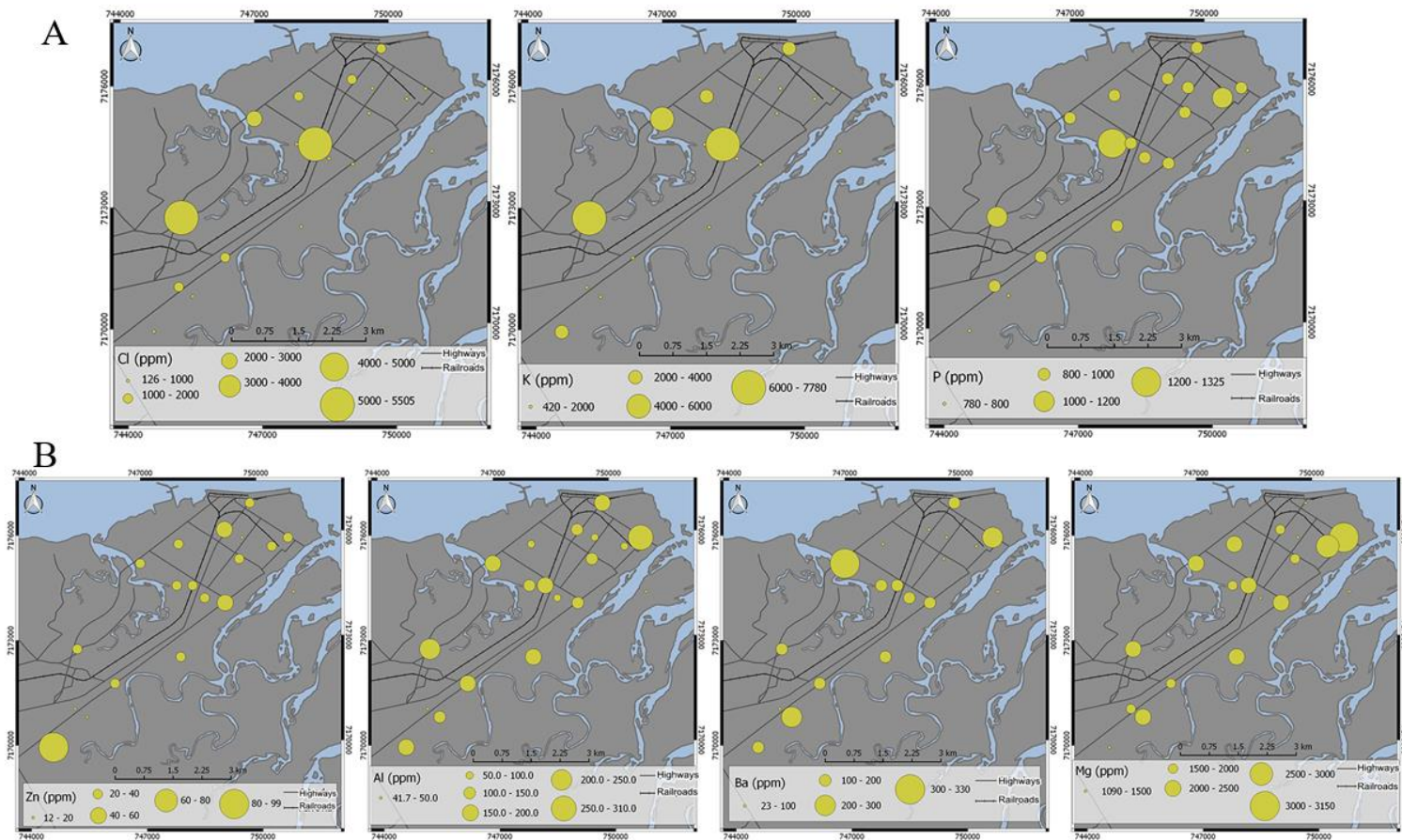


**Figure 2.** Maps of the analyzed elements according to the classification of probable emission source. (Fertilizers: Cl, K and P; Traffic: Zn, Al, Ba and Mg).

Sulphur is related to crude oil burn; this element is present in naval fuel and in low quality commercial diesel<sup>10</sup>. The distribution of S indicates that this element is abundant in sites near crossroads of heavy truck traffic and in the sampling site near the port (Figure 3A). Figure 3B

shows the distribution of Fe. The higher levels of this element were identified in sampling sites near the railway and train stations, hence, confirming the relationship between Fe levels and railways described in the literature<sup>17</sup>.

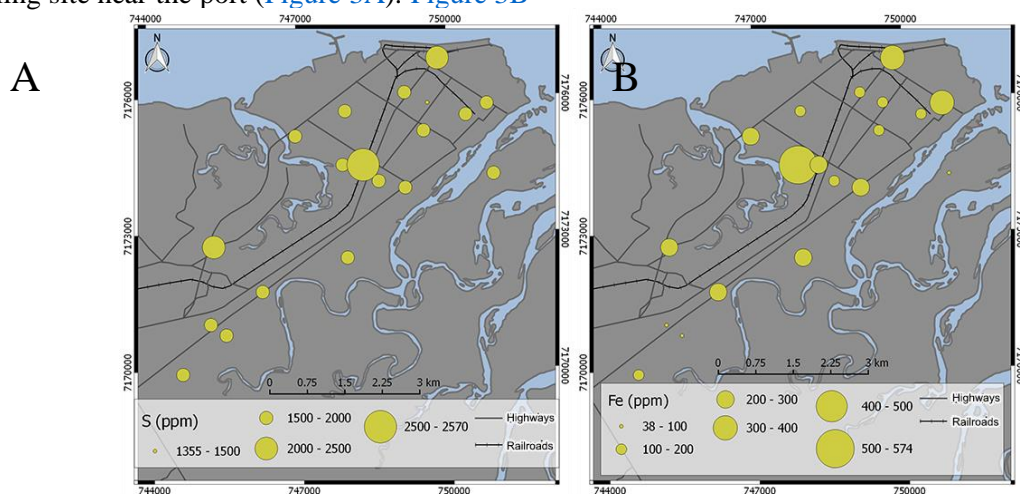


**Figure 3.** Maps of the analyzed elements according to the classification of probable emission source (A – Crude Oil and B – railroads).

#### 4. Conclusions

In this work we investigated the use of tree barks as an atmospheric pollution bioindicator aiming to determine the emission sources in a portuary context. We identified that high levels of K and Cl were detected near fertilizer warehouses. Furthermore, high levels of Fe were detected near railways and train stations. The low levels of the elements Zn, Al, Ba and Mg detected in a traffic restricted zone confirm the use of these elements as markers of vehicles traffic and validate the approach of using tree barks for air pollution biomonitoring.

#### 5. Acknowledgments

This work was funded by the Brazilian Ministry of Science, Technology and Innovation (MCTI), the Coordination for the Improvement of Higher Education Personnel - Brazil (CAPES) and the National Council for Scientific and Technological Development (CNPq).

#### 6. References

- [1] WHO, 7 million premature deaths annually linked to air pollution, WHO. (2014). <http://www.who.int> (accessed July 29, 2015).
- [2] Bell, M. L., Cifuentes, L.A., Davis, D.L., Cushing, E., Gusman Telles, A., Gouveia, N., Environmental health indicators and a case study of air pollution in Latin American cities, *Environmental Research* 111 (2011) 57–66. <https://doi.org/10.1016/j.envres.2010.10.005>.
- [3] Romieu, I., Álamo-Hernández, U., Texcalac-Sangrador, J. L., Pérez, L., Gouveia, N., McConell, R.. A contaminação atmosférica nas Américas: tendências, políticas e efeitos, in: *Determinantes Ambientais E Sociais Da Saúde*, Opas; Editora Fiocruz, Washington, 2011: pp. 475–495. <http://bases.bireme.br/cgi-bin/wxislind.exe/iah/online/?IsisScript=iah/iah.xis&src=google&base=LILACS&lang=p&nextAction=lnk&exprSearch=756802&indexSearch=ID> (accessed October 19, 2015).
- [4] Marć, M., Tobiszewski, M., Zabiegała, B., Guardia, M. de la, Namieśnik, J., Current air quality analytics and monitoring: A review, *Analytica Chimica Acta* 853 (2015) 116–126. <https://doi.org/10.1016/j.aca.2014.10.018>.
- [5] Carneiro, M.F.H., Ribeiro, F.Q., Fernandes-Filho, F.N., Lobo, D.J.A., Barbosa Jr., F., Rhoden, C.R., Mauad, T., Saldiva, P. H. N., Carvalho-Oliveira, R., Pollen abortion rates, nitrogen dioxide by passive diffusive tubes and bioaccumulation in tree barks are effective in the characterization of air pollution, *Environmental and Experimental Botany*. 72 (2011) 272–277. <https://doi.org/10.1016/j.envexpbot.2011.04.001>.
- [6] Guéguen, F., Stille, P., Millet, M., Air quality assessment by tree bark biomonitoring in urban, industrial and rural environments of the Rhine Valley: PCDD/Fs, PCBs and trace metal evidence, *Chemosphere* 85 (2011) 195–202. <https://doi.org/10.1016/j.chemosphere.2011.06.032>.
- [7] Senhou, A., Chouak, A., Cherkaoui, R., Moutia, Z., Lferde, M., Elyahyaoui, A., Khoukhi, T.E., Bounakhla, M., Embarche, K., Gaudry, A., Ayrault, S., Moskura, M., Sensitivity of biomonitors and local variations of element concentrations in air pollution biomonitoring, *Journal of Radioanalytical and Nuclear Chemistry* 254 (2002) 343–349. <https://doi.org/10.1023/A:1021688203179>.
- [8] Ferreira, A. B., Santos, J. O., Souza, S. O., Júnior, W. N. S., Alves, J. do P. H., Use of passive biomonitoring to evaluate the environmental impact of emissions from cement industries in Sergipe State, northeast Brazil, *Microchemical Journal* 103 (2012) 15–20. <https://doi.org/10.1016/j.microc.2011.12.008>.
- [9] Gurgatz, B. M., Carvalho-Oliveira, R., Oliveira, D. C. de, Jouscoski, E., Antoniaconi, G., Saldiva, P. H. do N., Reis, R. A., Atmospheric metal pollutants and environmental injustice: A methodological approach to environmental risk analysis using fuzzy logic and tree bark, *Ecological Indicators* 71 (2016) 428–437. <https://doi.org/10.1016/j.ecolind.2016.07.028>.
- [10] Bailey, D., Solomon, G., Pollution prevention at ports: clearing the air, *Environmental Impact Assessment Review* 24 (2004) 749–774. <https://doi.org/10.1016/j.eiar.2004.06.005>.

- [11] Silverman, D.T., Is diesel exhaust a human lung carcinogen?, *Epidemiology*. 9 (1998) 4–6. <https://www.ncbi.nlm.nih.gov/pubmed/9430259>.
- [12] Dawson, S. V., Alexeeff, G. V., Multi-Stage Model Estimates of Lung Cancer Risk from Exposure to Diesel Exhaust, Based on a U.S. Railroad Worker Cohort, *Risk Analysis* 21 (2001) 1–18. <https://doi.org/10.1111/0272-4332.211085>.
- [13] Pandya, R. J., Solomon, G., Kinner, A., Balmes, J. R., Diesel exhaust and asthma: hypotheses and molecular mechanisms of action., *Environ Health Perspect.* 110 (2002) 103–112. <https://www.ncbi.nlm.nih.gov/pubmed/11834468>.
- [14] Berechman, J., Tseng, P.-H., Estimating the environmental costs of port related emissions: The case of Kaohsiung, *Transportation Research Part D: Transport and Environment* 17 (2012) 35–38. <https://doi.org/10.1016/j.trd.2011.09.009>.
- [15] Campos Neto, C.A. da S., Pêgo Filho, B., Romminger, A. E., Ferreira, I. M., Portos brasileiros 2009: ranking, área de influência, porte e valor agregado médio dos produtos movimentados, (2009). <http://repositorio.ipea.gov.br/handle/11058/2606> (accessed January 13, 2017).
- [16] Guéguen, F., Stille, P., Dietze, V., Gieré, R., Chemical and isotopic properties and origin of coarse airborne particles collected by passive samplers in industrial, urban, and rural environments, *Atmospheric Environment* 62 (2012) 631–645. <https://doi.org/10.1016/j.atmosenv.2012.08.044>.
- [17] Gehrig, R., Hill, M., Lienemann, P., Zwicky, C. N., Bukowiecki, N., Weingartner, E., Baltensperger, U., Buchmann, B., Contribution of railway traffic to local PM10 concentrations in Switzerland, *Atmospheric Environment* 41 (2007) 923–933. <https://doi.org/10.1016/j.atmosenv.2006.09.021>.
- [18] Ernani, P. R., Bayer, C., Almeida, J.A. de, Cassol, P. C., Vertical mobility of cations as influenced by the method of potassium chloride application to variable charge soils, *Revista Brasileira de Ciência do Solo* 31 (2007) 393–401. <https://doi.org/10.1590/S0100-06832007000200022>.
- [19] Toledo, A. do R., Sistema pronominal possessivo em uso na Ilha dos Valadares, (2010). <http://dspace.c3sl.ufpr.br:8080/dspace/handle/1884/24437> (accessed November 20, 2015).

## Removal of pesticide residues after simulated water treatment: by-products and acetylcholinesterase inhibition

Rafael Oliveira Costa<sup>1</sup>, Polyana Soares Barcellos<sup>1</sup>, Maria Cristina Canela<sup>1</sup>

<sup>1</sup> Universidade Estadual do Norte Fluminense Darcy Ribeiro, 2000, Alberto Lamego Av, Campos dos Goytacazes, Rio de Janeiro, Brazil.

<sup>2</sup> Instituto Federal Fluminense, Campus Quissamã, 727, Amilcar Pereira da Silva Av, Quissamã, Rio de Janeiro, Brazil.

\* Corresponding author: Maria Cristina Cristina Canela, phone: e-mail address: [mccanela@gmail.com](mailto:mccanela@gmail.com)

### ARTICLE INFO

#### Article history:

Received: February 11, 2018

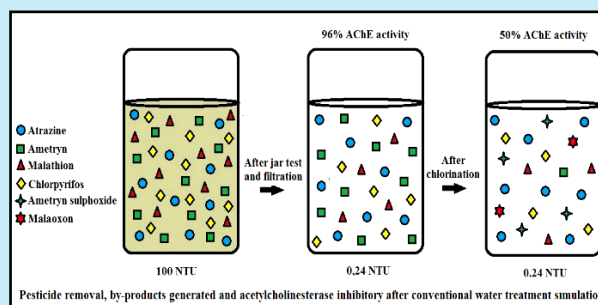
Accepted: June 10, 2018

Published: August 23, 2018

#### Keywords:

1. drinking water
2. pesticides
3. chlorination
4. by-products
5. acetylcholinesterase inhibition

**ABSTRACT:** Water is of extreme importance to living creatures. However, due to the actions of humans, water resources have been contaminated by many different compounds, including pesticides. Pesticides in water sources can cause damage to aquatic environments or to those who consume it. On this basis, it is important that water treatment systems can remove these pollutants from water. In this perspective, the objective is to investigate whether conventional water treatment can remove several pesticides, namely, atrazine, ametryn, malathion and chlorpyrifos. According to the results, it was observed that conventional treatment after filtration was not capable of removing these pesticides efficiently, with the organophosphorus pesticides (malathion and chlorpyrifos) removed in a higher percentage than the triazines (atrazine and ametryn). Post-chlorination reduced the pesticide levels, however, malaosxon and ametryn sulphoxide by-products were generated, which caused greater acetylcholinesterase inhibition.



### 1. Introduction

Due to its physical and chemical properties, water was essential for the emergence of the first living organisms, as well as their evolution. It is the most abundant compound in living systems, accounting for ~70% or more of the weight of most organisms, and it plays important roles in their metabolisms. Because it is an essential compound for survival, any contamination can cause damage to humans and the environment<sup>1</sup>.

The indiscriminate use of pesticides to accelerate food production, especially in developing countries, has resulted in contamination of natural waters, causing a serious threat to the environment in many parts of the world<sup>2</sup>.

Pesticides are chemical compounds used to kill different kinds of pests that cause damage to crop, such as insects, fungi and undesirable plants (weeds)<sup>3</sup>, as well as being used to protect food products during processing, storage and transport<sup>4</sup>. Pesticides, due to their nature, are potentially toxic to other organisms, including humans<sup>3</sup>.

Acute exposure to pesticides can lead to death or serious illness<sup>5</sup>. Chronic exposure can impair the function of the endocrine, nervous, renal, immune, reproductive, respiratory and cardiovascular systems<sup>6</sup>. From this perspective, there is evidence relating pesticide exposure and the incidence of chronic human diseases, including cancer<sup>7</sup>, Parkinson's disease<sup>8</sup>, Alzheimer's disease<sup>9</sup>, asthma<sup>10</sup>, multiple sclerosis<sup>11</sup>, diabetes<sup>12</sup>,

premature aging<sup>13</sup>, reproductive disorders,<sup>14,15</sup> cardiovascular disease<sup>16</sup> and chronic kidney disease<sup>17</sup>.

Brazil is the world's largest consumer of pesticides and is responsible for ~20% of the total<sup>18</sup>. In 2014, 317 active ingredients were commercialized in Brazil, consuming ~500 thousand tons of pesticides<sup>19</sup>.

Only 0.1% of the pesticides reach the target during application, while the remaining 99.9% has the potential to move to the environment, including surface and groundwater<sup>20</sup>. Thus, there is concern whether conventional water treatment systems can efficiently eliminate these contaminants. Only a few studies have been carried out with organic compounds in treated waters, and most of these studies are with pharmaceuticals and endocrine disrupters<sup>21</sup>.

Brazilian conventional water treatment facilities typically use coagulation, flocculation, sedimentation and filtration for the removal of suspended solids and dissolved organic carbon, followed by chlorination for disinfection. This system has been shown to be largely ineffective in removing emerging micropollutants (e.g.,

endocrine-disrupting compounds, pharmaceuticals, personal care products and pesticides) and the addition of chlorine can result in the reaction and transformation of these compounds<sup>21–23</sup>. Advanced treatment technologies, such as ozonation and advanced oxidation processes, activated carbon adsorption, reverse osmosis and nanofiltration, are effective in removing these compounds<sup>22</sup>. Despite this, due to their high cost, advanced processes in water treatment facilities are still limited, especially in developing countries, like Brazil<sup>24</sup>.

Therefore, the main objective of this work is to verify, by means of simulations, whether a conventional Brazilian water treatment system could remove some selected pesticide, namely, atrazine and ametryn, which belong to the class of triazines, and the organophosphorus pesticides, malathion and chlorpyrifos (Figure 1). These pesticides were chosen because they have recently been reported in the literature due to their high concentration in Brazilian surface waters, above the tolerable limit for aquatic life<sup>18</sup>.

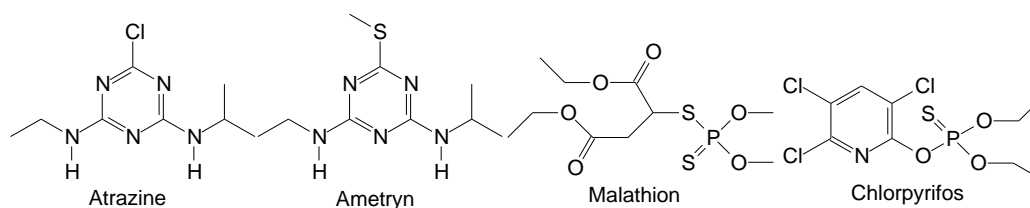


**Figure 1.** Pesticides used in this research.

## 2. Experimental

### 2.1. Materials and reagents

Atrazine (98.8% purity), ametryn (98.5% purity), chlorpyrifos (99.2% purity) and Malathion (99.1% purity) were purchased from Sigma-Aldrich. Aluminium sulfate ( $\text{Al}_2(\text{SO}_4)_3 \cdot 18\text{H}_2\text{O}$ , analytical grade) and calcium hydroxide ( $\text{Ca}(\text{OH})_2$ , analytical grade) were obtained from VETEC Química Fina Ltda. Kaolin was purchased from Prominérios Comércio de Minérios Ltda. and commercial sodium hypochlorite was obtained from Indústrias Anhembi Ltda. The concentration of the sodium hypochlorite solution was confirmed by a standard sodium thiosulfate titration<sup>25</sup>.

Stock solutions of  $800 \text{ mg L}^{-1}$  of the individual pesticides were prepared in pure acetone. All the

stock solutions were stored in amber glass bottles at  $4^\circ\text{C}$ .

The experimental artificial sample was prepared by adding a kaolin suspension with  $100 \pm 5$  NTU turbidity (TB100p MS Tecnopton) and 450 uH apparent color (Alfakit equipment)<sup>21</sup>. Organic and inorganic compounds were not added to artificial water because the aim was to isolate the variables and verify the treatment without interferences. The effect of a real matrix will be investigated in the next step of this work.

### 2.2. Experimental procedures

#### 2.2.1 Analytical method and recuperation tests

The method of analysis used to quantify the pesticides and to identify the by-products was based on the extraction/concentration of these

substances by means of solid phase extraction. Samples of 50 mL were submitted to solid phase extraction employing OPT 3 mL × 60 mg. Agilent cartridges were conditioned with 6.0 mL of methanol and 6.0 mL of ultrapure water in a 12-port vacuum manifold system. The analytes were then eluted using 7.5 mL of ethyl acetate with subsequent quantification by GC-MS.

#### Parent compound quantification

The extracts were analyzed by GC-MS (Shimadzu GC - 17A and MS - QP 5050) using selected ion monitoring mode. In the experiments, the injection volume was 1 µL and a VF-5ms capillary column (Varian, 30 m, I.D. 0.25 mm, 0.25 µm) was used. A flow rate of 1 mL min<sup>-1</sup> of helium gas, with a constant pressure of 203 kPa and a 1:10 split ratio was used. The oven temperature started from 100 °C then increased at 25 °C min<sup>-1</sup> to 250 °C and finally increased at 15 °C min<sup>-1</sup> to 270 °C. Temperatures were set at 240 °C in the injector and 230 °C in the interface to the detector. The ions monitored for atrazine detection were: m/z 215, 200 and 173; for ametryn: m/z 227, 212 and 170; for malathion: 173, 125 and 93; for chlorpyrifos: 314, 197 and 97. Quantification was performed by external standardization, with the area obtained compared with the appropriate analytical curve (Table 1)<sup>26</sup>.

#### By-product identification

The by-products of the pesticides were also analyzed by GC-MS using similar conditions as described for the parent compounds. A split ratio of 1:10, an injection volume of 1 µL and scan mode were used for this analysis. Compounds were identified using fragmentation analysis, and isotope clustering patterns were found with the aid of the NIST library.

Preliminary tests were carried out to evaluate the recovery of the pesticides in the aqueous matrixes used in the experiments to determine the efficiency of the extraction method. The pesticide recovery ratio was determined (in triplicate) by comparing peak areas from water samples spiked with a known amount of non-extracted pure standards. The linearity of the method, calibration equation, limit of detection (LOD) and limit of quantification (LOQ) were also determined (Table 1). The detection and quantification limits were calculated using the standard deviation of the blank (synthetic water extract after simulated water treatment without pesticides) from the following equations<sup>27</sup>:

$$LOD = 3.3 \times (\text{blank standard deviation})/\text{slope} \quad (\text{Equation 1}).$$

$$LOQ = 10 \times (\text{blank standard deviation})/\text{slope} \quad (\text{Equation 2}).$$

**Note:** Slope: Angular coefficient of the analytical curve.

**Table 1.** Detection (LOD) and quantification (LOQ) limits, mean percentage recovery (% R), calibration equation\* and coefficients of correlation ( $r^2$ ) for the experimental solutions.

Pesticide	Calibration equation	$r^2$	% R	LOD (ng L <sup>-1</sup> )	LOQ (ng L <sup>-1</sup> )
Atrazine	$y = 9.96 \cdot 10^5 x - 1.16 \cdot 10^4$	0.997	99±1	8.11	24.58
Ametryn	$y = 1.20 \cdot 10^6 x - 2.83 \cdot 10^4$	0.998	95±2	6.76	20.49
Malathion	$y = 1.88 \cdot 10^6 x - 3.63 \cdot 10^4$	0.998	112±3	4.29	13.02
Chlorpyrifos	$y = 1.14 \cdot 10^6 x - 1.51 \cdot 10^4$	0.997	79±2	7.08	21.44

\*Calibration equation was obtained by mixing the pesticides in synthetic water (100 NTU of turbidity) at concentrations of 0.48, 0.40, 0.32, 0.24, 0.16 and 0.08 mg L<sup>-1</sup>.

#### 2.2.2 Determining optimum operating conditions for jar test

The tests were carried out with the artificial sample mentioned in Section 2.1 using jar test

Trade Lab Ambiental equipment to obtain the ideal condition of turbidity removal. Then, the pair of values "coagulant dosage × coagulation pH" was varied.

An aluminum sulphate solution (1% w/v) was used to facilitate the coagulation in the water and a calcium hydroxide solution (0.5% w/v) was used for adjusting the pH values<sup>25</sup>.

### 2.2.3 Jar test procedures

Bench tests were performed in triplicate using the jar test method to reproduce the conventional water treatment systems, i.e., coagulation-flocculation and decantation, followed by filtration. The pesticides were added to synthetic water (pH corrected according to Section 2.2.2) at a concentration of 0.48 mg L<sup>-1</sup> for each compound, and their removal was verified according to Section 2.2.1.

The jar test was performed according to Brazilian standard NBR 12.216: 1992 and by the Practical manual of water analysis from the National Health Foundation to better represent the operations of the treatment plants of water, as follows:

Rapid mixture: dispersion of aluminum sulphate in 1 L of water sample to be treated, with a maximum speed of 100 rpm for 3 min;

Mechanized flocculation: total time of 10 min, with agitation speed of 50 rpm;

Decantation: the sample was left to decant for ~15 min, which corresponds to a sedimentation rate of 1.74 cm min<sup>-1</sup> (treatment plant with capacity of up to 1,000 m<sup>3</sup> day<sup>-1</sup>).

Filtration of the samples was done by gravity using 125 mm diameter filter paper. In the last step, chlorination, sodium hypochlorite was added in a dosage that resulted in 5 mg L<sup>-1</sup> of chlorine, a concentration as indicated by the Ministry of Health Ordinance N° 2914 of 12/12/2011. After this process, an aliquot of each test was removed and submitted to the analysis, as described in the following sections.

### 2.2.4 Acetylcholinesterase inhibitory activity

Determination of the AChE inhibitory activity was carried out according to the Ellman method, modified as follows<sup>28</sup>. This method is based on the amount of thiocholine released when AChE hydrolyses the substrate acetylthiocholine iodide. The product thiocholine reacts with Ellman's reagent (DTNB) to produce a yellow compound [5-thio-2-(nitrobenzoate)], which can be detected at 405 nm. In each well of a 96-well plate, 65 µL of PBS (0.2 mol·L<sup>-1</sup> phosphate buffer, pH 7.2), 10 µL

of sample\* and 10 µL of AChE (1300 U mg<sup>-1</sup>) were added. The mixture was kept at 37 °C for 3 h. Subsequently, 65 µL of 1.00 mmol L<sup>-1</sup> acetylcholine iodide and 65 µL of 1.00 mmol L<sup>-1</sup> Ellman's reagent (DTNB dissolved in 0.2 mol L<sup>-1</sup> phosphate buffer pH 7.2) were added. Then, the absorbance was measured at 405 nm using a microplate reader (ELX800 Biotec) in triplicate experiments. The enzymatic activity was calculated as a percentage of the velocities of each sample compared to the control. The inhibitory activity was calculated from one hundred percentage subtracted by the percentage of enzyme activity.

\*Control - 10 µL of ultrapure water. Chlorine - 10 µL chlorine solution (5 mg L<sup>-1</sup>). After filtration - 10 µL solution after filtration. Postchlorination - 10 µL solution after 30 min reaction time with chlorination.

## 3. Results and discussion

### 3.1 Determining optimum operating conditions for jar test

The optimal conditions for the treatment of 1 L of water at 100 NTU were using 20 mL of aluminum sulphate solution (1% w/v) and pH 10.5, or 15 mL of calcium hydroxide solution (0.5% w/v), conditions which provided a turbidity of 0.24 NTU and 0.0 uH apparent color. All results considered in this study meet the standards for turbidity and apparent color, set forth in Brazilian legislation from the Ministry of Health for drinking water standards. Therefore, these were the parameters used in the pesticide removal test in the simulation of conventional water treatment.

### 3.2 Pesticide removal

As shown in Figure 2, it was observed that after filtration, the pesticides were not removed efficiently. The organophosphorus compounds were removed in a higher percentage (malathion: 62.21 ± 0.01%, chlorpyrifos: 43.8 ± 0.9%) than the triazines (atrazine: 10.8 ± 0.6%, ametryn: 14.8 ± 0.3%). As the flake formation phenomenon in the treatment of water is carried out by electrostatic attraction, it is inferred that the organophosphorus compounds have been removed in greater percentage due to the presence of the phosphate group, which would allow a greater attraction to the

particles, and consequently, greater efficiency in the decantation/filtration process.

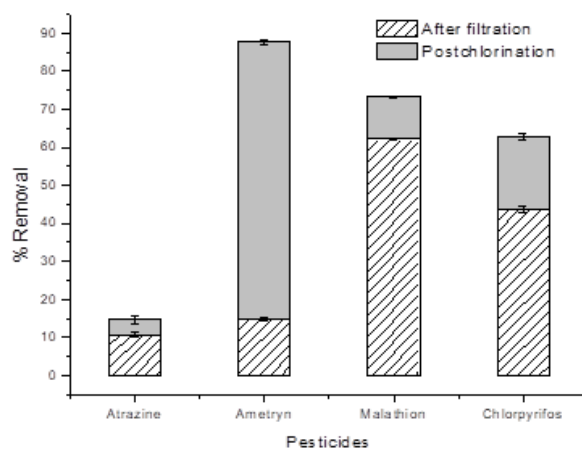


**Figure 2.** Average percentage of pesticide removal after treatment.

After the chlorination, the removal of pesticides increased, and lower and higher percentages were found for atrazine ( $15 \pm 1\%$ ) and ametryn ( $87.7 \pm 0.5\%$ ), respectively. The organophosphorus malathion and chlorpyrifos were eliminated by  $73.2 \pm 0.2\%$  and  $62.9 \pm 0.8\%$ , respectively. Despite the increased removal of pesticides, according to

**Figure 3**, two by-products were detected in the post-chlorination step. According to the NIST library, the first by-product is malaoxon and the second is an ametryn-derived compound, as shown in **Figure 3B**. Li *et al.*<sup>29</sup> reported that the oxidation of malathion by chlorination generates malaoxon.

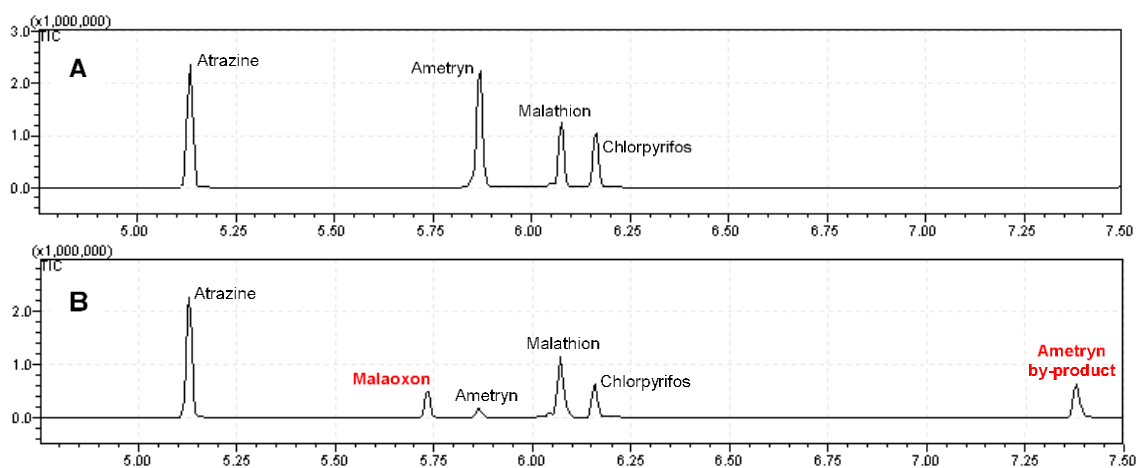


**Figure 3.** GC-MS chromatogram scan mode: A – After filtration; B – Post-chlorination.

Using the ametryn-derived fragmentation analysis (**Figure 4**), we found the molecular ion with a mass to charge ratio of 243, the molecular ametryn ion is  $m/z = 227$ , resulting in an increase equal to 16 in its mass value. This difference is consistent with the oxidation product of ametryn, derived from the reaction with sodium

hypochlorite, generating ametryn sulfoxide, as reported by Lopez and collaborators<sup>30</sup>. This by-product formation justifies the marked difference in the removal of ametryn compared with atrazine, due to the methyl sulfide group ( $R-S-CH_3$ ), which is susceptible to reaction with sodium hypochlorite.

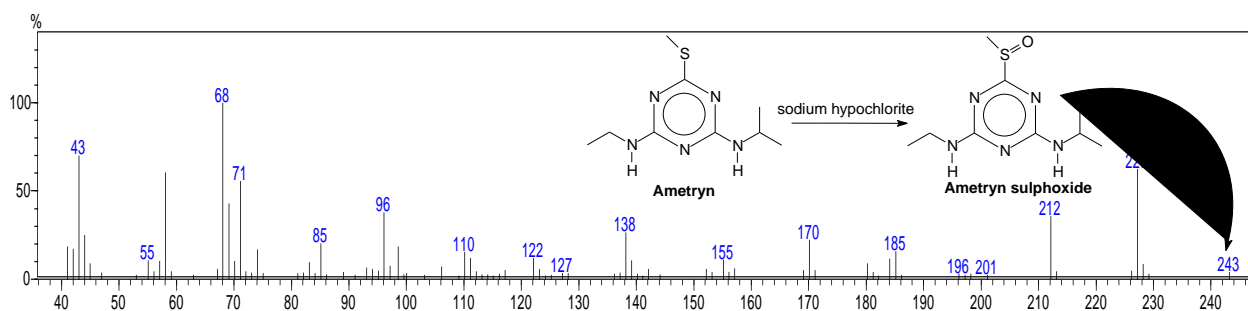


**Figure 4.** GC-MS mass spectra for ametryn by-product.

There are other studies on water treatment plant simulation that note that the conventional model is not efficient for the removal of pesticides, such as Soares *et al.*<sup>21</sup>, whose objective was to verify the removal of endosulfan, ethylenethiourea and 1,2,4-triazole. At the end of the experiments, they verified that 54% of endosulfan, 11% of ethylenethiourea and 18% of 1,2,4-triazole were removed<sup>21</sup>. Li *et al.*<sup>29</sup> also found that after the treatment process, the organophosphorus diazinon and tolclofos-methyl (initial concentration of 50  $\mu\text{g L}^{-1}$ ) were removed by *ca.* 63% and 49%, respectively, after filtration. These results are very similar to those found in the removal of the organophosphorus pesticides malathion and chlorpyrifos presented here.

### 3.3 Acetylcholinesterase inhibitory activity

According to Table 2, it is observed that the sample containing chlorine did not show significant difference to the control, in other words, chlorine was not capable of inhibiting the acetylcholinesterase enzyme. Alternatively, it is known that organophosphates have the ability to inhibit such enzymes<sup>31–33</sup>, which explains the inhibition generated after filtration, i.e., this treatment was not effective in removing such compounds. There are not studies demonstrating that atrazine and ametryn alone are capable of inhibiting AChE. However, during toxicity bioassays, the atrazine in combination with chlorpyrifos decreased significantly the acetylcholinesterase activity as compared to chlorpyrifos only treatments<sup>34</sup>. Studies show that atrazine enhances the uptake and facilitates the biotransformations of chlorpyrifos to chlorpyrifos-oxon<sup>35</sup>.

**Table 2.** Acetylcholinesterase activity (AChE).

Sample	% AChE activity
Control	100 $\pm$ 2
Chlorine	100 $\pm$ 1
After filtration	96 $\pm$ 1
Post-chlorination	51 $\pm$ 2

After chlorination, 50% enzyme inhibition was found, which is an indication that the compounds formed were more toxic than their parents. Based on Figure 3B, we observed the formation of two by-products, malaoxon and ametryn sulfoxide. It is known that the oxidation of organophosphorus generates more toxic products, the oxons, which are more efficient in inhibiting AChE<sup>27–29</sup>. In this perspective, we expected that the enzyme inhibition would be accentuated, since malaoxon was generated after the chlorination. The effect of ametryn sulfoxide is still unknown, however this will be investigated in the next step of this work.

## 4. Conclusions

Based on the results, we verified that the conventional water treatment was not effective in removing atrazine, ametryn, malathion and chlorpyrifos pesticides. Organophosphorus compounds were removed in higher percentages than the triazines.

It was observed that the post-chlorination water became more toxic, because the enzyme acetylcholinesterase activity reached at 50%, indicating that the malaoxon was one of the responsible by-products. It is not yet known if the ametryn oxidation by-product, ametryn sulfoxide, is capable of inhibiting this enzyme, this action will be verified in future experiments by testing only this by-product.

Based on the toxicity of pesticides and their post-chlorination by-products, water quality control measures and treatment systems improvement are necessary to allow further removal of these contaminants at levels that are not a hazard to the population.

## 5. Acknowledgments

The authors thank the INCTAA (FAPESP, proc. 465768/2014-8 and CNPq proc. 573894/2008-6) by the financial support.

## 6. References

- [1] Nelson, D. L., Cox, M. M., Lehninger Principles of Biochemistry, Artmed, Porto Alegre, 6th ed., 2014, ch2.
- [2] Sivagami, K., Krishna, R. R., Swaminathan, T., Photocatalytic degradation of pesticides in immobilized bead photo reactor under solar irradiation, *Sol. Energy* 103 (2014) 488-493. <https://doi.org/10.1016/j.solener.2014.02.001>.
- [3] WHO – World Health Organization, Geneva (2018), Pesticides [online], Available from: <<http://www.who.int/topics/pesticides/en/>>.
- [4] FAO - Food and Agriculture Organization of the United Nations, Roma (2010), International Code of Conduct on the Distribution and Use of Pesticides [online], Available from: <<http://www.fao.org/docrep/005/Y4544E/y4544e00.htm>>.
- [5] WHO – World Health Organization, Geneva (1990), Public health impact of pesticides used in agriculture [online], Available from: <<http://www.who.int/iris/handle/10665/61414>>.
- [6] Mostafalou, S., Abdollahi, M., Pesticides and human chronic diseases: Evidences, mechanisms, and perspectives, *Toxicol. Appl. Pharm.* 268 (2013) 157-177. <https://doi.org/10.1016/j.taap.2013.01.025>.
- [7] Koutros, S., Silverman, D. T., Alavanja, M. C. R., Andreotti, G., Lerro, C. C., Heltshe, S., Lynch, C. F., Sandler, D. P., Blair, A., Freeman, L. E. B., Occupational exposure to pesticides and bladder cancer risk, *Int. J. Epidemiol.* 45 (3) (2016) 792-805. <https://doi.org/10.1093/ije/dyv195>.
- [8] Pezzoli, G., Cereda, E., Exposure to pesticides or solvents and risk of Parkinson disease, *Neurology* 80 (22) (2013) 2035-2041. <https://doi.org/10.1212/WNL.0b013e318294b3c8>.
- [9] Jones, N., Alzheimer disease: risk of dementia and Alzheimer disease increases with occupational pesticide exposure, *Nat. Rev. Neurol.* 6 (7) (2010) 353. <https://doi.org/10.1038/nrneurol.2010.80>.
- [10] Amaral, A. F. S., Pesticides and asthma: challenges for epidemiology, *Front. Public Health* 2 (6) (2014) 1-3. <https://doi.org/10.3389/fpubh.2014.00006>.
- [11] Bonvicini, F., Marcello, N., Mandrioli, J., Pietrini, V., Vinceti, M., Exposure to pesticides and risk of amyotrophic lateral sclerosis: a population-based case-control study, *Ann. Ist. Super. Sanita.* 46 (3) (2010) 284-287. [https://doi.org/10.4415/ANN\\_10\\_03\\_10](https://doi.org/10.4415/ANN_10_03_10).
- [12] Jaacks, L. M., Staimez, L. R., Association of persistent organic pollutants and non-persistent pesticides with diabetes and diabetes-related health outcomes in Asia: a systematic review, *Environ. Int.* 76 (2015) 57-70. <https://doi.org/10.1016/j.envint.2014.12.001>.
- [13] Gravina, S., Vijg, J., Epigenetic factors in aging and longevity, *Pflug. Arch. Eur. J. Phy.* 459 (2) (2010) 247-258. <https://doi.org/10.1007/s00424-009-0730-7>.
- [14] Saadi, S., Abdollahi, M., Is there a link between human infertilities and exposure to pesticides? *Int. J. Pharmacol.* 8 (8) (2012) 708-710. <https://doi.org/10.3923/ijp.2012.708.710>.
- [15] Frazier, L. M., Reproductive disorders associated with pesticide exposure, *J. Agromedicine* 12 (1) (2007) 27-37. [https://doi.org/10.1300/J096v12n01\\_04](https://doi.org/10.1300/J096v12n01_04).
- [16] Morton, W. E., Hypertension in Oregon pesticide-formulating workers. *J Occup Med.* 17 (3) (1975) 182-185. Available from: <<https://www.ncbi.nlm.nih.gov/pubmed/1123687>>.

- [17] Siddharth, M., Datta, S. K., Bansal, S., Mustafa, M., Banerjee, B. D., Kalra, O. P., Tripathi, A.K., Study on organochlorine pesticide levels in chronic kidney disease patients: association with estimated glomerular filtration rate and oxidative stress, *J. Biochem. Mol. Toxicol.* 26 (6) (2012) 241-247. <https://doi.org/10.1002/jbt.21416>.
- [18] Albuquerque, A. F., Ribeiro, J. S., Kummrow, F., Nogueira, A. J. A., Montagner, C. C., Umbuzeiro, G. A., Pesticides in Brazilian freshwaters: a critical review, *Environ. Sci.: Processes Impacts* 18 (2016) 779-787. Available from: <http://pubs.rsc.org/en/content/articlelanding/2016/em/c6em00268d/unauth#!divAbstract>.
- [19] BRASIL, IBAMA – Ministério do Meio Ambiente, Relatórios de comercialização de agrotóxicos, Brasília, 2016. Available from: <http://www.ibama.gov.br/agrotoxicos/relatorios-de-comercializacao-de-agrotoxicos>.
- [20] Younos, T. M., Weigmann, D. L., Pesticides: A continuing dilemma, *J. Water Pollut. Con. F.* 60 (7) (1988) 1199-1205. Available from: <https://www.jstor.org/stable/i25043616?refreqid=excelsior%3Af302eef8f9935f088ff07fe88c6dad7b>.
- [21] Soares, A. F. S., Leão, M. M. D., Vianna Neto, M. R., Costa, E. P., Oliveira, M. C., Amaral, N. B., Efficiency of conventional drinking water treatment process in the removal of endosulfan, ethylenethiourea, and 1,2,4-triazole, *J. Water Supply Res. T.* 62 (6) (2013) 367-376. <https://doi.org/10.2166/aqua.2013.042>.
- [22] Westerhoff, P., Yoon, Y., Snyder, S., Wert, E. Fate of endocrine-disruptor, pharmaceutical, and personal care product chemicals during simulated drinking water treatment processes. *Environ Sci Technol.* 39 (2005) 6649-6663. <https://doi.org/10.1021/es0484799>.
- [23] Jin, X., Peldszus, S. Selection of representative emerging micropollutants for drinking water treatment studies: A systematic approach, *Sci. Total Environ.* 414 (2012) 653-663. <https://doi.org/10.1016/j.scitotenv.2011.11.035>.
- [24] Rigobello, E. S., Dantas, A. D., Di Bernardo, L., Vieira, E. M. Removal of diclofenac by conventional drinking water treatment processes and granular activated carbon filtration, *Chemosphere* 92 (2013) 184-191. <https://doi.org/10.1016/j.chemosphere.2013.03.010>.
- [25] BRASIL, Fundação Nacional de Saúde. Manual prático de análise de água. 4ª ed. - Brasília: Fundação Nacional de Saúde, 2013. Available from: [http://www.funasa.gov.br/site/wp-content/files\\_mf/manual\\_pratico\\_de\\_analise\\_de\\_a\\_gua\\_2.pdf](http://www.funasa.gov.br/site/wp-content/files_mf/manual_pratico_de_analise_de_a_gua_2.pdf).
- [26] Araújo, T. M. R., Canela, M. C., Miranda, P. C. M. L., Photochemical nitro-nitrite rearrangement in methyl parathion decay under tropical conditions, *J. Environ. Sci. Heal. B.* 48 (2013) 251-259. <https://doi.org/10.1080/03601234.2013.743750>.
- [27] Ribani, M., Bottoli, C. B. G., Collins, C. H., Jardim, I. C. S. F., Melo, L. F. C., Validação em métodos cromatográficos e eletroforéticos, *Quim. Nova* 27 (5) (2004) 771-780. <https://doi.org/10.1590/S0100-40422004000500017>.
- [28] Ellman, G. L., Courtney, D. K., Andres, V., Featherstone, R. M., A new and rapid colorimetric determination of acetylcholinesterase activity, *Biochem. Pharmacol.* 7 (2) (1961) 88-95. [https://doi.org/10.1016/0006-2952\(61\)90145-9](https://doi.org/10.1016/0006-2952(61)90145-9).
- [29] Li, W., Wu, R., Duan, J., Saint, C. P., Van Leeuwen, J., Impact of prechlorination on organophosphorus pesticides during drinking water treatment: Removal and transformation to toxic oxon byproducts, *Water Res.* 105 (2016) 1-10. <https://doi.org/10.1016/j.watres.2016.08.052>.
- [30] Lopez, A., Mascolo, G., Tiravanti, G., Passino, R., Degradation of herbicides (ametryn and isoproturon) during water disinfection by means of two oxidants (hypochlorite and chlorine dioxide), *Water Sci. Technol.* 35 (1997) 129-136. [https://doi.org/10.1016/S0273-1223\(97\)00018-8](https://doi.org/10.1016/S0273-1223(97)00018-8).
- [31] Fukuto, T. R., Mechanism of action of organophosphorus and carbamate insecticides, *Environ. Health Persp.* 87 (1990) 245-254. Available from:

<<https://www.ncbi.nlm.nih.gov/pmc/articles/PMC1567830/>>.

[32] Gälli, R., Rich, H. W., Scholtz, R., Toxicity of organophosphate insecticides and their metabolites to the water flea *Daphnia magna*, the Microtox test and na acetylcholinesterase inhibition test, *Aquat. Toxicol.* 30 (1994) 258-269. [https://doi.org/10.1016/0166-445X\(94\)90063-9](https://doi.org/10.1016/0166-445X(94)90063-9).

[33] Čolović, M. B., Krstić, D. Z., Ušćumlić, G. S., Vasić, V. M., Single and simultaneous exposure of acetylcholinesterase to diazinon, chlorpyrifos and their photodegradation products, *Pestic. Biochem. Phys.* 100 (1) (2011) 16-22. <https://doi.org/10.1016/j.pestbp.2011.01.010>.

[34] Belden J. B., Lydy, M. J., Effects of atrazine on acetylcholinesterase activity in midges (*Chironomus tentans*) exposed to organophosphorus insecticides, *Chemosphere* 44 (8) (2001) 1685-1689. [https://doi.org/10.1016/S0045-6535\(00\)00519-1](https://doi.org/10.1016/S0045-6535(00)00519-1).

[35] Belden, J. B., Lydy, M. J. Impact of atrazine on organophosphate insecticide toxicity, *Environ Toxicol. Chem.* 19 (2000) 2266-2274. <https://doi.org/10.1002/etc.5620190917>.